Some current topics in condensed matter physics

2012

M. E. Mora-Ramos, R. Pérez-Álvarez, L. M. Gaggero-Sager
(Eds.)

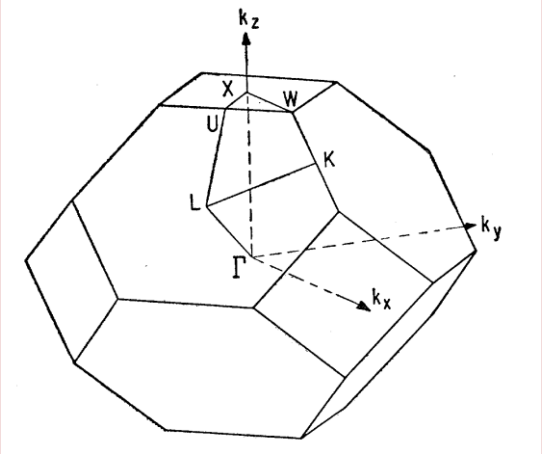

UAEM
Cuernavaca, México. 2012

Some current topics in condensed matter physics 2012

M. E. Mora-Ramos, R. Pérez-Álvarez,
L. M. Gaggero-Sager
(Eds.)

Cuerpo Académico de Física del Estado Sólido
Universidad Autónoma del Estado de Morelos
Cuernavaca. México. 2012

Some current topics in
condensed matter physics 2012
ISBN: 978-607-7771-68-5

Foreword

After the publication of the first in this series of electronic books, we present now to the physical community the second issue which corresponds to the year 2012. It contains some relevant contributions in several areas of the research frontier in Condensed Matter Physics.

In this occasion the editors apologize with those authors that sent their works –with high quality– early after the call. All kind of difficulties have contributed to the delay in the compilation, which has taken a time that we could have never imagined.

From now on the call for contributions is open to all colleagues that might be interested in putting their research works in the field in a format not limited by the length of the manuscript. They will appear as part of the third volume in the series, and can be sent to any of the editors below. We will be glad to communicate in order to comment the few formal requirements needed.

As commented in the foreword of the first volume, we have intentionally kept the bilingual format (english-spanish), looking for a wider diffusion of the contents via internet. Once more it is a pleasure to confirm that within this book meet very interesting contributions dealing with the most diverse fields, with different origins, and some of them being the fruits of the synergy between distant research groups, joined by the exciting world of the Condensed Matter Physics.

Cuernavaca, Mexico. June 2012

M. E. Mora-Ramos
(memora@uaem.mx)
R. Pérez-Álvarez (rpa@uaem.mx)
L. M. Gaggero-Sager (lgaggero@uaem.mx)

Luego de la publicación del primero de esta serie de libros electrónicos, presentamos a la comunidad el segundo, correspondiente al año 2012, con contribuciones relevantes en varias áreas de actividad de vanguardia de la Física de la Materia Condensada.

En esta ocasión debemos disculparnos con los autores que prontamente y con gran calidad nos hicieron llegar sus trabajos. Dificultades de todo tipo hicieron más demorado de lo que hubiéramos querido la salida de este segundo volumen.

Desde ahora ya estamos convocando a aquellos investigadores que puedan estar interesados en hacernos llegar sus resultados con vistas a la preparación del tercer volumen de esta serie. Pueden enviarlos a cualquiera de los editores. Con sumo gusto nos comunicaremos para comentarles las pocas exigencias de formato que usamos en estos libros.

Una vez más nos resulta grato constatar que en este libro confluyen contribuciones interesantes de varios y disímiles campos, de diferentes grupos, así como resultados de la sinergia entre colectivos que están distantes a veces miles de kilómetros pero que los une el apasionante mundo de la Física de la Materia Condensada.

Como comentamos en el prefacio del primer volumen de esta serie, hemos mantenido con toda intención el formato bilingüe (español-inglés), en aras de que los materiales puedan encontrar difusión vía *internet*.

Cuernavaca, Mexico. June 2012

M. E. Mora-Ramos
(memora@uaem.mx)
R. Pérez-Álvarez (rpa@uaem.mx)
L. M. Gaggero-Sager (lgaggero@uaem.mx)

Contents

Effective parameters for one-dimensional phononic crystals

J. Flores-Méndez, F. Pérez-Rodríguez

Abstract

We have developed a method for calculating the effective sound velocities for a 1D phononic crystal when the lattice constant is much smaller than the acoustic wave length and, therefore, the periodic medium can be regarded as a homogeneous one. The method is based on the expansion of the displacements field into plane waves, satisfying the Bloch theorem. The expansion allows us to obtain a wave equation for the amplitude of the macroscopic displacements field. From the form of this equation we identify the effective parameters, namely the effective sound velocities for the transverse and longitudinal macroscopic displacements in the homogenized 1D phononic crystal. We have obtained explicit expressions for the effective sound velocities in terms of the parameters of isotropic inclusions in the unit cell: mass density and elastic moduli. We have used these expressions for studying the dependence of the effective, transverse and longitudinal, sound velocities for a binary 1D phononic crystal upon the inclusion filling fraction. In particular, we present results for 1D phononic crystals composed of W-Al and Polyethylene-Si.

J. Flores-Méndez
Instituto de Física, Benemérita Universidad Autónoma de Puebla, Mexico.
e-mail: jflores@ifuap.buap.mx

F. Pérez-Rodríguez
Instituto de Física, Benemérita Universidad Autónoma de Puebla, Mexico.
e-mail: fperez@ifuap.buap.mx

Keywords: Phononic crystal, homogenization, elastic moduli, metamaterials.

1 Introduction

At present there is a great interest in fabricating artificial materials, having extraordinary properties, which considerably extend those of natural materials. Such a new class of materials is known as metamaterials. From the beginning, the photonic metamaterials, possessing negative index of refraction, have intensively been investigated. It was established that such an unusual optical property is found in periodic structures (photonic crystals) whose dielectric function is spatially modulated. A peculiarity of the photonic metamaterials is the high dielectric contrast between the components. The negative refraction has been observed in double negative metamaterials with simultaneously-negative effective permittivity and permeability (see, for example, the works [1–6]). However, this phenomenon is also manifest in anisotropic materials, as simple as a one-dimensional (1D) photonic crystal or superlattice, having elements in the effective permittivity tensor of different sign (see Refs. [7–10]). Analogously, metamaterials with uncommon acoustic properties have also searched among phononic crystals (PCs), i.e. materials with periodic modulation of their elastic properties. As in the photonic case, the calculation of the effective parameters of a phononic crystal is an important task.

Several homogenization theories, which are valid when the acoustic wave length is much longer than the lattice constant of the phononic crystal, have been proposed (see, for example, Refs. [11–15]). Among homogenization theories, we can identify two commonly-used approaches. One of them provides effective acoustic parameters within the framework of multiple scattering [11–13]. The second one, which is based on the Fourier formalism, makes use of the expansion of the microscopic acoustic field into plane waves [14,15]. The latter approach is of particular interest because it can be applied to different geometries of the inclusions inside the unit cell without substantial or complicated modifications. Here, we will precisely use the Fourier formalism to calculate the effective acoustic parameters of a 1D phononic crystal. As in the case of 1D photonic crystals, such

an inherently-anisotropic elastic system is a potential metamaterial. However, the main goal of the present work is to pay the way for the development of a general homogenization theory of (1D, 2D or 3D) elastic phononic crystals on the basis of the plane wave expansion.

We have organized the chapter as follows. In Sec. 2, we will present the Fourier formalism applied to a binary elastic superlattice. The numerical and analytical methods for calculating the dispersion relation for acoustic modes are commented in Sec. 3. The proposed method for calculating the effective acoustic parameters for a phononic superlattice, which is based upon the derivation of the wave equation for the macroscopic displacements field, is described in Sec. 4. Finally (Sec. 5), we shall apply the derived explicit formulas for the effective sound velocities to binary superlattices composed of W-Al and Polyethylene-Si.

2 Binary elastic superlattice

Let us consider a one-dimensional phononic crystal (or elastic superlattice) composed of alternating layers of isotropic elastic materials, A and B (Fig. 1). Their thicknesses are, respectively, d and $a-d$, where a is the lattice constant. Assuming that the z-axis is parallel

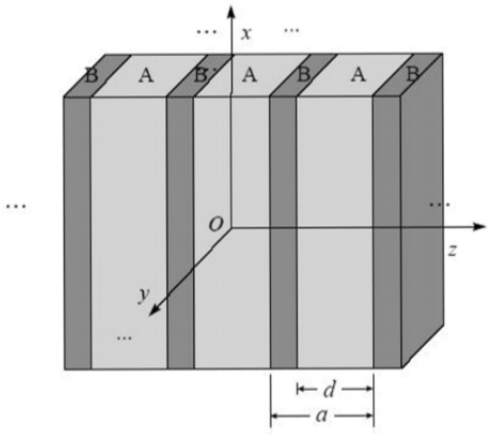

Fig. 1 Scheme of the binary superlattice.

to the superlattice growth direction, the mass density ρ, as well as the longitudinal and transverse sound velocities, C_l and C_t, turn out to be functions of the z-coordinate only. In this case, the second Newton's law for the displacement vector $\mathbf{u}(z,t)$, in the absence of external forces, acquires the form [16,17]:

$$\frac{\partial \sigma_{ik}}{\partial x_k} = \rho(z)\frac{\partial^2 u_i}{\partial t^2}. \tag{1}$$

Here, the Cauchy stress tensor σ_{ij} is expressed in terms of the strain tensor

$$u_{ik} = \frac{1}{2}\left(\frac{\partial u_i}{\partial x_k} + \frac{\partial u_k}{\partial x_i}\right), \tag{2}$$

according to the relation

$$\sigma_{ik} = 2\rho(z)C_t^2(z)u_{ik} + \rho(z)(C_l^2(z) - 2C_t^2(z))u_{ll}\delta_{ik}, \tag{3}$$

where δ_{ik} is the Kronecker's delta. Substituting Eqs. (2) and (3) into Eq. (1), we obtain the wave equation for an elastic inhomogeneous medium as [18,19]:

$$\rho\frac{\partial^2 u_i}{\partial t^2} = \nabla\cdot(\rho C_t^2\nabla u_i) + \nabla\cdot\left(\rho C_t^2\frac{\partial \mathbf{u}}{\partial x_i}\right) + \frac{\partial}{\partial x_i}\left[(\rho C_l^2 - 2\rho C_t^2)\nabla\cdot\mathbf{u}\right]. \tag{4}$$

Because of the periodicity of the functions $\rho(z)$, $C_l(z)$, and $C_t(z)$, we can expand them into Fourier series as

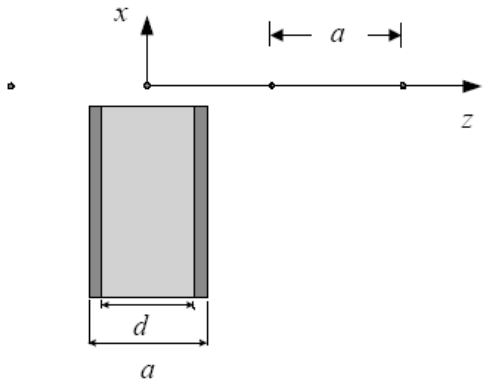

Fig. 2 Unit cell of the binary superlattice.

$$\rho(z) = \sum_{G_z} \rho(G_z) e^{iG_z z}, \tag{5}$$

$$C_{11}(z) = \rho(z) C_l^2(z) = \sum_{G_z} \Lambda(G_z) e^{iG_z z}, \tag{6}$$

$$C_{44}(z) = \rho(z) C_t^2(z) = \sum_{G_z} \tau(G_z) e^{iG_z z}, \tag{7}$$

where C_{11} and C_{44} are the longitudinal and transversal elastic constants for an isotropic elastic medium, and the components for the vectors of the reciprocal lattice are expressed as

$$G_z = \frac{2\pi}{a} n, \quad n = 0, \pm 1, \pm 2, \pm 3, \ldots \tag{8}$$

The component C_{12} for an isotropic medium is given by the relation:

$$C_{12}(z) = C_{11}(z) - 2C_{44}(z). \tag{9}$$

According to our geometry (see Figs. 1 and 2), the Fourier coefficients $\rho(G_z)$, appearing in Eqs. (5), can be calculated with the formula

$$\begin{aligned} \rho(G_z) &= \frac{1}{a} \int_{-a/2}^{a/2} \rho(z) e^{-iG_z z} dz \\ &= \rho_B \delta_{0G_z} + (\rho_A - \rho_B) F(G_z), \end{aligned} \tag{10}$$

where $F(G_z)$ is the form factor of the inclusion A,

$$F(G_z) = f \frac{\sin(G_z d/2)}{G_z d/2}, \tag{11}$$

and the ratio $f = d/a$ is its filling fraction. Similarly, the Fourier coefficients $\Lambda(G_z)$ and $\tau(G_z)$ of the expansions (6) and (7) can respectively be written as

$$\Lambda(G_z) = \Lambda_B \delta_{0G_z} + (\Lambda_A - \Lambda_B) F(G_z), \tag{12}$$

$$\tau(G_z) = \tau_B \delta_{0G_z} + (\tau_A - \tau_B) F(G_z). \tag{13}$$

For a periodic system, the solution of Eq. (4) should satisfy the Bloch theorem [20]. Therefore, we can write the displacement vector in the form

$$\mathbf{u}(\mathbf{r}, t) = e^{-i\omega t} e^{i\mathbf{K}\cdot\mathbf{r}} \mathbf{u}_{\mathbf{K}}(z), \tag{14}$$

where $\mathbf{u}_{\mathbf{K}}(z)$ is a periodic function with the same period as for the superlattice, and ω is the frequency. We should note that the component K_z is here the Bloch wave number and $\mathbf{K}_{\|}$ is an independent vector parallel to the $x-y$ plane. After expanding the function $\mathbf{u}_{\mathbf{K}}(z)$ into Fourier series, we get

$$\mathbf{u}(\mathbf{r},t) = e^{-i\omega t} e^{i\mathbf{K}\cdot\mathbf{r}} \sum_{G_z} \mathbf{u}_{\mathbf{K}}(G_z) e^{iG_z z}. \tag{15}$$

It is worth mentioning that the Fourier formalism for solving the wave equation (4) allows us to avoid the application of boundary conditions for the displacement vector $\mathbf{u}(\mathbf{r})$, since the structural information of the system is explicitly contained in the Fourier coefficients $\mathbf{u}_{\mathbf{K}}(G_z)$. This is owing to the fact that the boundary conditions for $\mathbf{u}(\mathbf{r})$ are consistent with the wave equation (4).

Substituting Eqs. (5)-(7), and (15) into (4), we obtain

$$\begin{aligned}\sum_{G_z'} \big\{ & \tau(G_z - G_z')\mathbf{u}(G_z')(\mathbf{K}_{\|} + (K_z + G_z')\hat{z}) \cdot (\mathbf{K}_{\|} + (K_z + G_z)\hat{z}) \\ & + \tau(G_z - G_z')\mathbf{u}(G_z') \cdot (\mathbf{K}_{\|} + (K_z + G_z)\hat{z})\,(\mathbf{K}_{\|} + (K_z + G_z')\hat{z}) \\ & + \Lambda(G_z - G_z')\mathbf{u}(G_z') \cdot (\mathbf{K}_{\|} + (K_z + G_z')\hat{z})\,(\mathbf{K}_{\|} + (K_z + G_z)\hat{z}) \\ & - 2\tau(G_z - G_z')\mathbf{u}(G_z') \cdot (\mathbf{K}_{\|} + (K_z + G_z')\hat{z})\,(\mathbf{K}_{\|} + (K_z + G_z)\hat{z}) \\ & - \omega^2 \rho(G_z - G_z')\mathbf{u}(G_z') \big\} = 0 \end{aligned} \tag{16}$$

We can rewrite Eq. (16) in dyadic form as

$$\sum_{G_z'} \left[\overleftrightarrow{B}\,(G_z, G_z') - \omega^2 \rho(G_z - G_z')\ \overleftrightarrow{I} \right] \cdot \mathbf{u}(G_z') = \mathbf{0}, \tag{17}$$

where

$$\begin{aligned} \overleftrightarrow{B}\,(G_z, G_z') = {} & \tau(G_z - G_z')(\mathbf{K}_{\|} + (K_z + G_z')\hat{z}) \cdot (\mathbf{K}_{\|} + (K_z + G_z)\hat{z})\ \overleftrightarrow{I} \\ & + \tau(G_z - G_z')(\mathbf{K}_{\|} + (K_z + G_z')\hat{z})\,(\mathbf{K}_{\|} + (K_z + G_z)\hat{z}) \\ & + \Lambda(G_z - G_z')(\mathbf{K}_{\|} + (K_z + G_z)\hat{z})\,(\mathbf{K}_{\|} + (K_z + G_z')\hat{z}) \\ & - 2\tau(G_z - G_z')(\mathbf{K}_{\|} + (K_z + G_z)\hat{z})\,(\mathbf{K}_{\|} + (K_z + G_z')\hat{z}), \end{aligned} \tag{18}$$

and $\overleftrightarrow{I}$ is the unit dyadic [$(\overleftrightarrow{I})_{ij} = \delta_{ij}$].

3 Phononic dispersion relation

3.1 Numerical diagonalization

The inverse $\nu(G_z, G'_z)$ of matrix $\rho(G_z, G'_z) \equiv \rho(G_z - G'_z)$ in Eq. (18) satisfies the relation

$$\sum_{G'_z} \nu(G_z, G'_z)\rho(G'_z, G''_z) = \delta_{G_z, G''_z}, \tag{19}$$

and its elements are directly calculated by using the expression

$$\begin{aligned}\nu(G_z, G'_z) &= \nu(G_z - G'_z) \\ &= \frac{1}{a}\int_{-a/2}^{a/2} \frac{1}{\rho(z)} e^{-i(G_z - G'_z)z} dz \\ &= \frac{1}{\rho_B}\delta_{G_z, G'_z} + \left(\frac{1}{\rho_A} - \frac{1}{\rho_B}\right) F(G_z - G'_z).\end{aligned} \tag{20}$$

Multiplying Eq. (18) by $\nu(G_z, G'_z)$ (20), we get

$$\sum_{G'_z} \left[\overleftrightarrow{M}(G_z, G'_z) - \omega^2 \delta_{G_z, G'_z} \overleftrightarrow{I}\right] \cdot \mathbf{u}(G'_z) = \mathbf{0}, \tag{21}$$

where we have introduced the dyadic $\overleftrightarrow{M}(G_z, G'_z)$:

$$\overleftrightarrow{M}(G_z, G'_z) = \sum_{G''_z} \nu(G_z, G''_z) \overleftrightarrow{B}(G''_z, G'_z). \tag{22}$$

The system (21) represents a homogeneous system of algebraic equations, which has a nontrivial solution if the determinant of the associated matrix is identical to zero, i.e.

$$\det\left\{\overleftrightarrow{M}(G_z, G'_z) - \omega^2 \delta_{G_z, G'_z} \overleftrightarrow{I}\right\} = 0. \tag{23}$$

The condition (23) provides the dispersion relation $\omega(K_z)$ for vibrational eigenmodes in the PC. It should be noted that such a phononic dispersion parametrically depends upon the wave vector component $\mathbf{K}_{\|}$. Thus, the phononic dispersion can be straightforwardly calculated by numerically diagonalizing the matrix $\overleftrightarrow{M}(G_z, G'_z)$. In doing that, we

should use a finite matrix of sufficiently large size to guarantee accurate results.

3.2 Analytical procedure

The phononic dispersion for modes propagating along the crystal growth can be analytically calculated. Indeed, the wave equation (4) can be separated into two equations for the principal polarizations: one equation for the transverse modes with displacement vector

$$\mathbf{u}_t(z) = (u_x(z), u_y(z), 0), \tag{24}$$

and the other one for the longitudinal modes, whose displacement is parallel to the z-axis,

$$\mathbf{u}_l(z) = (0, 0, u_z(z)). \tag{25}$$

Substituting the expressions

$$\mathbf{u} = \mathbf{u}_t + \mathbf{u}_l, \tag{26}$$

(24) and (25) into (4), we get

$$\rho(z)\frac{\partial^2 \mathbf{u}_t}{\partial t^2} = \frac{\partial}{\partial z}\left(\rho(z)C_t^2(z)\frac{\partial \mathbf{u}_t}{\partial z}\right), \tag{27}$$

$$\rho(z)\frac{\partial^2 \mathbf{u}_l}{\partial t^2} = \frac{\partial}{\partial z}\left(\rho(z)C_l^2(z)\frac{\partial \mathbf{u}_l}{\partial z}\right). \tag{28}$$

Let us consider transverse modes with polarization vector along the x-axis. From Eq. (27), we can write

$$\rho(z)\frac{\partial^2 u_x}{\partial t^2} = \frac{\partial}{\partial z}\left(\rho(z)C_t^2(z)\frac{\partial u_x}{\partial z}\right). \tag{29}$$

Inside the homogeneous media A and B, namely in the regions $-d/2 < z < d/2$ and $-(a-d/2) < z < -d/2$ (see Figs. 1 and 2), this equation can be rewritten as

$$\frac{\partial^2 u_x}{\partial t^2} = C_{t,A}^2 \frac{\partial^2}{\partial z^2} u_x, \qquad -d/2 < z < d/2, \tag{30}$$

$$\frac{\partial^2 u_x}{\partial t^2} = C_{t,B}^2 \frac{\partial^2}{\partial z^2} u_x, \quad -(a-d/2) < z < -d/2. \tag{31}$$

Assuming $u_x(x,t) \sim e^{-i\omega t}$, the solutions of equations (30) and (31) can be expressed in the form

$$u_x(z) = De^{iK_z^A z} + Ee^{-iK_z^A z}, \qquad -d/2 < z < d/2, \tag{32}$$

$$u_x(z) = Fe^{iK_z^B z} + He^{-iK_z^B z}, \quad -(a-d/2) < z < -d/2, \tag{33}$$

where

$$K_z^A = \omega/C_{t,A}, \qquad K_z^B = \omega/C_{t,B}. \tag{34}$$

The solutions (32) and (33) should satisfy boundary conditions at $z = -d/2$, which are given by [16,17]

$$u_x(-d/2-0) = u_x(-d/2+0), \tag{35}$$

$$\rho_A C_{t,A}^2 \frac{\partial}{\partial z} u_x(-d/2-0) = \rho_B C_{t,B}^2 \frac{\partial}{\partial z} u_x(-d/2+0). \tag{36}$$

The boundary conditions at the interface $z = -d/2$, lead to two algebraic equations for the amplitudes D, E, F, and H:

$$Fe^{-iK_z^B d/2} + He^{iK_z^B d/2} = De^{-iK_z^A d/2} + Ee^{iK_z^A d/2}, \tag{37}$$

$$K_z^B C_{44,B}\left[Fe^{-iK_z^B d/2} - He^{iK_z^B d/2}\right] = K_z^A C_{44,A}\left[De^{-iK_z^A d/2} - Ee^{iK_z^A d/2}\right] \tag{38}$$

Here, we used $\rho_A C_{t,A}^2 = C_{44,A}$ and $\rho_B C_{t,B}^2 = C_{44,B}$. The displacements field inside the region $d/2 < z < a - d/2$ (see Figs. 1 and 2) can be determined by requiring that it satisfy the Bloch theorem, i.e.

$$u_x(z+a) = e^{iK_z a} u_x(z), \tag{39}$$

where K_z is the Bloch wave vector. Hence,

$$u_x(z) = e^{iK_z a}\left[Fe^{iK_z^B(z-a)} + He^{-iK_z^B(z-a)}\right], \qquad d/2 < z < a - d/2. \tag{40}$$

Now, we should apply boundary conditions for the displacements field at the interface $z = d/2$:

$$u_x(d/2-0) = u_x(d/2+0), \tag{41}$$

$$\rho_A C_{t,A}^2 \frac{\partial}{\partial z} u_x(d/2-0) = \rho_B C_{t,B}^2 \frac{\partial}{\partial z} u_x(d/2+0). \tag{42}$$

Substituting Eqs. (32) and (40) into Eqs. (41) and (42), we obtain other two equations for the amplitudes D, E, F, and H:

$$De^{iK_z^A d/2} + Ee^{-iK_z^A d/2} = e^{iK_z a}\left[Fe^{-iK_z^B(a-d/2)} + He^{iK_z^B(a-d/2)}\right], \tag{43}$$

$$K_z^A C_{44,A}\left[De^{iK_z^A d/2} - Ee^{-iK_z^A d/2}\right] = K_z^B C_{44,B} e^{iK_z a}\left[Fe^{-iK_z^B(a-d/2)} - He^{iK_z^B(a-d/2)}\right]. \tag{44}$$

The resulting system of algebraic equations for D, E, F, and H is homogeneous and, therefore, it has a nontrivial solution if its determinant

$$\Delta = \begin{vmatrix} e^{-iK_z^A d/2} & e^{iK_z^A d/2} & -e^{-iK_z^B d/2} & -e^{iK_z^B d/2} \\ K_z^A C_{44,A} e^{-iK_z^A d/2} & -K_z^A C_{44,A} e^{iK_z^A d/2} & -K_z^B C_{44,B} e^{-iK_z^B d/2} & K_z^B C_{44,B} e^{iK_z^B d/2} \\ e^{iK_z^A d/2} & e^{-iK_z^A d/2} & -e^{i(K_z a - K_z^B(a-d/2))} & -e^{i(K_z a + K_z^B(a-d/2))} \\ K_z^A C_{44,A} e^{iK_z^A d/2} & -K_z^A C_{44,A} e^{-iK_z^A d/2} & -K_z^B C_{44,B} e^{i(K_z a - K_z^B(a-d/2))} & K_z^B C_{44,B} e^{i(K_z a + K_z^B(a-d/2))} \end{vmatrix} \tag{45}$$

is equal to zero. The condition $\Delta = 0$ leads to the phononic dispersion relation $\omega(K_z)$, which can be written in the form

$$\cos(K_z a) = \cos(K_z^A d)\cos(K_z^B d_B) - \frac{1}{2}\left[\frac{K_z^A \rho_A C_{t,A}^2}{K_z^B \rho_B C_{t,B}^2} + \frac{K_z^B \rho_B C_{t,B}^2}{K_z^A \rho_A C_{t,A}^2}\right] \sin(K_z^A d)\sin(K_z^B d_B), \tag{46}$$

where $d_B = a - d$.

The phononic dispersion for transverse modes with polarization vector along the y-axis is exactly the same as in Eq. (46). Besides, the dispersion relation for the longitudinal modes, propagating along the growth direction, can be similarly calculated. Nevertheless, it can be directly obtained from Eq. (46) by substituting the transverse velocities, $C_{t,A}$ and $C_{t,B}$, therein for the longitudinal ones, $C_{l,A}$ and $C_{l,B}$.

4 Effective acoustic parameters

In the case when the wave length of sound is much larger than the lattice constant of the phononic crystal, this artificial periodic heterostructure can be modeled as a homogeneous medium with effective acoustic parameters. In this section, we shall calculate the effective sound velocities for both transverse and longitudinal vibrational modes, propagating along the growth direction of a superlattice like that considered in the previous sections.

From the Bloch theorem, given by Eq. (15), we can write the displacements field as

$$\mathbf{u}(\mathbf{r},t) = e^{-i\omega t}\left\{ e^{i\mathbf{K}\cdot\mathbf{r}}\mathbf{u}_{\mathbf{K}}(0) + e^{i\mathbf{K}\cdot\mathbf{r}}\sum_{G_z\neq 0}\mathbf{u}_{\mathbf{K}}(G_z)e^{iG_z z}\right\}. \tag{47}$$

Assuming $\mid K_z a \mid \ll 1$ and $\mathbf{K}_{\parallel} = 0$, the first term on the r.h.s. of Eq. (47) describes the smooth variations of the displacement vector $\mathbf{u}(\mathbf{r},t)$ as a function of the coordinates, whereas the second term therein is associated with the rapid oscillations (fluctuations) over the unit cell. So, we can define the average (macroscopic) displacements field as

$$\mathbf{U}(\mathbf{r},t) \equiv e^{-i\omega t}e^{i\mathbf{K}\cdot\mathbf{r}}\mathbf{u}_{\mathbf{K}}(0) = e^{-i\omega t}e^{i\mathbf{K}\cdot\mathbf{r}}\mathbf{U}_0 \tag{48}$$

According to Eq. (21), the Fourier coefficients $\mathbf{u}(G_z)$ satisfy the system of equations

$$\sum_{G_z'}\overleftrightarrow{D}(G_z,G_z')\cdot\mathbf{u}(G_z') = \mathbf{0}, \tag{49}$$

where we have introduced the dyadic

$$\overleftrightarrow{D}(G_z,G_z') = \overleftrightarrow{M}(G_z,G_z') - \omega^2\delta_{G_z,G_z'}\overleftrightarrow{I}. \tag{50}$$

One can express the coefficients $\mathbf{u}(G_z \neq 0)$ in terms of $\mathbf{U}_0$ by using Eq. (49) for $G_z \neq 0$. Thus,

$$\mathbf{u}(G_z) = -\sum_{G_z'\neq 0}\overleftrightarrow{D}_S^{-1}(G_z,G_z')\overleftrightarrow{D}(G_z',0)\cdot\mathbf{U}_0. \tag{51}$$

Here, $\overleftrightarrow{D}_S\,(G_z,G'_z)$ is a submatrix, obtained from $\overleftrightarrow{D}\,(G_z,G'_z)$ (50) after eliminating its block rows (columns) with $G_z=0$ ($G'_z=0$). As it was demonstrated in Ref. [21], the inverse of the submatrix $\overleftrightarrow{D}_S\,(G_z,G'_z)$ is related with the inverse of the matrix $\overleftrightarrow{D}\,(G_z,G'_z)$ according to the formula:

$$\overleftrightarrow{D}_S^{\,-1}\,(G_z,G'_z)=\overleftrightarrow{D}^{\,-1}\,(G_z,G'_z) - \overleftrightarrow{D}^{\,-1}\,(G_z,0)\left\{\overleftrightarrow{D}^{\,-1}\,(0,0)\right\}^{-1}\overleftrightarrow{D}^{\,-1}\,(0,G'_z), \quad (52)$$

where, $\overleftrightarrow{D}^{\,-1}\,(0,0)$ is a 3×3 block, which is obtained from the original matrix $\overleftrightarrow{D}^{\,-1}\,(G_z,G'_z)$ (50) of infinite size, and $\{\ldots\}^{-1}$ symbolizes the inverse of the 3×3 matrix block.

Let us rewrite Eq. (49) for $G_z=0$ as

$$\omega^2\mathbf{U}_0=\overleftrightarrow{M}\,(0,0)\cdot\mathbf{U}_0+\sum_{G'_z\neq 0}\overleftrightarrow{D}\,(0,,G'_z)\cdot\mathbf{u}(G'_z). \quad (53)$$

Substituting Eqs. (51) and (52) into Eq. (53), we obtain the macroscopic wave equation:

$$\omega^2\mathbf{U}_0=\overleftrightarrow{M}_{\rm eff}\,(K_z)\cdot\mathbf{U}_0, \quad (54)$$

where the effective matrix $\overleftrightarrow{M}_{\rm eff}$ is given by

$$\overleftrightarrow{M}_{\rm eff}\,(K_z)=\left\{\overleftrightarrow{D}^{\,-1}\,(K_z;0,0)\right\}^{-1}+\omega^2\,\overleftrightarrow{I}\,. \quad (55)$$

From the macroscopic wave equation (54), we can define an effective dyadic representing the Christoffel tensor, divided by the mass density, as

$$(\overleftrightarrow{\Gamma}/\rho)_{\rm eff}=\overleftrightarrow{M}_{\rm eff}\,(K_z)/K_z^2. \quad (56)$$

Thus,

$$\left(\frac{\overleftrightarrow{\Gamma}}{\rho}\right)_{\rm eff}=\frac{1}{K_z^2}\left\{\overleftrightarrow{D}^{\,-1}\,(K_z;0,0)\right\}^{-1}+\left(\frac{\omega}{K_z}\right)^2\overleftrightarrow{I}\,. \quad (57)$$

In the situation, considered here, of acoustic waves propagating along the growth direction, the effective tensor (57) turns out to be diagonal, i.e. $(\overleftrightarrow{\Gamma}/\rho)_{\mathrm{eff},ij} = C_{\mathrm{eff},i}\delta_{ij}$ with $C_{\mathrm{eff},x} = C_{\mathrm{eff},y}$. The principal values $C_{\mathrm{eff},x}(= C_{\mathrm{eff},y})$ and $C_{\mathrm{eff},z}$ are, in fact, the effective sound velocities for transverse and longitudinal modes, respectively. It should be emphasized that formula (57) is valid in the long wavelength limit, i.e. when both $K_z \to 0$ and $\omega \to 0$.

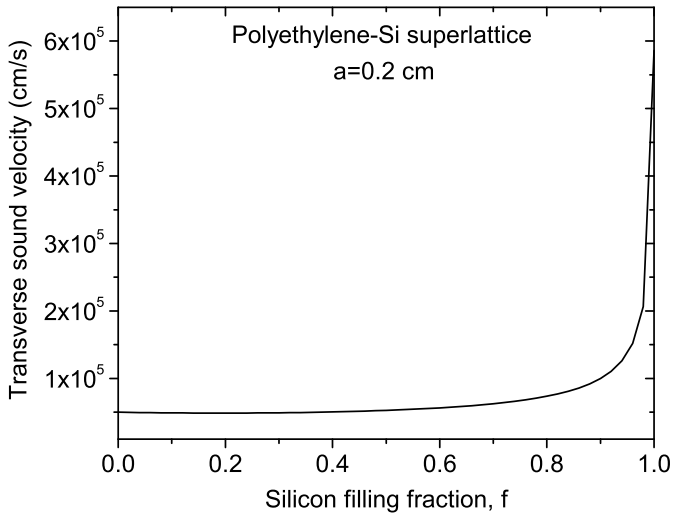

Fig. 3 Effective sound velocity for *transverse* vibrational modes propagating along the growth direction of a Polyethylene-Si superlattice.

5 Numerical results and discussion

Let us apply the derived formula (57) for calculating the effective sound velocities of modes propagating along the growth direction of specific binary 1D phononic crystals. First, we shall consider a polyethylene-silicon superlattice having a period $a = 0.2$cm. The parameters used in the calculations are: mass densities $\rho_A = 2.32$ gr/cm^3 and $\rho_B = 0.89$ gr/cm^3, transverse sound velocities $C_{t,A} =$

5.86×10^5 cm/s and $C_{t,B} = 0.5 \times 10^5$ cm/s, and longitudinal sound velocities $C_{l,A} = 8.45 \times 10^5$ cm/s and $C_{l,B} = 1.9 \times 10^5$ cm/s for silicon and polyethylene, respectively (the material parameters were taken from Ref. [20]). In the numerical calculations, 300 plane waves were needed to achieve good convergence of the results.

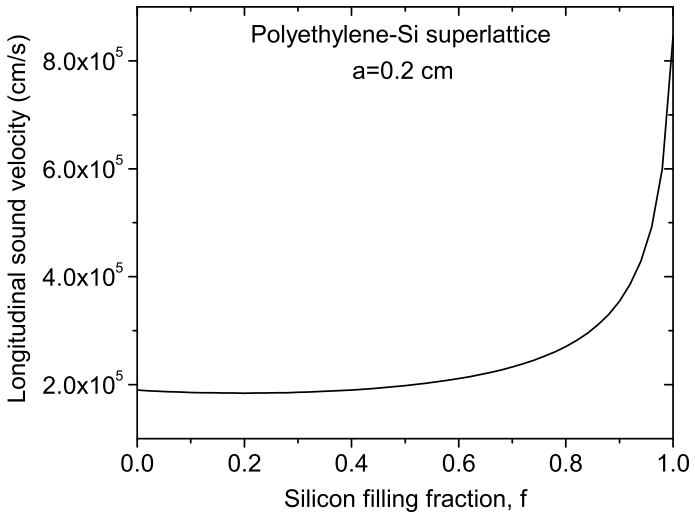

Fig. 4 Effective sound velocity for *longitudinal* vibrational modes propagating along the growth direction of a Polyethylene-Si superlattice.

Figs. 3 and 4 show the dependencies of the transverse ($C_{\text{eff},t}$) and longitudinal ($C_{\text{eff},l}$) effective sound velocities upon the silicon filling fraction f ($f = d/a$). As it is seen, both transverse and longitudinal effective sound velocities slowly vary with increasing the silicon filling fraction f up to $f \approx 0.9$. In contrast, at $f > 0.9$, the slopes of the curves $C_{\text{eff},t}(f)$ and $C_{\text{eff},l}(f)$ are relatively large.

Figs. 5 and 6 exhibit numerically-calculated effective parameters, $C_{\text{eff},t}$ and $C_{\text{eff},l}$, for a W-Al 1D phononic crystal. The parameters used here are [20]: $\rho_A = 2.69$ gr/cm^3 and $\rho_B = 19.3$ gr/cm^3, transverse sound velocities $C_{t,A} = 3.22 \times 10^5$ cm/s and $C_{t,B} = 2.88 \times 10^5$ cm/s, and longitudinal sound velocities $C_{l,A} = 6.45 \times 10^5$ cm/s and $C_{l,B} = 5.21 \times 10^5$ cm/s for aluminium and tungsten, respectively. In

this case, the effective sound velocity for transverse [longitudinal] modes decreases with the Al filling fraction f up to its minimum value at $f \approx 0.45$. For larger values of f (i.e. in the interval $0.5 < f < 1$) the effective parameter $C_{\mathrm{eff},t}$ [$C_{\mathrm{eff},l}$] increases with f.

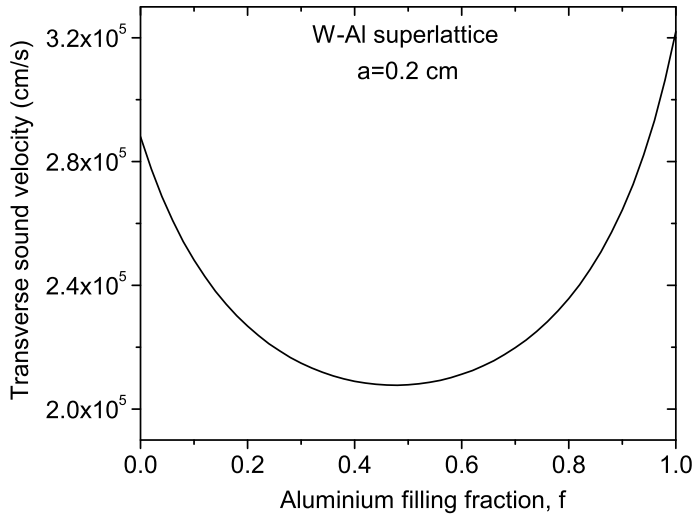

Fig. 5 Effective sound velocity for *transverse* vibrational modes propagating along the growth direction of a W-Al superlattice.

In order to verify our numerical results (Figs. 3-6), we shall derive analytical expressions for the effective sound velocities $C_{\mathrm{eff},t}$ and $C_{\mathrm{eff},l}$ in the case when the "microscopic" displacement vector slowly varies in each layer of the superlattice, i.e. when

$$K_z^A d \ll 1, \qquad K_z^B d_B \ll 1. \tag{58}$$

After expanding the dispersion relation (46) in powers of the parameters (58) up to quadratic terms and using Eq. (34), we obtain the expression:

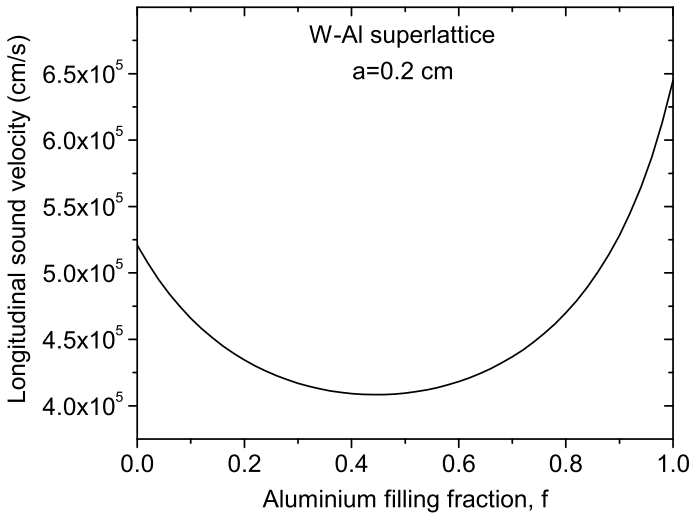

Fig. 6 Effective sound velocity for *longitudinal* vibrational modes propagating along the growth direction of a W-Al superlattice.

$$C_{\mathrm{eff},t} = \left\{ \frac{f^2}{C_{t,A}^2} + \frac{(1-f)^2}{C_{t,B}^2} + \left[\frac{\rho_A C_{t,A}}{\rho_B C_{t,B}} + \frac{\rho_B C_{t,B}}{\rho_A C_{t,A}} \right] \frac{f}{C_{t,A}} \frac{(1-f)}{C_{t,B}} \right\}^{-1/2} . \tag{59}$$

Here, the effective sound velocity for transverse vibrational modes has been defined as $C_{\mathrm{eff},t} = \omega / K_z$. The expression for the effective sound velocity of longitudinal modes is obtained by writing the subindex l instead of t in Eq. (59). We have found that our numerical results, shown in Figs. 3-6, coincide with those predicted by equation (59) and the corresponding one for longitudinal modes.

6 Conclusions

We have derived explicit formulas for the calculation of the effective sound velocities in a 1D phononic crystal in the long-wavelength limit. The formulas were applied for analyzing the dependence of the effective, transverse and longitudinal, sound velocities upon the inclu-

sion filling fraction for binary superlattices composed of Polyethylene-Si and W-Al. In the later case, the contrast of material parameters is relatively larger and, as a result, at Al filling fractions $f \approx 0.45$, the effective sound velocity for both transverse ($C_{\text{eff},t}$) and longitudinal ($C_{\text{eff},l}$) modes, propagating along the superlattice growth direction, takes values smaller than the sound velocity for each component (W or Al). For this reason, we can say that the homogenized 1D W-Al phononic crystal behaves as a metamaterial. It should be emphasized that these results coincide with those obtained from analytical expressions for the effective sound velocities, which were derived from the exact phononic dispersion by assuming that the microscopic field slowly varies inside each layer of the unit cell.

Although the homogenization theory developed here is valid only for phononic crystals with one-dimensional periodicity and isotropic inclusions, it shows the usefulness of the plane wave expansion method to obtain explicit expressions for the effective acoustic parameters. The generalization of this approach to 2D and 3D periodic elastic structures with anisotropic inclusions and arbitrary contrast of the materials parameters will be presented elsewhere.

Acknowledgments

J. F.-M. thanks the Consejo Nacional de Ciencia y Tecnología (CONACYT) for financial support. F. P.-R. and the group of "Materiales Avanzados" (BUAP-CA-250) acknowledge the support from the scientific groups "Física del Estado Sólido" (UAEMOR-CA-27) and "Propiedades Electrónicas, Ópticas y Magnéticas de Materiales" (UAZ-CA-136) through PROMEP-SEP projects.

References

1. J. B. Pendry, A. J. Holden, D. J. Robbins, and W. J. Stewart, "Magnetism from conductors and enhanced nonlinear phenomena", *IEEE Trans. Microw. Theory Tech.* **47**, 2075 (1999).
2. D. R. Smith, W. J. Padilla, D. C. Vier, S. C. Nemat-Nasser, and S. Schultz, "Composite medium with simultaneously negative permeability and permittivity", *Phys. Rev. Lett.* **84**, 4184–4187 (2000).
3. L. Zhang, G. Tuttle, C. M. Soukoulis, "GHz magnetic response of split ring resonators", *Photon. Nanostruct.* **2**, 155–159 (2004).

4. C. Enkrich, M. Wegener, S. Linden, S. Burger, L. Zschiedrich, F. Schmidt, J. F. Zhou, Th. Koschny, and C. M. Soukoulis, "Magnetic metamaterials at telecommunication and visible frequencies", *Phys. Rev. Lett.* **95**, 203901, 1–4 (2005).
5. S. Zhang, W. Fan, N. C. Panoiu, K. J. Malloy, R. M. Osgood, and S. R. J. Brueck, "Experimental demonstration of near-infrared negative-index metamaterials", *Phys. Rev. Lett.* **95**, 137404, 1–4 (2005).
6. J. A. Reyes-Avendaño, U. Algredo-Badillo, P. Halevi, and F. Pérez-Rodríguez, "From photonic crystals to metamaterials: the bianisotropic response", *New J. Phys.* **13**, 073041, 1–33 (2011).
7. V. A. Podolskiy and E. E. Narimanov, "Strongly anisotropic waveguide as a nonmagnetic left-handed system", *Phys. Rev. B* **71**, 201101(R), 1–4 (2005).
8. B. Wood, J. B. Pendry, and D. P. Tsai, "Directed subwavelength imaging using a layered metal-dielectric system", *Phys. Rev. B* **74**, 115116, 1–8 (2006).
9. A. L. Rakhmanov, V. A. Yampolskii, J. A. Fan, F. Capasso, F. Nori, "Layered superconductors as negative-refractive-index metamaterials", *Phys. Rev. B* **81**, 075101, 1–6 (2010).
10. B. Zenteno-Mateo, V. Cerdán-Ramírez, B. Flores-Desirena, M. P. Sampedro, E. Juárez-Ruiz, and F. Pérez-Rodríguez, "Effective permittivity tensor for a metal-dielectric superlattice", *Progress in Electromagnetics Research Letters (PIER Lett.)* **22**, 165–174 (2011).
11. J. Mei, Zh. Liu, W. Wen, and P. Sheng, "Effective mass density of fluid-solid composites", *Phys. Rev. Lett.* **96**, 024301, 1–4 (2006).
12. D. Torrent, A. Håkansson, F. Cervera, and J. Sánchez-Dehesa, "Homogenization of two-dimensional clusters of rigid rods in air", *Phys. Rev. Lett.* **96**, 204302, 1–4 (2006).
13. D. Torrent and J. Sánchez-Dehesa, "Effective parameters of clusters of cylinders embedded in a nonviscous fluid or gas", *Phys. Rev. B* **74**, 224305, 1–10 (2006).
14. A. A. Krokhin, J. Arriaga, and L. Gumen, "Speed of sound in periodic elastic composites", *Phys. Rev. Lett.* **91**, 264302, 1–4 (2003).
15. L. N. Gumen, J. Arriaga, A. A. Krokhin, "Metafluid with anisotropic dynamic mass", *Low Temp. Phys./Fizika Nizkikh Temperatur* **37**, 1221–1224 (2011).
16. L. D. Landau, E. M. Lifshitz, "Theory of elasticity" (Butterworth - Heinemann, New York, 1986).
17. L. M. Brekhovskikh, O. A. Godin, "Acoustics of layered media I: Plane and quasi-plane waves" (Springer, Berlin, 1998).
18. M. S. Kushwaha, P. Halevi, G. Martínez, L. Dobrzynski, and B. Djafari-Rouhani, "Theory of acoustic band structure of periodic elastic composites", *Phys. Rev. B* **49**, 2313-2322 (1994).
19. M. S. Kushwaha, "Classical band structure of periodic elastic composites", *Int. J. Mod. Physics B* **10**, 977-1094 (1996).
20. Ch. Kittel, "Introduction to solid state physics" (Wiley, New York, 1995).
21. V. Cerdán-Ramírez, B. Zenteno-Mateo, M. P. Sampedro, M. A. Palomino-Ovando, B. Flores-Desirena, and F. Pérez-Rodríguez, "Anisotropy effects in homogenized magnetodielectric photonic crystals", *J. Appl. Phys.* **106**, 103520, 1-8 (2009).

Acoustic transmittance of a multilayer system with a linear variation of impedances

J. J. Rodríguez Pérez, R. A. Reyes-Villagrana, A. Enciso-Muñoz, and D. A. Contreras-Solorio

Abstract

Using the transfer matrix method we calculate the frequency dependence of the transmission of longitudinal elastic waves for a layered structure where the characteristic acoustic impedance of the layers with odd numbering follows a linear distribution. The central layer has the highest value of impedance while the end layers have the smallest ones. The inserted even layers have the same impedance as the incident medium, which is water. The structure presents intervals of stopbands and very flat passbands. We compare the transmission with that of a regular structure where all the layers with odd numbering have the same value of impedance. We also make a comparison of the transmission with that of an inverted structure where the central barrier has the smallest value of impedance while the end layers have the highest values.

1 Introduction

Since many decades ago, the search for energy, electronic, optical and acoustic filters is an active field. In particular, there are proposals of energy band-pass filters using quantum superlattices with a Gaussian potential profile [1,2]. These structures allow the incident electrons to be nearly totally transmitted when the impinging electron energy is in the passband. Also, a complete reflection occurs when the impinging energy is in the stopband. The characteristics of the bands can be adjusted modifying the parameters of the superlattice and of

Unidad Académica de Física de la Universidad Autónoma de Zacatecas. Apartado Postal C-580, 98060 Zacatecas, Zac., Mexico. e-mail: D. A. C. S.: dacs10@yahoo.com.mx

the Gaussian distribution. On the other hand, following the preceding idea, there is also a proposal of a multilayer optical structure where the refractive index varies according to the envelope of a Gaussian function [3]. This structure acts as an omnidirectional mirror. For sound, the characteristic acoustic impedance is one of the main acoustical properties of a material. The difference of the impedance values between two media, causes reflection at the interface. Formerly a multilayer structure with Gaussian variation of the acoustic impedance was studied [4]. In this work we propose a multilayer acoustic structure where the impedance values of the layers with odd numbering has a linear profile. The central layer has the maximum value of impedance and the end layers have the minimum value. The acoustic impedance of the inserted layers with even number is the same as that of the incident medium. This type of variation provides a smoothly varying impedance for the layers, which can improve the transmission of the structure. We make a theoretical study of the frequency dependence of the transmittance for this structure following a formalism of transfer matrix used for electromagnetic waves, which we have adapted to acoustic waves [5]. We obtain stopbands with 100% reflectivity and very flat passbands. We also calculate the transmission for a regular structure where all the layers with odd numbering have the same value of impedance, and for an inverted structure where the central layer has the minimum impedance and the layers at the ends have the maximum impedances.This type of structures can be constructed experimentally using layers with composite materials where the acoustic impedance can be tailored by varying the volume fractions of the components in the composite [6,7]. Another possible way to construct these structures is by using layers of porous silicon. This material has been widely used for the fabrication of optical devices, including optical filters where the refractive index can be varied through a variation of the porosity [3]. There are also studies of the variation of acoustical properties, including the acoustical impedance, due to the variation of the porosity [8,9]. Recently, acoustic multilayer mirrors have been made using porous silicon [10].

2 Theoretical model and calculation method

To calculate the transmittance, we use the theory of Refs.[5][11][12]. We consider a structure of N plane multilayers. The layers are perpendicular to the x axis. Each j layer has a width d_j and characteristic impedance Z_j given by

$$Z_j = \rho_j c_j \tag{1}$$

Where ρ_j and c_j are, respectively, the density and the sound speed for the j material. We consider longitudinal elastic plane waves propagating in the $x-z$ plane, coming from the left in a medium with impedance Z_0. The plane wave is incident on the structure of N plane multilayers. At the right side of the structure, the wave propagates in a medium S with impedance Z_s. We can write the wave function for each layer in the following form

$$P_j = A_j e^{i(\mathbf{k}_j \cdot \mathbf{r} - \omega t)} + B_j e^{i(\mathbf{k'}_j \cdot \mathbf{r} - \omega t)} \tag{2}$$

P_j represents the propagating pressure perturbation. The first and the second terms on the right-hand side of Eq. (2) represent propagation to the right and to the left, respectively, i.e. the forward and the backward waves. The index $j = 0$ represents the medium at the left side of the structure with impedance Z_0. In the medium S with $j = N+1$ we consider only propagation to the right, consequently $B_s = 0$. $\mathbf{k_j}$ y $\mathbf{k'_j}$ are the forward and backward wavevectors for medium j, t is the time, ω the angular frequency, and i the imaginary unit. A solid can support both longitudinal and transverse elastic waves, and a fluid only transmits elastic longitudinal waves. If a longitudinal wave in a fluid is incident obliquely on the interface with a solid, both type of waves can be transmitted in the solid. However, at normal incidence, the character of the longitudinal wave is preserved, without generation of transverse waves in the solid. Then, for oblique incidence, our theory is valid only for fluid layers. If the wave is incident at an angle θ_0 with the normal to the structure, the Law of Snell gives

$$\frac{1}{c_0}\sin\theta_0 = \frac{1}{c_1}\sin\theta_1 = \cdots = \frac{1}{c_j}\sin\theta_j = \cdots = \frac{1}{c_N}\sin\theta_N = \frac{1}{c_s}\sin\theta_s \tag{3}$$

The wave propagation from medium 0 to medium S through the multilayer structure is described by

$$\begin{bmatrix} A_0 \\ B_0 \end{bmatrix} = \begin{bmatrix} M_{11}\, M_{12} \\ M_{21}\, M_{22} \end{bmatrix} \cdot \begin{bmatrix} A_S \\ 0 \end{bmatrix} \tag{4}$$

Where the (2×2) transfer matrix is given by

$$\begin{bmatrix} M_{11}\, M_{12} \\ M_{21}\, M_{22} \end{bmatrix} = D_0^{-1} \left[\prod_{j=1}^{N} D_j\, P_j\, D_j^{-1} \right] D_S \tag{5}$$

The matrix D_j is called the dynamical or transmission matrix, and arises from the continuity conditions on the pressure and the displacement normal to the interface between media $j-1$ and j. The matrix P_j is the kinematical or propagation matrix inside the j layer. If it is supposed that the media are lossless, the matrices are given by

$$D_j = \begin{bmatrix} 1 & 1 \\ \frac{\cos\theta_j}{Z_j} & -\frac{\cos\theta_j}{Z_j} \end{bmatrix}, \qquad P_j = \begin{bmatrix} e^{ik_j d_j \cos\theta} & 0 \\ 0 & e^{-ik_j d_j \cos\theta} \end{bmatrix} \tag{6}$$

We define the transmittance T as the transmitted power by the waves through the structure, normal to the structure, divided by the power of the incident waves, normal to the structure. It is given in terms of the transfer matrix by

$$T = \left| \frac{< V_t > \cdot \hat{n}}{< V_i > \cdot \hat{n}} \right| \tag{7}$$

Where V_t is the vector of transmitted power, V_i the vector of incident power, and $\hat{n}$ the unit vector normal to the structure. The angle brackets denote average over time. V is similar to the Poynting vector in electromagnetism. Its temporal average is given by [11]

$$\langle V \rangle = \frac{1}{2} \frac{A^2}{Z} \hat{u} \tag{8}$$

Here, A is the amplitude of the pressure wave and $\hat{u}$ the unit vector in the direction of propagation of the wave.

The transmittance T, in terms of the transfer matrix, is given by

$$T = \frac{Z_0 \cos\theta_s}{Z_s \cos\theta_0} \left| \frac{1}{M_{11}} \right| \tag{9}$$

The reflectance R is given by

$$R = T - 1 \tag{10}$$

3 Results

We consider that the structure is situated in water, with $Z = 1.5$ MRayl and $c = 1480 m/s$. For the layers with odd numbering we make a linear variation of the impedance values. The impedance profile of the structure is shown schematically in Fig. 1.

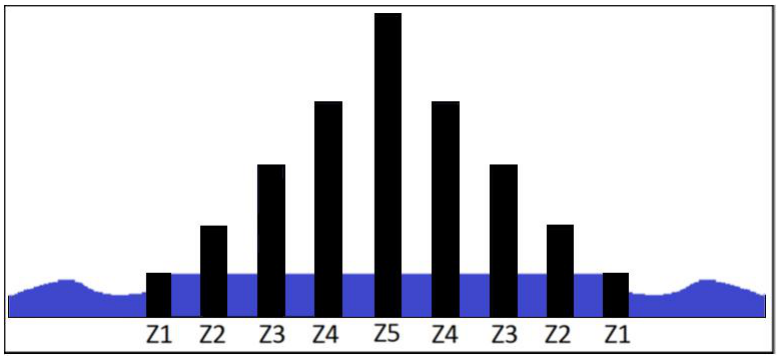

Fig. 1 Schematic impedance profile of the structure.

We consider that the maximum value of the impedance is Z_{max}=3.5 MRayl and the minimum value is Z_{min}=2.0 MRayl. The central layer has the maximum value and the layers at the ends have the minimum value. The other odd layers have corresponding linear values between the maximum and the minimum impedances. The layers with even numbering consist also of water.

For the calculations, it is necessary to know for each value of Z, the corresponding value of the sound velocity c in order to calculate the matrix P. For that purpose, for the interval of impedances from 0.7 to 1.6 MRayl, we make an average of the density and the velocity

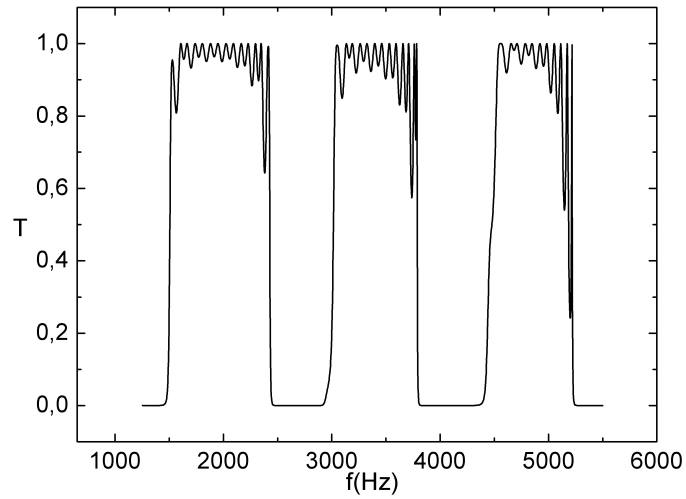

Fig. 2 Structure with 17 odd layers. $Zmax = 3.5$ MRayl for central layer, $Zmin = 2.0$ MRayl for end layers. Odd layers have 0.15 m thick, even layers with 0.45 m thick.

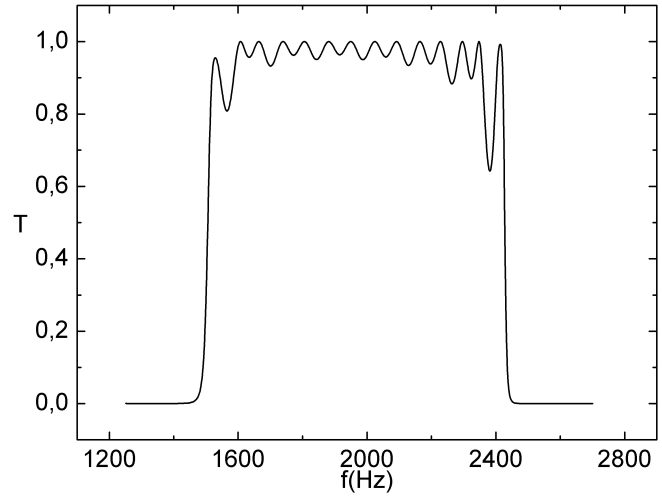

Fig. 3 Detail of the first passband of Fig. 2.

of sound for several liquids. For the interval of impedances from 1.6 to 2.5 MRayl we make the average of densities and sound velocities for plastics, and for the interval of impedances from 2.5 to 4.5 MRayl the average is made for solids. For each interval we construct a linear relationship between the density and the velocity of sound and find the proportionality constant. Finally we make an average of the three constants and we obtain the relationships

$$\begin{aligned} \rho &= 0.52c, \\ c &= \sqrt{\frac{Z}{0.52}} \end{aligned} \tag{11}$$

The values for the impedances, densities and sound velocities were obtained from Ref. [13].

The spectrum of allowed frequencies for the acoustical multilayer structure consists of quasi-bands of discrete values of eigenfrequencies or passbands, separated by gaps or stopbands, where there is no transmission of sound. In Fig. 2 we present the frequency dependence of the transmission T for normal incidence of the longitudinal waves for a structure of 33 layers, where 17 have linear variation of impedances. The layers thickness with variable impedance is 0.15 m and the layers of water in between have a thickness of 0.45 m. We observe several stopbands and passbands. The flatness of the passbands is conspicuous. Fig. 3 shows a detail of the first passband of Fig. 2, and we appreciate more easily the passband flatness. We present in Fig. 4 the transmission spectrum for a regular structure where all the 17 odd layers have the same value of impedance, $Z = 3.5$ MRayl.

The thicknesses of the layers are the same of those of Fig. 2. We see that in this case the regular structure has well defined stopbands but it does not have flat passbands. The transmission in the passbands for the structure with regular profile is poorer due to the more abrupt change of impedances. The oscillations in the passbands correspond to the eigenfrequencies of the structure and are more prominent in the regular structure than that of the other structure with linear variable impedance; we will appreciate this better in the next figure. We show in Fig. 5 for comparison the second passband of Fig. 4 and the passband of Fig. 3. We see that the difference between the two spectra is notable, a structure with regular profile can work as an acoustic

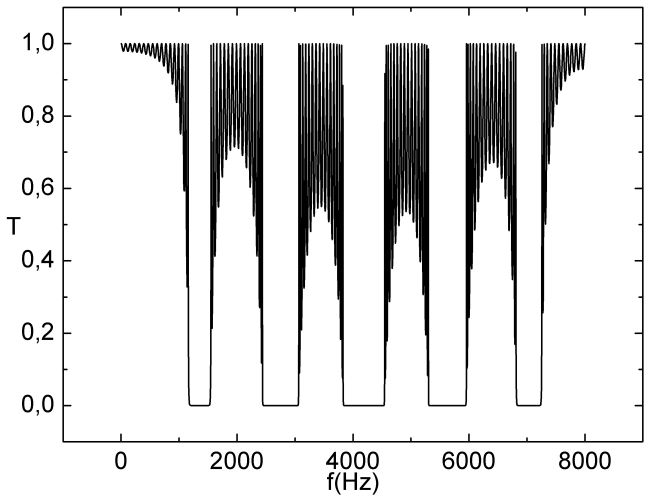

Fig. 4 Regular structure with 17 odd layers of $Z = 3.5$ MRayl. Odd layers have 0.15 m thick, even layers with 0.45 m thick.

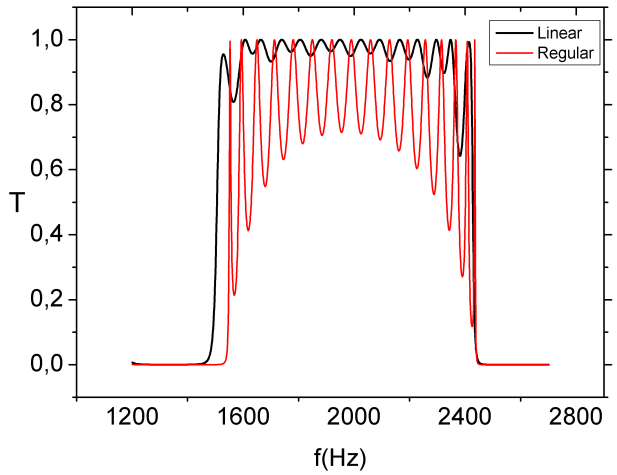

Fig. 5 Comparison of the first passband of the linear structure of Fig. 3 (in black) with the second passband of the regular structure of Fig. 4 (in red).

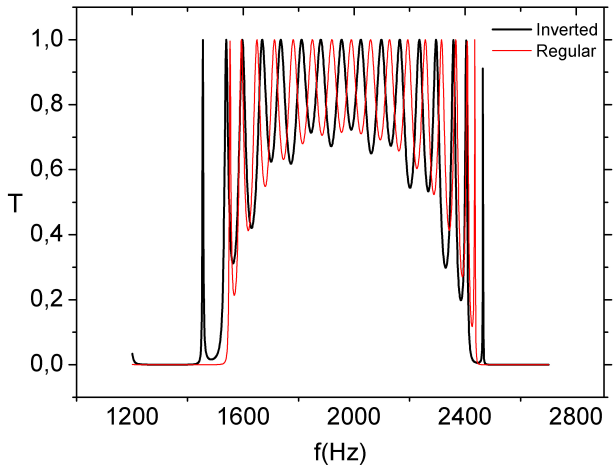

Fig. 6 In black: Transmittance for an inverted structure of 17 odd layers with $Zmin = 2.0$ MRayl for the central layer and $Zmax = 3.5$ MRayl for end layers. In red: transmittance for the regular structure of Figs. 4 and 5.

mirror, but it is bad as an acoustic filter. We also calculated the transmittance for an inverted linear structure with 17 odd layers, where the central layer has the minimum value of impedance and the layers at the ends have the maximum value. We present in Fig. 6 the transmittance for this structure and, for comparison, the transmittance for the regular structure of Fig. 5. We see that the oscillations for the inverted structure are even more pronounced than that for the regular structure. This fact is due to the more abrupt change of impedances in the inverted structure than for the regular one.

4 Conclusions

Using a method of transfer matrix, we have made studies in order to propose a layered structure where the characteristic impedance of the layers with odd numbers follows a linear profile of values and the inserted layers with even number have a constant value of acoustic impedance. Flat transmission bands and reflection bands are obtained by properly choosing the structure parameters. When a longitudinal

plane wave of sound is incident on the layered structure, has very high transmittance if the frequency lies in a passband and completely reflected if the frequency lies in a stopband. This kind of structure can have potential applications, such as acoustic mirrors and filters allowing selected intervals of frequencies to pass through.

ACKNOWLEDGEMENTS

This work has been supported partially by Universidad Autónoma de Zacatecas and Consejo Zacatecano de Ciencia y Tecnologá (COZCyT).

References

1. H. H. Tung and C. P. Lee, *An energy band-pass filter using superlattice structures*, IEEE J. Quantum Electron. 32, 507-512 (1996).
2. I. Gómez, F. Domínguez-Adame, E. Diez, and V. Bellani, *Electron transport across a Gaussian superlattice*, J. Appl. Phys. 85(7), 3916-3918 (1999).
3. J. Arriaga and X. Saldaña, *Band structure and reflectivity of omnidirectional Si-based mirrors with a Gaussian profile refractive index*, J. Appl. Phys. 100(4), 044911 (2006).
4. J. Madrigal-Melchor, R. A. Reyes Villagrana, X. Saldaa, S. Jelev-Vlaev and D. A. Contreras-Solorio, *Acoustic layered filter with a Gaussian distribution of impedances*, SLAFES Book of Abstracts Iguazú, Argentina (2008).
5. P. Yeh, *Optical waves in layered media*, Wiley, New York, 1988.
6. K. K. Shung and M. Zipparo, *Ultrasonic transducers and arrays*, IEEE Eng. Med. Biol. Mag.6, 20, 1996.
7. R. Zhang, W. Cao, Q. Zhou, JH Cha, KK Shung, and Y Huang, *Acoustic properties of alumina colloidal/polymer nano-composite film on silicon*, IEEE Trans. Ultrason., Ferroelect., Freq. Contr. 54, 467, 2002.
8. A. D. Y. Boumaiza, Z. Hadjoub and L. Deboub, *Porosity effects on different measured acoustic parameters of porous silicon*, J. Mat. Sci. Letts. 18, 295 1999.
9. M. D. A.Doghmane, I. Hadjoub and Z. Hadjoub, *Prediction of elastic parameters of photoluminescent porous Si*, ICTON-MW, 1, 2007.
10. A. Reinhardt and P. A. Snow, *Theoretical study of acoustic band-gap structures made of porous silicon*, Phys. Stat. Sol. (a) , 204, 1528, 2007.
11. W. C. Elmore and M. A. Heald, *Physics of waves*, Dover, New York, 1985.
12. L. M. Brekhovskikh, *Waves in layered media*, Academic Press, New York, 1960.
13. http://www.ondacorp.com consulted September 30, 2011.

Matrices de Transferencia, Rigidez, Distensión y otras, y el problema $\omega - d$ en la Física de sistemas multicapas

R. Pérez-Álvarez, Miguel E. Mora-Ramos, and Luis M. Gaggero-Sager

Abstract

La idea de este trabajo es en primer lugar listar y comentar las definiciones y propiedades más elementales de las distintas matrices de transferencia, así como de las matrices de rigidez (*stiffness*) y de distensión o compliancia (*compliance*). Esto nos llevará a la solución de los problemas de contorno estándares que aparecen en el estudio de modos elásticos, electrónicos, electromagnéticos, y aún otros, en los sistemas multicapas. Un aspecto aparentemente secundario, pero de gran importancia práctica y teórica es el llamado *Problema* ω-d; comentaremos las diversas soluciones propuestas así como sus limitaciones para, finalmente, proponer algunos caminos a explorar.

Transfer, Stiffness, Compliance, and other related matrices, and the ω-d problem in the Physics of multilayered systems

The aim of this work is, in first place, to list and comment the definitions and basic properties of the different transfer matrices and also of the stiffness and compliance matrices. This leads to the solution of the standard boundary problems appearing in the study of elastic, electronic, electromagnetic, and even other kinds of modes in multilayered systems. A problem that might look as a second order one;

R. Pérez-Álvarez
Universidad Autónoma del Estado de Morelos. Facultad de Ciencias, Ave. Universidad 1001, Cuernavaca, Morelos, Mexico.
e-mail: rpa@uaem.mx

M. E. Mora-Ramos
Universidad Autónoma del Estado de Morelos. Facultad de Ciencias.
e-mail: memora@uaem.mx

L. M. Gaggero-Sager
Universidad Autónoma del Estado de Morelos. Facultad de Ciencias.
e-mail: lgaggero@uaem.mx

but that reveals to be of capital importance is the so-called ω-*d problem*. We shall comment the diverse solutions proposed as well as their limitations in order to, finally, present some of the plausible different ways to explore.
Physics and Astronomy Classification Scheme: 73.21.-b, 73.22.-f, 73.63.-b

Keywords: electron states, elastic modes, electromagnetic modes, onedimensional problems, transfer matrix, stiffness matrix, compliance matrix, bound and virtual bound states, multilayer systems.

1 Introducción

Desde hace alrededor de 40 años tienen un auge espectacular los sistemas nanoscópicos debido a sus posibles usos en la nanoelectrónica y otras ciencias aplicadas [1-7]. Entre estos hay sistemas cuasicerodimensionales[1], cuasiunidimensionales[2] y cuasibidimensionales. A estos últimos prestaremos nuestra máxima atención. Como ejemplos de estos sistemas tenemos los pozos cuánticos, simples o múltiples, a capas o gradados, tensionados o no, construidos por dopamiento deltaico o no deltaico, etc., superredes también de muy diversos tipos, sistemas cuasirregulares[3][8,9], etc.

Para reconstruir la estructura electrónica a partir de las características de los materiales masivos suelen usarse diversas variantes de la Aproximación de la Función Envolvente (EFA: Envelope Function Approximation) [3]. Cuando se trata de una sola banda estos formalismos suelen llamarse de Masa Efectiva (EMA: Effective Mass Aproximation), probablemente porque el parámetro más relevante es una masa efectiva. En rigor esta magnitud depende de la posición por lo que en su día se trabajó mucho en lograr una formulación que tuviese en cuenta este factor. En su versión más aceptada [10,11] esta teoría tiene como ecuación maestra la ecuación de Schrödinger con masa variable, a saber:

[1] Quantum Dots, por ejemplo

[2] Quantum Wires, por ejemplo

[3] Fibonacci, Thue-Morse, Rudin-Shapiro, etc.

$$\left[\hat{\mathbf{p}}\cdot\left(\frac{1}{m(\mathbf{r})}\hat{\mathbf{p}}\right)+V(\mathbf{r})\right]\Psi(\mathbf{r})=E\Psi(\mathbf{r})\,. \tag{1}$$

Para sistemas en que la masa y el potencial varían con una sola coordenada cartesiana, pongamos que z, tendremos que

$$-\frac{\hbar^2}{2}\frac{d}{dz}\left[\frac{1}{m(z)}\frac{dF(z)}{dz}\right]+\left(V(z)+\frac{\hbar^2\kappa^2}{2m(z)}-E\right)F(z)=0 \tag{2}$$

$$\Psi(\mathbf{r})=F(z)\,\frac{\exp(i\boldsymbol{\kappa}\cdot\boldsymbol{\rho})}{\sqrt{A}} \tag{3}$$

$$\boldsymbol{\kappa}=(\kappa_x,\kappa_y) \tag{4}$$

$$\boldsymbol{\rho}=(x,y)\,, \tag{5}$$

y A es el área en el plano xy a los efectos de normalización.

Ya en este caso se avizora el tipo de característica y dificultad con que chocaremos en este tipo de problemas. Por lo pronto se nota que el operador que caracteriza la ecuación maestra es de tipo Sturm-Liouville. Otros muchos tipos de modos de diversas excitaciones elementales de muy diversos campos de la Física siguen ecuaciones (o sistemas de ecuaciones) diferenciales con esta propiedad. En [7] se puede ver un compendio, susceptible de ser ampliado, de un conjunto grande de excitaciones cuya ecuación de movimiento en sistemas a capas adopta la forma

$$\frac{d}{dz}\left[\mathbf{B}(z)\cdot\frac{d\mathbb{F}(z)}{dz}+\mathbf{P}(z)\cdot\mathbb{F}(z)\right]+\mathbf{Y}(z)\cdot\frac{d\mathbb{F}(z)}{dz}+\mathbf{W}(z)\cdot\mathbb{F}(z)=0 \tag{6}$$

Por "sistemas a capas", como la expresión lo indica, entenderemos sistemas formados por la yuxtaposición de capas de modo que las intercaras resulten paralelas; a menos que se indique lo contrario, se supondrá que estas intercaras son perfectas.

En todos los casos que estudiaremos aquí la ecuación de movimiento es un sistema de ecuaciones diferenciales -que en los modelos más sencillos se reduce a una- y sucede que es invariante frente a las traslaciones arbitrarias en los planos de las capas. Por esta razón los estados se pueden etiquetar por cierto vector de onda de dos componentes $\boldsymbol{\kappa}$ y suponer que la dependencia de las coordenadas en este plano es de onda plana ($\propto \exp(i\boldsymbol{\kappa}\cdot\boldsymbol{\rho})$, donde $\boldsymbol{\rho}$ es el vector de posición

en este plano). De este modo el problema 3D pasa a ser formalmente 1D en la coordenada perpendicular a los planos, que llamaremos z.

Por supuesto que si pensamos en el sistema físico, éste usualmente tiene estructura en los planos paralelos a las intercaras por lo que tomar la dependencia $\propto \exp(i\boldsymbol{\kappa}\cdot\boldsymbol{\rho})$ siempre es una aproximación que promedia en el plano $\boldsymbol{\rho}$. Los modelos matemáticos de los cuales nosotros partimos ya han hecho esta suposición de alguna manera más o menos explícita.

Resulta que el problema 1D así obtenido, para una clase muy amplia de sistemas y problemas, es un sistema de ecuaciones diferenciales de segundo orden ordinarias acopladas. De esta manera todos estos problemas específicos se enmarcan en un mismo problema general del cual pasan a ser casos particulares. $\mathbb{F}(z)$ es el *campo* bajo estudio: función de onda -o envolvente- si de estados electrónicos se trata, amplitud de oscilación si estudiamos Elasticidad, o una componente del campo eléctrico en ciertos problemas de la Electrodinámica. $\mathbf{B}(z)$, $\mathbf{P}(z)$, $\mathbf{Y}(z)$, y $\mathbf{W}(z)$ son matrices cuadradas de orden N. Como $\mathbb{F}(z)$ tiene N componentes nos referiremos a esta magnitud como un *vector*; queda entendido que no es un vector en el sentido que lo es el vector de posición $\mathbf{r}$, la velocidad $\mathbf{v}$ o la fuerza $\mathbf{f}$, caracterizados por la manera en que cambian ante una transformación ortogonal de las coordenadas. La denominación de vector aquí se usa en el sentido de que tiene varias componentes (más exactamente N) y en todo caso porque la función $\mathbb{F}(z)$ es un vector en el espacio vectorial funcional asociado al sistema de ecuaciones (6). El punto $\cdot$ indica el producto usual de matrices o producto contraído.

En la Fig. (1) se da una idea del sistema bajo estudio. Cuando tengamos este sistema tal cual diremos que tenemos una *heteroestructura* y en principio, para el análisis general que hacemos aquí, a menos que se diga lo contrario, los anchos pueden ser cualesquiera. En su momento estudiaremos casos particulares de interés, como son, por ejemplo, los pozos cuánticos ($\mu = 1$), las heterouniones ($\mu = 0$. El dominio L está yuxtapuesto al dominio R), las superredes truncadas (también llamadas medios localmente periódicos), las heteroestructuras cuasirregulares (QH: Quasiregular Heterostructures), etc.

Aunque aquí hemos llamado a estas estructuras "casos particulares", aún ellas son sistemas bastante genéricos. Se puede intentar una lista más amplia que, aunque nunca será exhaustiva, contendrá como veremos muchas más situaciones diversas que se pueden enmarcar en

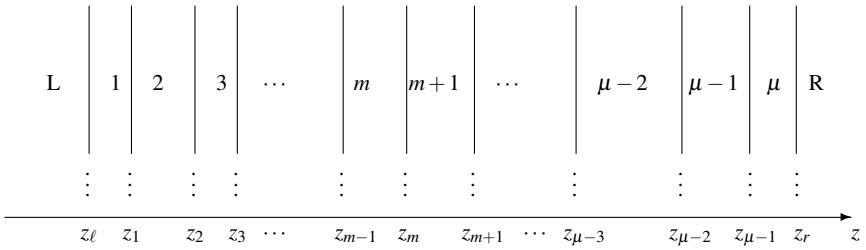

Fig. 1 Esquema general del sistema bajo estudio. Tenemos μ capas emparedadas por sendas capas semiinfinitas L a la izquierda y R a la derecha. Según el convenio escogido la capa m se encuentra limitada por las intercaras $(m-1)$ y m cuyas coordenadas son respectivamente z_{m-1} y z_m. El índice m va de 1 a μ y $z_0 \equiv z_\ell$, $z_\mu \equiv z_r$. A menos que se diga otra cosa, la capa L va de $-\infty$ a z_ℓ mientras que R va de z_r a $+\infty$.

alguno de los casos enunciados en el párrafo anterior. Nos referimos, por ejemplo a las siguientes: Capas de inversión [2,4,12-16]; Pozos cuánticos simples o múltiples indexpozo!cuántico múltiple [2,4,14-16]; Heteroestructuras de confinamiento separado [2,4,14-16]; Barreras simples o múltiples [2,4,14-16]; Pozos δ dopados simples o múltiples (ver [17-19] y las referencias que allí se dan); Superredes [2,4,14-16]; Multisuperredes [2,4,14-16]; Heteroestructuras digitales (ver [20,21] y las referencias que allí se dan); Superredes de masa (ver [22] y las referencias que allí se dan); y un largo etcétera. Esta lista no agota el conjunto de sistemas a capas. De hecho, se pueden construir combinaciones de los que enunciamos aquí. La adición de impurezas, por ejemplo, abre el abanico de posibilidades, dando lugar a las llamadas *estructuras moduladas*. Lo de *politipo* no va sólo con las superredes; podemos estudiar una QH politipo, donde los ladrillos básicos a partir de los cuales se construye la estructura es a su vez una pareja, trío, o conjunto cualquiera de capas.

En todos los casos hay que considerar la cuestión relativa a las *condiciones de contorno* (*boundary conditions*, en inglés), o sea las condiciones que satisfacen estos campos para $z \to +\infty$ y $z \to -\infty$, o si ponemos barreras infinitas en z_ℓ y/o z_r, los valores que los campos y/o sus derivadas tienen en estos extremos. Otra cuestión parecida, pero de un estilo distinto, son las condiciones que satisfacen estos campos en las intercaras (*matching boundary conditions*, en inglés). Ambos asuntos tienen mucha importancia y serán discutidos en detalle más adelante.

Las distintas capas también se llamarán lajas o dominios, y usualmente son porciones homogéneas de materiales (GaAs, AlAs, C, Co, etc). Esto último significa que las matrices en (6) sean seccionalmente constantes. No obstante, es bueno aclarar que la mayor parte de lo que sigue no presupone esta hipótesis.

La situación que analizaremos, por lo demás muy común, es aquella en la que conocemos parámetros de los medios por separado, considerados infinitos, y a partir de estos datos queremos hallar magnitudes asociadas a la heteroestructura como un todo. Para el análisis es muy valioso el concepto de *pseudomedio extendido* [23], entendido como cualquier medio que coincida con el dado en la región espacial que éste ocupa en la heteroestructura. Se prueba rigurosamente que todas estas extensiones dan el mismo resultado al empalmar. Cuando los parámetros son constantes dentro de cada laja la extensión natural y más cómoda es suponer un medio con estos parámetros en todo punto. Si los parámetros no son constantes podemos imaginar cualquier extensión con tal de que coincida con el medio en su región.

Aún en problemas en que el campo $\mathbb{F}$ es continuo, muchos autores escriben la ecuación (6) en cada laja por separado, con lo cual desaparecen o se simplifican sustancialmente los términos en la primera derivada. La segunda condición de empalme (continuidad de la forma lineal asociada $\mathbb{A} = \mathbf{B}(z) \cdot \mathbb{F}'(z) + \mathbf{P}(z) \cdot \mathbb{F}(z)$) tiene que ser introducida entonces *con la mano*, es decir argumentándola con criterios ajenos a (6). Estos dos enfoques, que en algún sentido son opuestos, llevan a confusiones y es importante en cada caso saber el ámbito de cumplimiento de la ecuación con que trabajamos: si estamos trabajando con una ecuación de ámbito *global*, o sea que rige el comportamiento del sistema para todo z en la región de interés, o si trabajamos con una ecuación de ámbito *local*, o sea válida para una laja concreta.

Para hallar los modos de las excitaciones elementales descritas por una ecuacin como la (6), en un sistema como el de la Fig. 1, se han ideado muchas alternativas que con más o menos éxito abordan este problema en el sinnúmero de situaciones particulares de interés. De este modo surgieron las distintas matrices de transferencia, tanto en el problema electrónico como en el de modos elásticos, las matrices de rigidez (*stiffness*) y de admitancia (*compliance*), mayormente en el mundo de la Elasticidad, etc. Uno de los propósitos del presente trabajo es poner en orden y comparar todas estas definiciones en el marco general de la ecuacin (6). Por otro lado, por muchos de estos

procedimientos, aparece el llamado problema $\omega - d$, el cual es un escollo importantísimo a la hora de los cálculos numéricos. Al final de este trabajo discutiremos las opciones propuestas para evitar, o al menos paliar esta dificultad.

La primera parte de lo que aquí se expone puede encontrarse en el libro [7], aunque hemos querido comentar las partes que en el libro no se explicitan. Ya la parte de matrices de stiffness y compliance son desarrollos obtenidos después que el libro saliera.

2 Matrices de Transferencia Completa M y Asociada T

A continuación un apretado resumen de las definiciones y propiedades básicas de las matrices de transferencia completa (FTM) y de transferencia asociada (ATM). Muchos más detalles se pueden ver en [7]. Las partes matemáticas se pueden ver en varios libros clásicos [24-30].

La ecuación maestra (6) es un sistema de N ecuaciones diferenciales ordinarias lineales de segundo orden. Por tanto su espacio de soluciones es expandible por $2N$ vectores linealmente independientes (LI) $\mathbb{F}_j(z)$; a estos corresponden sendas derivadas $\mathbb{F}'_j(z)$ y formas lineales $\mathbb{A}_j(z) = \mathbf{B}(z) \cdot \mathbb{F}'_j(z) + \mathbf{P}(z) \cdot \mathbb{F}_j(z)$. Como se verá más adelante, resulta ventajoso definir un bicampo $\Phi(z)$ de $2N$ componentes, de las cuales las N primeras coinciden con las de $\mathbb{F}(z)$, mientras que el resto coincide con las componentes de $\mathbb{F}'(z)$. Análogamente se define el bicampo $\Psi(z)$ de orden $2N$ con las componentes de $\mathbb{F}(z)$ y $\mathbb{A}(z)$. De la misma manera se construyen los conjuntos de vectores $\{\Phi_j(z); j = 1,2,\cdots,2N\}$ y $\{\Psi_j(z); j = 1,2,\cdots,2N\}$. Con las $\Phi_j(z)$ se forma la matriz $2N \times 2N$ $\mathbb{N}(z)$ y con las $\Psi_j(z)$ la matriz $\mathbb{Q}(z)$.

Tanto los valores del campo como de sus derivadas -léase forma lineal- en cualquier punto se puede expresar como una combinación lineal de las $2N$ soluciones linealmente independientes. Finalmente este hecho se puede expresar matemáticamente mediante la ecuación básica de transferencia entre dos puntos: o bien

$$\Phi(z_2) = \mathbf{M}(z_2, z_1) \cdot \Phi(z_1) \,, \tag{7}$$

o bien

$$\Psi(z_2) = \mathbf{T}(z_2, z_1) \cdot \Psi(z_1) \ , \tag{8}$$

donde $\mathbf{M}(z_2, z_1)$ es la Matriz de Transferencia Completa (FTM: *Full Transfer Matrix*), mientras que $\mathbf{T}(z_2, z_1)$ es la llamada Matriz de Transferencia Asociada (ATM: *Associated Transfer Matrix*). En [7] se pueden ver las propiedades más importantes de estos entes y las relaciones entre ellos. En estilo telegráfico:

$$\Phi(z_2) = \begin{vmatrix} \mathbb{F}(z_2) \\ \mathbb{F}'(z_2) \end{vmatrix} = \mathbf{M}(z_2, z_1) \cdot \begin{vmatrix} \mathbb{F}(z_1) \\ \mathbb{F}'(z_1) \end{vmatrix} = \mathbf{M}(z_2, z_1) \cdot \Phi(z_1) \tag{9}$$

$$\mathbf{M}(z_2, z_1) = \mathbb{N}(z_2) \cdot [\mathbb{N}(z_1)]^{-1} \tag{10}$$

$$\mathbf{M}(z, z) = \mathbb{I} \tag{11}$$

$$\mathbf{M}(z_2, z_0) = \mathbf{M}(z_2, z_1) \cdot \mathbb{C}(z_1) \cdot \mathbf{M}(z_1, z_0) \tag{12}$$

$$\text{Det } [\mathbf{M}(z_2, z_1)] = \frac{\text{Det } [\mathbb{B}(z_1)]}{\text{Det } [\mathbb{B}(z_2)]} \text{ Det } [\mathbb{T}(z_2, z_1)] \ . \tag{13}$$

$$\Psi(z_2) = \begin{vmatrix} \mathbb{F}(z_2) \\ \mathbb{A}(z_2) \end{vmatrix} = \mathbf{T}(z_2, z_1) \cdot \begin{vmatrix} \mathbb{F}(z_1) \\ \mathbb{A}(z_1) \end{vmatrix} = \mathbf{T}(z_2, z_1) \cdot \Psi(z_1) \tag{14}$$

$$\mathbf{T}(z_2, z_1) = \mathbb{Q}(z_2) \cdot [\mathbb{Q}(z_1)]^{-1} \tag{15}$$

$$\mathbf{T}(z, z) = \mathbb{I} \tag{16}$$

$$\mathbf{T}(z_2, z_0) = \mathbf{T}(z_2, z_1) \cdot \mathbf{T}(z_1, z_0) \tag{17}$$

$$\text{Det } [\mathbf{T}(z_2, z_1)] = \mathrm{e}^{\int_{z_1}^{z_2} dz \text{Tr} \left[[\mathbb{B}(z)]^{-1} \cdot \left(\mathbb{P}(z) - \mathbb{P}^{\dagger}(z) \right) \right]} \tag{18}$$

$$\mathbf{J} = \mathbf{T}(z_2, z_1)^{\dagger} \cdot \mathbf{J} \cdot \mathbf{T}(z_2, z_1) \ . \tag{19}$$

$$\mathbf{T}(z_2, z_1) = \mathbb{R}(z_2) \cdot \mathbf{M}(z_2, z_1) \cdot [\mathbb{R}(z_1)]^{-1} \ . \tag{20}$$

En estas expresiones y en las que siguen $\mathbb{I}$ es la matriz identidad del orden adecuado ($2N$ en las fórmulas anteriores). Como quiera que la derivada de $\mathbb{F}$ puede ser discontinua, en la propiedad (12) es necesario introducir la llamada matriz de acople (*coupling matrix*) $\mathbb{C}(z_1) = \mathbb{M}(z_1+, z_1-)$. En la propiedad análoga para $\mathbb{T}$ no es necesario tal artificio pues la ATM transfiere magnitudes que son continuas en todo punto. Por su parte

$$\mathbb{R}(z) = \begin{Vmatrix} \mathbb{I} & \mathbb{O} \\ \mathbb{P}(z) & \mathbb{B}(z) \end{Vmatrix} \tag{21}$$

es la llamada matriz relacionadora (*relating matrix*). Se tiene, además que

$$\mathbb{C}(z) = [\mathbb{R}(z+)]^{-1} \cdot \mathbb{R}(z-) \; . \tag{22}$$

La propiedad (19) es la que caracteriza el carácter simpléctico de la ATM. La matriz auxiliar $\mathbf{J}$ viene dada por

$$\mathbf{J} = \begin{Vmatrix} 0 & -\mathbf{I} \\ \mathbf{I} & 0 \end{Vmatrix}. \tag{23}$$

El carácter simpléctico de la ATM implica que esta matriz tiene determinante de módulo unidad. Esto no contradice la propiedad (18) pues también se puede demostrar que el integrando en dicha propiedad es imaginario puro. En muchos casos de interés esta propiedad se simplifica extraordinariamente y termina en que la ATM tiene determinante unidad.

Por otro lado, (8) es equivalente a

$$\mathbb{F}(z_2) = \mathbf{T}_{AA}(z_2, z_1) \cdot \mathbb{F}(z_1) + \mathbf{T}_{AD}(z_2, z_1) \cdot \mathbb{A}(z_1) \tag{24}$$

$$\mathbb{A}(z_2) = \mathbf{T}_{DA}(z_2, z_1) \cdot \mathbb{F}(z_1) + \mathbf{T}_{DD}(z_2, z_1) \cdot \mathbb{A}(z_1) \; . \tag{25}$$

Este es un sistema de dos ecuaciones, matriciales por supuesto, en cuatro *incógnitas*: $\mathbb{F}(z_1)$, $\mathbb{F}(z_2)$, $\mathbb{A}(z_1)$ y $\mathbb{A}(z_2)$. La matriz $2N \times 2N$ $\mathbf{T}$ se ha expresado a través de sus 4 bloques $N \times N$, a saber $\mathbf{T}_{AA}, \mathbf{T}_{AD}, \mathbf{T}_{DA}$ y $\mathbf{T}_{DD}$. Por supuesto que lo mismo se puede hacer con la FTM y tendríamos los bloques $\mathbf{M}_{AA}, \mathbf{M}_{AD}, \mathbf{M}_{DA}$ y $\mathbf{M}_{DD}$.

Ejemplo: Ecuación de masa efectiva en un intervalo donde la masa (m) y el potencial (V)son constantes.

$$\mathbf{M}(z,z_0) = \begin{Vmatrix} \cos(k(z-z_0)) & \frac{\sin(k(z-z_0))}{k} \\ -k\sin(k(z-z_0)) & \cos(k(z-z_0)) \end{Vmatrix} \tag{26}$$

$$\mathbf{T}(z,z_0) = \begin{Vmatrix} \cos(k(z-z_0)) & m\frac{\sin(k(z-z_0))}{k} \\ -\frac{k}{m}\sin(k(z-z_0)) & \cos(k(z-z_0)) \end{Vmatrix} \tag{27}$$

$$k = \sqrt{\frac{2m}{\hbar^2}(V-E)}\,. \tag{28}$$

3 Matrices de Transferencia de coeficientes

Otro enfoque de este asunto algo diferente es el que sigue.

Supongamos que la región L : $\{z < z_\ell\}$ (left) está separada de la región R : $\{z > z_r\}$ (right) por una región intermedia M descrita por $\mathbf{T}(z,z_0)$ (ver Figura 2). Pudiéramos pensar que M tiene estructura y que es, por ejemplo, la unión ($\bigcup$) de las lajas intermedias en la Fig. (1). Para la discusión que sigue da igual. El caso es que supondremos que toda la información de la región intermedia M está dada y contenida en la ATM $\mathbf{T}(z,z_0)$ que está definida y es conocida al menos $\forall\, z, z_0 \in$ M. Entonces

$$\Psi(z) = \begin{cases} \sum_{j=1}^{2N} a_j(\mathrm{L})\Psi_j(z) & z \le z_\ell \\ \sum_{j=1}^{2N} a_j(\mathrm{R})\Psi_j(z) & z \ge z_r \end{cases}\,. \tag{29}$$

Si ahora construimos sendos vectores con los coeficientes en cada lado, podremos escribir:

$$\Psi(z) = \begin{cases} \mathbb{Q}(\mathrm{L}:z)\cdot\mathbf{a}(\mathrm{L}) & z \le z_\ell \\ \mathbf{T}(z,z_\ell)\cdot\Psi(z_\ell) & z_\ell \le z \le z_r \\ \mathbb{Q}(\mathrm{R}:z)\cdot\mathbf{a}(\mathrm{R}) & z \ge z_r \end{cases}\,. \tag{30}$$

Estamos suponiendo que Ψ es continua en z_ℓ y z_r. Entonces

$$\mathbb{Q}(\mathrm{R}:z_r)\cdot\mathbf{a}(\mathrm{R})=\mathbf{T}(z_r,z_\ell)\cdot\mathbb{Q}(\mathrm{L}:z_\ell)\cdot\mathbf{a}(\mathrm{L})$$

$$\mathbf{a}(\mathrm{R})=\mathbf{K}(\mathrm{R},\mathrm{L})\cdot\mathbf{a}(\mathrm{L}) \tag{31}$$

$$\mathbf{K}(\mathrm{R},\mathrm{L})=[\mathbb{Q}(\mathrm{R}:z_r)]^{-1}\cdot\mathbf{T}(z_r,z_\ell)\cdot\mathbb{Q}(\mathrm{L}:z_\ell) \tag{32}$$

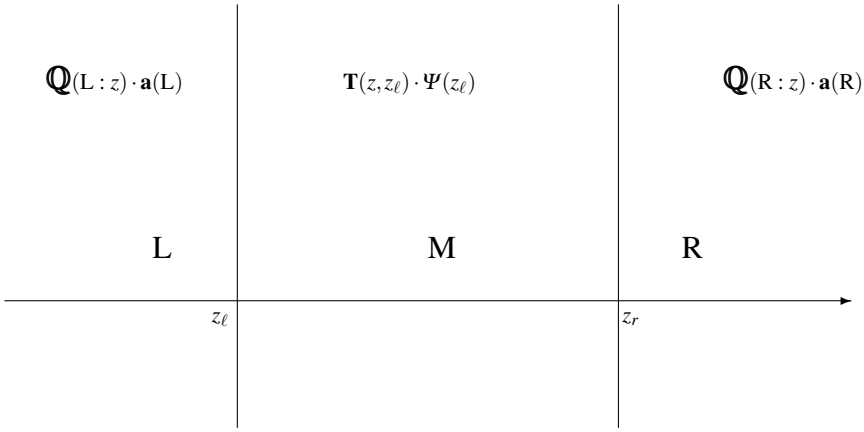

Fig. 2 Esquema de una región central emparedada por sendas regiones semiinfinitas L y R, donde las soluciones se describen por los coeficientes $\mathbf{a}(\mathrm{L})$ y $\mathbf{a}(\mathrm{R})$; en la región central M se supone conocida la matriz de transferencia asociada $\mathbf{T}(z,z_\ell)$.

$\mathbf{K}(\mathrm{R},\mathrm{L})$ es la Matriz de Transferencia de Coeficientes (CTM: Coefficient Transfer Matrix).

Notar que no ponemos etiqueta de dominio a la ATM $\mathbf{T}(z,z_0)$. Podríamos haber puesto $\mathbf{T}(\mathrm{M}:z,z_0)$ pero sería sobrecargar sin necesidad la notación pues $\mathbf{T}$ es una propiedad absolutamente global. Por la misma razón se puede decir que para el presente argumento no importa si M es simple o compuesto.

Propiedades elementales de $\mathbf{K}(\mathrm{R},\mathrm{L})$

1. $\mathbf{M}(z,z_0)$ y $\mathbf{T}(z,z_0)$ no dependen de la base $\{\mathbb{F}_j(z)\}$ escogida. $\mathbf{K}(\mathrm{R},\mathrm{L})$ sí depende de esta elección.
2. Si escogemos para el medio L/R la base canónica[4] en z_ℓ/z_r tendremos que $\mathbf{K}(\mathrm{R},\mathrm{L})=\mathbf{T}(z_r,z_\ell)$.

[4] Una base de soluciones es canónica en un punto cuando todas las componentes de cada vector son nulas excepto la j-ésima componente del vector j-ésimo, la cual es igual a la unidad.

3. Análogamente, el Det $[\mathbf{K}(\mathrm{R},\mathrm{L})]$ depende del sistema bajo estudio y de la base de funciones LI seleccionada.
4. Un caso interesante es aquel en que $z_r = z_\ell = \bar{z}$. Entonces $\mathbf{T}(z_r, z_\ell) = \mathbf{T}(\bar{z},\bar{z}) = \mathbf{I}_{2N}$, y $\mathbf{K}(\mathrm{R},\mathrm{L}) = [\mathbb{Q}(\mathrm{R}:\bar{z})]^{-1} \cdot \mathbb{Q}(\mathrm{L}:\bar{z})$. Esta $\mathbf{K}(\mathrm{R},\mathrm{L})$ es la que permite relacionar los coeficientes de dos regiones contiguas. Si escogiésemos las bases en ambos medios de manera que $\Psi(\mathrm{L}:z_\ell)$ y $\Psi(\mathrm{R}:z_r)$ tomasen los mismos valores, tendríamos que $\mathbf{K}(\mathrm{R},\mathrm{L}) = \mathbf{I}_{2N}$, lo cual es a todas luces un resultado trivial.
5. La matriz de transferencia de coeficientes cumple una propiedad de encadenamiento semejante a la que cumplen FTM y ATM. Sean las regiones $\mathrm{L}:\{z < z_\ell\}$ (*left*), $\mathrm{M}:\{z_\ell < z < z_r\}$ (*middle*), y $\mathrm{R}:\{z > z_r\}$ (*right*), con $z_\ell < z_r$. Y supongamos ahora que describimos M en términos de una única base de funciones LI, independientemente de que M sea simple o compuesto. Esto es algo que, formalmente, siempre se puede hacer y permite formalmente referirnos a un único set de coeficientes $a_j(\mathrm{M})$.

$$\mathbf{a}(\mathrm{R}) = \mathbf{K}(\mathrm{R},\mathrm{L}) \cdot \mathbf{a}(\mathrm{L}) \tag{33}$$

$$\mathbf{K}(\mathrm{R},\mathrm{L}) = \mathbf{K}(\mathrm{R},\mathrm{M}) \cdot \mathbf{K}(\mathrm{M},\mathrm{L}) \tag{34}$$

$$\mathbf{K}(\mathrm{R},\mathrm{M}) = [\mathbb{Q}(\mathrm{R}:z_r)]^{-1} \cdot \mathbb{Q}(\mathrm{M}:z_r) \tag{35}$$

$$\mathbf{K}(\mathrm{M},\mathrm{L}) = [\mathbb{Q}(\mathrm{M}:z_\ell)]^{-1} \cdot \mathbb{Q}(\mathrm{L}:z_\ell) \tag{36}$$

   Aquí estamos estudiando el mismo problema esquematizado en la Figura (2) pero ahora suponemos que lo que conocemos son las matrices de coeficientes $\mathbf{K}(\mathrm{R},\mathrm{M})$ y $\mathbf{K}(\mathrm{M},\mathrm{L})$.
6. La CTM relaciona *dominios*, mientras que la FTM y la ATM relacionan *puntos*.

En [7] se pueden ver matrices de transferencia de coeficientes específicas: RCTM (Reduced Coefficient Transfer Matrix), PM (Propagation Matrix), SVTM (State Vector Transfer Matrix).

Ejemplo: Ecuación de masa efectiva en un intervalo donde la masa y el potencial son constantes.

Pongamos que R y L son dos dominios contiguos y que z_s es la coordenada de la intercara. Continuando con nuestras costumbres relativas a la notación, agreguemos el argumento R/L a las magnitudes que caracterizan a dicho dominio. En lo que sigue, y hasta que no di-

gamos otra cosa, trabajaremos con bases de funciones exponenciales. Entonces

$$\mathbf{K}(\mathrm{R},\mathrm{L}) = [\mathbf{Q}(\mathrm{R}:z_s)]^{-1}\cdot\mathbf{Q}(\mathrm{L}:z_s) \tag{37}$$

$$\vdots$$

$$\mathbf{K}(\mathrm{R},\mathrm{L}) = \frac{1}{2}\begin{Vmatrix} \left(1+\frac{m(\mathrm{R})\,k(\mathrm{L})}{m(\mathrm{L})\,k(\mathrm{R})}\right)\mathrm{e}^{-\theta(\mathrm{R})+\theta(\mathrm{L})} & \left(1-\frac{m(\mathrm{R})\,k(\mathrm{L})}{m(\mathrm{L})\,k(\mathrm{R})}\right)\mathrm{e}^{-\theta(\mathrm{R})-\theta(\mathrm{L})} \\ \left(1-\frac{m(\mathrm{R})\,k(\mathrm{L})}{m(\mathrm{L})\,k(\mathrm{R})}\right)\mathrm{e}^{+\theta(\mathrm{R})+\theta(\mathrm{L})} & \left(1+\frac{m(\mathrm{R})\,k(\mathrm{L})}{m(\mathrm{L})\,k(\mathrm{R})}\right)\mathrm{e}^{+\theta(\mathrm{R})-\theta(\mathrm{L})} \end{Vmatrix} \tag{38}$$

$$\theta(\mathrm{R}) = ik(\mathrm{R})(z_s - z_0(\mathrm{R})) \tag{39}$$

$$\theta(\mathrm{L}) = ik(\mathrm{L})(z_s - z_0(\mathrm{L}))\,. \tag{40}$$

Hemos llamado $z_0(\mathrm{R})/z_0(\mathrm{L})$ a la coordenada del punto donde se anulan los argumentos de las soluciones LI en el dominio R/L. Lo usual es tomar al menos uno de los dos igual a la coordenada de la intercara.

Escribamos la fórmula (38) tomando $z_0(\mathrm{L}) = z_0(\mathrm{R}) = z_s$. Pudiera parecer un poco excéntrico, y lo es, pero hagámoslo:

$$\mathbf{K}_{z_s=z_0(\mathrm{L})=z_0(\mathrm{R})}(\mathrm{R},\mathrm{L}) = \frac{1}{2}\begin{Vmatrix} 1+\frac{m(\mathrm{R})\,k(\mathrm{L})}{m(\mathrm{L})\,k(\mathrm{R})} & 1-\frac{m(\mathrm{R})\,k(\mathrm{L})}{m(\mathrm{L})\,k(\mathrm{R})} \\ 1-\frac{m(\mathrm{R})\,k(\mathrm{L})}{m(\mathrm{L})\,k(\mathrm{R})} & 1+\frac{m(\mathrm{R})\,k(\mathrm{L})}{m(\mathrm{L})\,k(\mathrm{R})} \end{Vmatrix} = \mathbf{K}_{(r)}(\mathrm{R},\mathrm{L}) \tag{41}$$

$\mathbf{K}_{(r)}(\mathrm{R},\mathrm{L})$ es la RCTM.

4 Matrices de scattering

4.1 Definición

En la definición de las matrices **K**'s se usa el criterio de poner los coeficientes a un lado de la intercara en función de los coeficientes al otro lado (ver esquema (3)). Para lo que sigue da igual pensar en la intercara como en una Heteroestructura con capas intermedias. Dividamos los coeficientes en dos grupos: los de las ondas (soluciones

LI) que viajan de izquierda a derecha, y los de ondas que viajan de derecha a izquierda. A los primeros les añadimos el supraíndice "+"; a los segundos el supraíndice "-". Así las cosas, se tiene que

$$\begin{vmatrix} \mathbf{a}^+(\mathrm{R}) \\ \mathbf{a}^-(\mathrm{R}) \end{vmatrix} = \mathbf{K}(\mathrm{R},\mathrm{L}) \cdot \begin{vmatrix} \mathbf{a}^+(\mathrm{L}) \\ \mathbf{a}^-(\mathrm{L}) \end{vmatrix}. \tag{42}$$

Esto crea una división en bloques de $\mathbf{K}$ de dimensión mitad.

$$\mathbf{K} = \begin{Vmatrix} \mathbf{K}_{11} & \mathbf{K}_{12} \\ \mathbf{K}_{21} & \mathbf{K}_{22} \end{Vmatrix}. \tag{43}$$

Existe otro criterio distinto; vea, por ejemplo [31,32,46,47,48,49,50], y las referencias que allí se dan. Este nuevo criterio conduce a las llamadas *matrices de scattering* (SM). Consiste en poner las salidas (*output*), $\mathbf{a}^-(\mathrm{L})$ y $\mathbf{a}^+(\mathrm{R})$, en términos de las entradas (*input*) $\mathbf{a}^+(\mathrm{L})$ y $\mathbf{a}^-(\mathrm{R})$, o sea

$$\begin{vmatrix} \mathbf{a}^-(\mathrm{L}) \\ \mathbf{a}^+(\mathrm{R}) \end{vmatrix} = \mathbf{S}(\mathrm{R};\mathrm{L}) \cdot \begin{vmatrix} \mathbf{a}^+(\mathrm{L}) \\ \mathbf{a}^-(\mathrm{R}) \end{vmatrix} \tag{44}$$

$$\mathbf{S} = \begin{Vmatrix} \mathbf{S}_{11} & \mathbf{S}_{12} \\ \mathbf{S}_{21} & \mathbf{S}_{22} \end{Vmatrix}. \tag{45}$$

Nótese que $\mathbf{K}(\mathrm{R},\mathrm{L})$ indica transferencia de los coeficientes de un dominio a otro, mientras que $\mathbf{S}(\mathrm{R};\mathrm{L})$ indica relación entre dichos coeficientes pero no de transferencia, sino de tipo *scattering* según se define en (44).

La literatura puede crear algunas confusiones pues se usa con bastante frecuencia el nombre de "matriz de *scattering*" para lo que estamos denominando CTM, RCTM, y para estas $\mathbf{S}$'s. Hay razones para pensar que la $\mathbf{S}$ tiene *más* derecho a llevar este nombre.

Existe otro género de confusiones relacionado con la misma definición. Además del orden en que están los coeficientes $\mathbf{a}^-(\mathrm{L})$, $\mathbf{a}^+(\mathrm{R})$, $\mathbf{a}^+(\mathrm{L})$, y $\mathbf{a}^-(\mathrm{R})$ en (44), son igualmente válidas otras elecciones [**?**] en las que $\mathbf{S}$ se define mediante una ecuación como (44) en la que se ha permutado el orden de las amplitudes entrantes o las salientes, o ambas. En estas cuatro maneras posibles de escoger la matriz de scattering está contenida la misma física, pero las fórmulas pueden adoptar dife-

Fig. 3 Esquema de scattering. Entre L y R puede haber una simple intercara -L y R empalmados directamente- o cualquier estructura intermedia.

rentes formas específicas; de una se pasa a la otra *bailando* los cuatro bloques de **S**. En lo que sigue nos ajustaremos a la definición (44).

Abundemos en algo que ya tocamos algunas páginas atrás. Para definir las SM se alude a la dirección en que se propagan las ondas-soluciones. Al decir esto todos pensamos inmediatamente en el problema unidimensional de Schrödinger y en las soluciones $\exp(ikz)$ y $\exp(-ikz)$. Pero esta imagen de ondas propagándose y dispersándose falla para energías que sean clásicamente prohibidas pues en este caso las soluciones no son propagantes, sino exponenciales reales ($\exp(-|k|z)$ y $\exp(|k|z)$). Habrá que poner de todas formas las soluciones LI en dos grupos, en dependencia de si sean propagantes hacia un lado o hacia el otro cuando se varía de manera continua la energía y se hace adecuadamente la prolongación analítica del vector de onda k. La regla clave es sustituir k por $i|k|$ pero siempre será saludable prestarle la debida atención a este punto y no hacerlo mecánicamente.

Antes de seguir adelante anotemos algo relevante. La introducción de las SMs usualmente se justifica o fundamenta sobre la base del análisis de las ondas propagantes hacia un lado y otro. Pero nada impide hacer una división de cualquier base en dos mitades cada una de N soluciones LI, sean propagantes o no. La CTM **K** se dividiría en bloques de tamaño N y se podrían introducir las SMs. Estas SMs no tendrían, por supuesto, la interpretación en términos de entrada y salida (*input* y *output*), pero satisfarían las relaciones (53)-(56), (57)-(60), y aún otras; en principio todas aquellas en que no se use explícitamente el carácter propagante de la base en cuestión.

Ejemplo: Ecuación de masa efectiva en un intervalo donde la masa y el potencial son constantes.

Calculemos la SM que conecta dos intervalos -L y R- separados por una intercara en el punto z_s para el caso de EMT (EFA a una banda). En general tenemos que

$$\mathbf{S} = \begin{Vmatrix} -\frac{1-C}{1+C}\,\mathrm{e}^{2\theta(L)} & \frac{2}{1+C}\,\mathrm{e}^{-\theta(R)+\theta(L)} \\ \frac{2C}{1+C}\,\mathrm{e}^{-\theta(R)+\theta(L)} & \frac{1-C}{1+C}\,\mathrm{e}^{-2\theta(R)} \end{Vmatrix} \tag{46}$$

$$= \frac{1}{1+C}\,\frac{1}{\mathrm{e}^{\theta(R)-\theta(L)}} \begin{Vmatrix} -(1-C)\,\mathrm{e}^{\theta(R)+\theta(L)} & 2 \\ 2C & (1-C)\,\mathrm{e}^{-\theta(R)-\theta(L)} \end{Vmatrix} \tag{47}$$

Hemos usado la notación

$$C = \frac{m(R)}{m(L)}\,\frac{k(L)}{k(R)}\,. \tag{48}$$

Análogamente, son evidentes las siguientes fórmulas para los coeficientes de reflexión y trasmisión de izquierda a derecha, y de derecha a izquierda[5]:

$$r = -\frac{1-C}{1+C}\,\mathrm{e}^{2\theta(L)} \tag{49}$$

$$t = \frac{2C}{1+C}\,\mathrm{e}^{-\theta(R)+\theta(L)} \tag{50}$$

$$r' = \frac{1-C}{1+C}\,\mathrm{e}^{-2\theta(R)} \tag{51}$$

$$t' = \frac{2}{1+C}\,\mathrm{e}^{-\theta(R)+\theta(L)}\,. \tag{52}$$

Esta **S** relaciona dos intervalos *contigüos*. Por eso no es de extrañar que si hacemos $m(R) = m(L)$ y $V(R) = V(L)$, obtengamos el resultado trivial $r = r' = 0$ y $t = t' = 1$.

[5] Ver fórmulas (63) más adelante

Veamos a continuación algunas propiedades interesantes de estas matrices. En lo que sigue, excepto en los casos en que se diga lo contrario, sobreentenderemos que las matrices **K** y **S** llevan los mismos argumentos, (R,L) en el primer caso, y $(\mathrm{R};\mathrm{L})$ en el segundo.

4.2 Relación entre S *y* K

Escribiendo las ecuaciones (42)-(43) y (44)-(45) en forma expandida para los vectores de coeficientes $\mathbf{a}^{+}(\mathrm{R})$, $\mathbf{a}^{-}(\mathrm{L})$, etc, e igualando, por simple comparación se pueden ver las relaciones entre los bloques de **K** y los de **S**.

$$\mathbf{S}_{11} = -\mathbf{K}_{22}^{-1} \cdot \mathbf{K}_{21} \tag{53}$$
$$\mathbf{S}_{12} = \mathbf{K}_{22}^{-1} \tag{54}$$
$$\mathbf{S}_{21} = \mathbf{K}_{11} - \mathbf{K}_{12} \cdot \mathbf{K}_{22}^{-1} \cdot \mathbf{K}_{21} \tag{55}$$
$$\mathbf{S}_{22} = \mathbf{K}_{12} \cdot \mathbf{K}_{22}^{-1} \,. \tag{56}$$

O análogamente

$$\mathbf{K}_{11} = \mathbf{S}_{21} - \mathbf{S}_{22} \cdot \mathbf{S}_{12}^{-1} \cdot \mathbf{S}_{11} \tag{57}$$
$$\mathbf{K}_{12} = \mathbf{S}_{22} \cdot \mathbf{S}_{12}^{-1} \tag{58}$$
$$\mathbf{K}_{21} = -\mathbf{S}_{12}^{-1} \cdot \mathbf{S}_{11} \tag{59}$$
$$\mathbf{K}_{22} = \mathbf{S}_{12}^{-1} \,. \tag{60}$$

4.3 Determinantes de S *y* K

Planteémonos el cálculo del determinante de la Matriz de Scattering **S**. Para ello usemos las fórmulas que dan el determinante de una matriz en términos de sus bloques [26]. Supondremos que las inversas involucradas existen. Entonces

$$\begin{aligned}\text{Det}\,[\mathbf{S}] &= \text{Det}\,[\mathbf{S}_{11}]\,\text{Det}\,[\mathbf{S}_{22}-\mathbf{S}_{21}\cdot\mathbf{S}_{11}^{-1}\cdot\mathbf{S}_{12}]\\ &\vdots\\ &= (-1)^N\,\frac{\text{Det}\,[\mathbf{K}_{11}]}{\text{Det}\,[\mathbf{K}_{22}]}\,.\end{aligned} \tag{61}$$

Ver más detalles en [7].

K y **S** dependen de la base escogida. Por eso no es concebible un Teorema tan simple como el de **T** (Det $[\mathbf{T}] = \exp(i\Theta)$, con Θ dada por el sistema original de ecuaciones) para el determinante de **K** y/o **S**. Pero sí que hay una relación entre ellas: (61).

Sin gran dificultad se puede demostrar una fórmula en cierto sentido *inversa* de la que acabamos de obtener, o sea una expresión para el determinante de **K** en términos de los determinantes de ciertos bloques de **S**. En efecto

$$\begin{aligned}\text{Det}\,[\mathbf{K}] &= \text{Det}\,[\mathbf{K}_{22}]\,\text{Det}\,[\mathbf{K}_{11}-\mathbf{K}_{12}\cdot\mathbf{K}_{22}^{-1}\cdot\mathbf{K}_{21}]\\ &= \frac{\text{Det}\,[\mathbf{S}_{21}]}{\text{Det}\,[\mathbf{S}_{12}]}\,.\end{aligned} \tag{62}$$

4.4 Amplitudes de reflexión y transmisión

Imaginemos un experimento de dispersión donde se lanza una onda de izquierda a derecha sobre la región dispersora, y se investiga la onda reflejada y la trasmitida. Esta es una situación que se puede caracterizar por las ecuaciones (44) y (45) con tal de poner $\mathbf{a}^-(\mathrm{R}) = 0$. El coeficiente de proporcionalidad que queda entonces entre la amplitud incidente $\mathbf{a}^+(\mathrm{L})$ y la reflejada $\mathbf{a}^-(\mathrm{L})$ se denomina *coeficiente de reflexión* y lo denotaremos por **r**. Análogamente, se define el coeficiente de transmisión **t** para este experimento como el coeficiente de proporcionalidad entre la amplitud trasmitida $\mathbf{a}^+(\mathrm{R})$ y la incidente $\mathbf{a}^+(\mathrm{L})$. De manera completamente similar definamos los coeficientes de reflexión y transmisión $\mathbf{r}'$ y $\mathbf{t}'$ respectivamente cuando se hace un experimento de dispersión lanzando un haz desde la derecha. Entonces es prácticamente evidente que

$$\mathbf{S} = \left\| \begin{matrix} \mathbf{r} & \mathbf{t}' \\ \mathbf{t} & \mathbf{r}' \end{matrix} \right\|. \tag{63}$$

Si tenemos en cuenta estas definiciones así como las relaciones entre **S** y **K**, tendremos que

$$\mathbf{K} = \left\| \begin{matrix} \mathbf{t} - \mathbf{r}' \cdot (\mathbf{t}')^{-1} \cdot \mathbf{r} & \mathbf{r}' \cdot (\mathbf{t}')^{-1} \\ -(\mathbf{t}')^{-1} \cdot \mathbf{r} & (\mathbf{t}')^{-1} \end{matrix} \right\|. \tag{64}$$

4.5 Composición de matrices de scattering

Pongámonos de nuevo en la situación en que tenemos los dominios L, M y R (de izquierda a derecha). Aquí M puede ser una capa o μ de ellas; para lo que sigue da igual; el caso es que ahora no nos ocuparemos de una eventual *estructura interna* del dominio central M. Como ya explicamos más arriba, formalmente se puede trabajar con una única base de soluciones LI que expanda el espacio de soluciones en todo M. Para fijar ideas se pudiera pensar que tomamos una base en el dominio o capa $m = 1$, y buscamos su prolongación a la capa $m = 2$ imponiendo las adecuadas condiciones de empalme en la intercara entre los dominios 1 y 2, y que repetimos el procedimiento prolongando estas funciones a los dominios $m = 3, 4, ..., \mu - 2, \mu - 1$, cuidándonos mucho de *ser buenos chicos* en todas las intercaras. Situados en este enfoque del problema, si lo quisiéramos resolver en términos de SM's encararíamos la tarea de hallar la SM de toda la estructura ($\mathbf{S}(\mathrm{R};\mathrm{L})$) a partir de las SM de las parejas de dominios ($\mathbf{S}(\mathrm{R};\mathrm{M})$ y ($\mathbf{S}(\mathrm{M};\mathrm{L})$). Recordemos las definiciones de estas matrices:

$$\begin{vmatrix} \mathbf{a}^-(\mathrm{L}) \\ \mathbf{a}^+(\mathrm{M}) \end{vmatrix} = \mathbf{S}(\mathrm{M};\mathrm{L}) \cdot \begin{vmatrix} \mathbf{a}^+(\mathrm{L}) \\ \mathbf{a}^-(\mathrm{M}) \end{vmatrix}, \tag{65}$$

$$\begin{vmatrix} \mathbf{a}^-(\mathrm{M}) \\ \mathbf{a}^+(\mathrm{R}) \end{vmatrix} = \mathbf{S}(\mathrm{R};\mathrm{M}) \cdot \begin{vmatrix} \mathbf{a}^+(\mathrm{M}) \\ \mathbf{a}^-(\mathrm{R}) \end{vmatrix}, \tag{66}$$

$$\mathbf{S}_{\mathrm{L}} = \mathbf{S}(\mathrm{M};\mathrm{L}) = \begin{Vmatrix} \mathbf{r}_{\mathrm{L}} & \mathbf{t}'_{\mathrm{L}} \\ \mathbf{t}_{\mathrm{L}} & \mathbf{r}'_{\mathrm{L}} \end{Vmatrix} \tag{67}$$

$$\mathbf{S}_{\mathrm{R}} = \mathbf{S}(\mathrm{R};\mathrm{M}) = \begin{Vmatrix} \mathbf{r}_{\mathrm{R}} & \mathbf{t}'_{\mathrm{R}} \\ \mathbf{t}_{\mathrm{R}} & \mathbf{r}'_{\mathrm{R}} \end{Vmatrix} . \tag{68}$$

En la Figura (4) se pueden ver las amplitudes en cada capa.

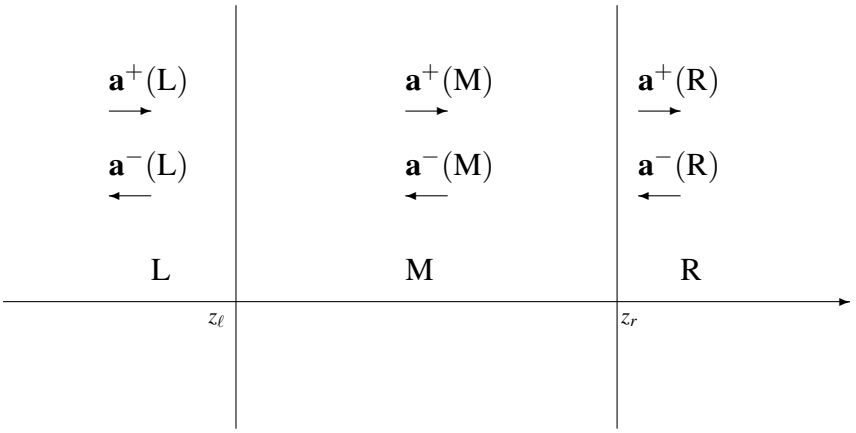

Fig. 4 Esquema de una región central emparedada por sendas regiones semiinfinitas L y R, donde las soluciones se describen por los coeficientes $\mathbf{a}^{\pm}(\mathrm{L})$, $\mathbf{a}^{\pm}(\mathrm{M})$ y $\mathbf{a}^{\pm}(\mathrm{R})$.

Despejando las amplitudes de la capa intermedia en una de estas ecuaciones y sustituyéndolas en la otra obtendremos las amplitudes en el dominio R en función de las amplitudes en L. La matriz que las enlaza no es otra que $\mathbf{S}(\mathrm{R};\mathrm{L})$. El resultado de esta operación es:

$$\mathbf{S} = \mathbf{S}(\mathrm{R};\mathrm{L}) = \begin{Vmatrix} \mathbf{r} & \mathbf{t}' \\ \mathbf{t} & \mathbf{r}' \end{Vmatrix} \tag{69}$$

$$\mathbf{r} = \mathbf{r}_{\mathrm{L}} + \mathbf{t}'_{\mathrm{L}} \cdot \mathbf{r}_{\mathrm{R}} \cdot (\mathbf{I}_N - \mathbf{r}'_{\mathrm{L}} \cdot \mathbf{r}_{\mathrm{R}})^{-1} \cdot \mathbf{t}_{\mathrm{L}} \tag{70}$$

$$\mathbf{t} = \mathbf{t}_{\mathrm{R}} \cdot (\mathbf{I}_N - \mathbf{r}'_{\mathrm{L}} \cdot \mathbf{r}_{\mathrm{R}})^{-1} \cdot \mathbf{t}_{\mathrm{L}} \tag{71}$$

$$\mathbf{r}' = \mathbf{r}'_{\mathrm{R}} + \mathbf{t}_{\mathrm{R}} \cdot (\mathbf{I}_N - \mathbf{r}'_{\mathrm{L}} \cdot \mathbf{r}_{\mathrm{R}})^{-1} \cdot \mathbf{r}'_{\mathrm{L}} \cdot \mathbf{t}'_{\mathrm{R}} \tag{72}$$

$$\mathbf{t}' = \mathbf{t}'_{\mathrm{L}} \cdot \mathbf{t}'_{\mathrm{R}} + \mathbf{t}'_{\mathrm{L}} \cdot \mathbf{r}_{\mathrm{R}} \cdot (\mathbf{I}_N - \mathbf{r}'_{\mathrm{L}} \cdot \mathbf{r}_{\mathrm{R}})^{-1} \cdot \mathbf{r}'_{\mathrm{L}} \cdot \mathbf{t}'_{\mathrm{R}} . \tag{73}$$

En [47] se dan fórmulas equivalentes.

De aquí se ve la conveniencia de introducir una operación especial y nueva entre matrices cuadradas del mismo orden. Vamos a definir un

tipo especial de producto por la siguiente regla de composición. Sean $\mathbf{X}$ y $\mathbf{Y}$ dos matrices de orden $2N$. Denotemos como de costumbre $\mathbf{Z}_{ij}$ a los bloques de orden N de $\mathbf{Z}$, $\mathbf{X}_{ij}$ a los de $\mathbf{X}$, y $\mathbf{Y}_{ij}$ a los de $\mathbf{Y}$. Entonces que el *"producto"* de $\mathbf{X}$ por $\mathbf{Y}$ es $\mathbf{Z}$ se puede denotar como sigue

$$\mathbf{Z} = \mathbf{Y} \bigotimes \mathbf{X} \tag{74}$$

$$\begin{vmatrix} \mathbf{Z}_{11} & \mathbf{Z}_{12} \\ \mathbf{Z}_{21} & \mathbf{Z}_{22} \end{vmatrix} = \begin{vmatrix} \mathbf{Y}_{11} & \mathbf{Y}_{12} \\ \mathbf{Y}_{21} & \mathbf{Y}_{22} \end{vmatrix} \bigotimes \begin{vmatrix} \mathbf{X}_{11} & \mathbf{X}_{12} \\ \mathbf{X}_{21} & \mathbf{X}_{22} \end{vmatrix}, \tag{75}$$

y se define por las siguientes igualdades

$$\mathbf{Z}_{11} = \mathbf{X}_{11} + \mathbf{X}_{12} \cdot \mathbf{Y}_{11} \cdot (\mathbf{I}_N - \mathbf{X}_{22} \cdot \mathbf{Y}_{11})^{-1} \cdot \mathbf{X}_{21} \tag{76}$$

$$\mathbf{Z}_{12} = \mathbf{X}_{12} \cdot \mathbf{Y}_{12} + \mathbf{X}_{12} \cdot \mathbf{Y}_{11} \cdot (\mathbf{I}_N - \mathbf{X}_{22} \cdot \mathbf{Y}_{11})^{-1} \cdot \mathbf{X}_{22} \cdot \mathbf{Y}_{12} \tag{77}$$

$$\mathbf{Z}_{21} = \mathbf{Y}_{21} \cdot (\mathbf{I}_N - \mathbf{X}_{22} \cdot \mathbf{Y}_{11})^{-1} \cdot \mathbf{X}_{21} \tag{78}$$

$$\mathbf{Z}_{22} = \mathbf{Y}_{22} + \mathbf{Y}_{21} \cdot (\mathbf{I}_N - \mathbf{X}_{22} \cdot \mathbf{Y}_{11})^{-1} \cdot \mathbf{X}_{22} \cdot \mathbf{Y}_{12} \, . \tag{79}$$

Con esta operación de composición de matrices en mente, las ecuaciones (69)-(73) pueden condensarse así:

$$\mathbf{S} = \mathbf{S}_{\mathrm{R}} \bigotimes \mathbf{S}_{\mathrm{L}} \tag{80}$$

$$\mathbf{S}(\mathrm{R};\mathrm{L}) = \mathbf{S}(\mathrm{R};\mathrm{M}) \bigotimes \mathbf{S}(\mathrm{M};\mathrm{L}) \, . \tag{81}$$

$\mathbf{S}(\mathrm{M};\mathrm{L})$ tiene el lugar de $\mathbf{X}$ en la definición general, mientras que $\mathbf{S}(\mathrm{R};\mathrm{M})$ tiene el de $\mathbf{Y}$ y $\mathbf{S}(\mathrm{R};\mathrm{L})$ el de $\mathbf{Z}$.

Notar el orden de los factores de este *producto* tan *sui generis*. Si $\mathbf{K}(\mathrm{R},\mathrm{L}) = \mathbf{K}(\mathrm{R},\mathrm{M}) \cdot \mathbf{K}(\mathrm{M},\mathrm{L})$, entonces ponemos $\mathbf{S}(\mathrm{R};\mathrm{L}) = \mathbf{S}(\mathrm{R};\mathrm{M}) \bigotimes \mathbf{S}(\mathrm{M};\mathrm{L})$, conservando el orden de la *multiplicación* y el encadenamiento de los argumentos ($\mathrm{R}\underbrace{\mathrm{MM}}\mathrm{L}$).

4.6 La operación $\bigotimes$

Hagamos una pequeña digresión matemática. Llamemos $\mathscr{S}^{2N}$ al conjunto de matrices del mismo orden, siendo este orden *par* ($= 2N$). La operación $\bigotimes$ tiene algunas propiedades interesantes. Por ejemplo:

1. Cerradura. Es evidente que al efectuar la operación $\bigotimes$ entre matrices de orden $2N$ obtenemos matrices de este mismo orden. Dicho en otras palabras: no nos salimos de $\mathscr{S}^{2N}$.
2. Matriz *identidad* con respecto a esta operación. No es difícil ver que la matriz que tiene este papel es

$$\mathbf{E} = \begin{Vmatrix} 0_N & \mathbf{I}_N \\ \mathbf{I}_N & 0_N \end{Vmatrix}, \tag{82}$$

pues

$$\mathbf{S} \bigotimes \mathbf{E} = \mathbf{E} \bigotimes \mathbf{S} = \mathbf{S} \qquad \forall \;\; \mathbf{S} \in \mathscr{S}^{2N} . \tag{83}$$

3. Matriz *inversa* respecto de esta operación. Se trata de buscar una matriz que satisfaga la propiedad

$$\mathbf{S} \bigotimes \mathbf{S}^{(i)} = \mathbf{S}^{(i)} \bigotimes \mathbf{S} = \mathbf{E} . \tag{84}$$

Si

$$\mathbf{S} = \begin{Vmatrix} \mathbf{r} & \mathbf{t}' \\ \mathbf{t} & \mathbf{r}' \end{Vmatrix}, \tag{85}$$

no es difícil comprobar que

$$\mathbf{S}^{(i)} = \begin{Vmatrix} -(\mathbf{t}')^{-1} \cdot \mathbf{r} \cdot \left[\mathbf{t} - \mathbf{r}' \cdot (\mathbf{t}')^{-1} \cdot \mathbf{r}\right]^{-1} & \left[\mathbf{t}' - \mathbf{r} \cdot (\mathbf{t})^{-1} \cdot \mathbf{r}'\right]^{-1} \\ \left[\mathbf{t} - \mathbf{r}' \cdot (\mathbf{t}')^{-1} \cdot \mathbf{r}\right]^{-1} & -(\mathbf{t})^{-1} \cdot \mathbf{r}' \cdot \left[\mathbf{t}' - \mathbf{r} \cdot (\mathbf{t})^{-1} \cdot \mathbf{r}'\right]^{-1} \end{Vmatrix}. \tag{86}$$

4. Asociatividad. Es algo laborioso pero directo comprobar que

$$\left[\mathbf{S}(R;2) \bigotimes \mathbf{S}(2;1)\right] \bigotimes \mathbf{S}(1;L) = \mathbf{S}(R;2) \bigotimes \left[\mathbf{S}(2;1) \bigotimes \mathbf{S}(1;L)\right] \tag{87}$$

Debido a esto se pueden obviar los signos de agrupación y poner simplemente

$$\mathbf{S}(R;2)\bigotimes\mathbf{S}(2;1)\bigotimes\mathbf{S}(1;L)\ . \tag{88}$$

Las propiedades 1-4 hacen que $\mathscr{S}^{2N}$ tenga estructura de *Grupo* respecto de $\bigotimes$.

4.7 Interpretación matemática y física de las matrices de coeficientes y de scattering

Ante todo introduzcamos el concepto de *"base prolongada de* L *a* R*"*. Tomemos una base en la region L y para cada función de la base hallemos la solución correspondiente en la region R, o sea la solución que es igual a la función base dada en L y que satisface las condiciones de empalme en cada intercara y, por supuesto, el sistema de ecuaciones para todo valor de la variable independiente z. Notar que se puede hallar la base prolongada aplicando la ATM $\mathbf{T}(z,z_\ell)$ con $z\in$ R a cada funcion base en L, o sea

$$\Psi_j^{(prol)}(\mathrm{R}:z)=\mathbf{T}(z,z_\ell)\cdot\Psi_j(\mathrm{L}:z_\ell)\ \ ;\ \ z\in\mathrm{R}\ . \tag{89}$$

Entonces es un hecho trivial que si usamos una base cualquiera en L, pero usamos su prolongación en R, los coeficientes de cualquier solución serán los mismos en L y en R. Por lo tanto la matriz de coeficientes es la matriz unidad usual, y la de scattering es también la unidad pero respecto de la operación de composición de SMs. En fórmulas:

$$\mathbf{K}(\mathrm{R},\mathrm{L})=\mathbf{I}_{2N} \tag{90}$$

$$\mathbf{S}(\mathrm{R};\mathrm{L})=\mathbf{E}\ . \tag{91}$$

E también es de orden $2N$ pero no es necesario indicarlo pues siempre aparece con este número de filas y columnas.

Si usamos las bases prolongadas, los coeficientes de reflexión son cero y los de trasmisión uno. O sea

$$\mathbf{r} = \mathbf{r}' = \mathbf{I}_N \tag{92}$$

$$\mathbf{t} = \mathbf{t}' = 0_N \, . \tag{93}$$

Este es un ejemplo sencillo pero muy ilustrativo de que las CTMs y las SMs dependen muy fuertemente de las bases escogidas.

Otro ejemplo menos trivial es aquel en que usamos en ambas regiones extremas (L y R) sendas bases canónicas. Entonces las matrices $\mathbb{Q}$ son iguales a la identidad $\mathbf{I}$, y la matriz de coeficientes $\mathbf{K}(\mathrm{R},\mathrm{L})$ coincide con la ATM $\mathbf{T}(z_\ell, z_r)$.

Usar las bases reducidas en L y/o R da otra solución a este problema, distinta a las dos anteriores, pero sin ningún valor notable que sea independiente del sistema físico.

Ninguno de los dos primeros ejemplos anteriores (bases prolongada y canónica) es lo que se hace usualmente. Los dos primeros ejemplos son pura matemática. Lo más visto es que se toma una base de ondas planas ($\Lambda(z)\exp[ik(z-z_0)]$) tanto a la izquierda (región L) como a la derecha (región R). Si se toma z_0 como z_ℓ (z_r) tendremos la base reducida en L (R). La elección de estas soluciones LI, sean reducidas o no, se corresponde más bien con el hecho de que los físicos saben preparar y medir las características de paquetes de tales ondas. Entonces las CTMs, las SMs y las matrices de reflexión y transmisión dejan de tener estos valores notables ($\mathbf{I}$, 0, etc.)y toman otros valores con mas significación física. Incluso se ve con bastante frecuencia que los medios L y R son del mismo material, o sea que poseen los mismos parámetros constitutivos, y se escoge entonces la misma base ($\Lambda(z)\exp[ik(z-z_0)]$) en ambas regiones. La expresión "la misma base" desde un punto de vista formal es incorrecta pues se trata de funciones definidas en dominios diferentes, pero espero que el lector sepa de qué estamos hablando. Se trata de funciones definidas en dominios diferentes pero con la misma regla para asignar a cada elemento del dominio su transformado; en este caso, con el mismo z_0.

Digamos unas palabras del significado de la inversa de una CTM $\mathbf{K}(\mathrm{R},\mathrm{L})$, o sea $\mathbf{K}(\mathrm{R},\mathrm{L})^{-1}$. Esta matriz tambien es una CTM: la que lleva de R a L, o sea $\mathbf{K}(\mathrm{R},\mathrm{L})^{-1} = \mathbf{K}(\mathrm{L},\mathrm{R})$. En el caso de las CTM esta operación está bien definida pues el orden de los argumentos de $\mathbf{K}$ cuenta.

Cuando queremos hacer esto mismo, o algo parecido, con las SMs el análisis se complica algo. El orden de los argumentos en las SMs

no cuenta. A la inversa de una $\mathbf{K}$ ($\mathbf{K}^{-1}$) le corresponde una SM que resulta la inversa (i) de la SM que corresponde a $\mathbf{K}$, o sea $\mathbf{S}^{(i)}$.

Recalquemos que la composición de matrices de scattering es una operación diferente a la multiplicación de matrices. Lo que se hace en CTMs multiplicando, con las SMs hay que aplicar la operación de composición $\otimes$. De paso: si hubiésemos escogido otro orden de los coeficientes en la definición de las SMs, la matriz *unidad* respecto de $\otimes$ sería $\mathbf{I}$ en lugar de nuestra $\mathbf{E}$. Pero hacer tal cosa escondería peligrosamente el carácter totalmente diferente de $\otimes$ respecto de la multiplicación usual de matrices.

5 Definición de las matrices de stifness, compliance y Poincaré

A continuación haremos un brevísimo estudio de las matrices llamadas de *Stiffness*, *Compliance*, y de *Poincaré*. Éstas tienen interés doble. Por un lado son variantes para analizar analíticamente nuestros problemas. Desde ese punto de vista cobra importancia el estudio de sus propiedades formales. Por otro lado, varios autores *venden* unas u otras como opciones para evitar o paliar los problemas numéricos.

La ecuación básica de transferencia entre dos puntos

$$\mathbf{T}(z_2, z_1) \cdot \Psi(z_1) = \Psi(z_2) \tag{94}$$

se puede poner como

$$\mathbf{T}_{AA}(z_2, z_1) \cdot \mathbb{F}(z_1) + \mathbf{T}_{AD}(z_2, z_1) \cdot \mathbb{A}(z_1) = \mathbb{F}(z_2) \tag{95}$$
$$\mathbf{T}_{DA}(z_2, z_1) \cdot \mathbb{F}(z_1) + \mathbf{T}_{DD}(z_2, z_1) \cdot \mathbb{A}(z_1) = \mathbb{A}(z_2)\,. \tag{96}$$

En principio caben cuatro variantes básicas, a las que se podrían agregar variantes triviales. Listemos las básicas:

- Si tomamos $\mathbb{F}(z_2)$ y $\mathbb{A}(z_2)$ como variables dependientes estamos usando el formalismo $\mathbf{T}$ y su ecuación definitoria es (95)-(96).

- Si tomamos $\mathbb{A}(z_1)$ y $\mathbb{A}(z_2)$ como variables dependientes estamos usando el formalismo de la *Matriz de Stiffness* [**?**] $\mathbf{E}$ y su ecuación definitoria es

$$\mathbf{E}_{11}(z_2,z_1)\cdot\mathbb{F}(z_1)+\mathbf{E}_{12}(z_2,z_1)\cdot\mathbb{F}(z_2)=\mathbb{A}(z_1) \tag{97}$$
$$\mathbf{E}_{21}(z_2,z_1)\cdot\mathbb{F}(z_1)+\mathbf{E}_{22}(z_2,z_1)\cdot\mathbb{F}(z_2)=\mathbb{A}(z_2)\ . \tag{98}$$

  Nota: No se debe confundir la matriz de *stiffness* $\mathbf{E}(z,z_0)$, dependiente de dos variables espaciales, con la matriz numérica $\mathbf{E}$. Esta última no depende de ningún argumento y es simplemente la matriz unidad para la operación $\bigotimes$.
- Si tomamos $\mathbb{F}(z_1)$ y $\mathbb{F}(z_2)$ como variables dependientes estamos usando el formalismo de la *Matriz de Compliance* [**?**] $\mathbf{L}$ y su ecuación definitoria es

$$\mathbf{L}_{11}(z_2,z_1)\cdot\mathbb{A}(z_1)+\mathbf{L}_{12}(z_2,z_1)\cdot\mathbb{A}(z_2)=\mathbb{F}(z_1) \tag{99}$$
$$\mathbf{L}_{21}(z_2,z_1)\cdot\mathbb{A}(z_1)+\mathbf{L}_{22}(z_2,z_1)\cdot\mathbb{A}(z_2)=\mathbb{F}(z_2)\ . \tag{100}$$

  Atención a los problemas de notación. No se debe confundir esta matriz con la del operador de la ecuación maestra.
- Si elegimos tres puntos arbitrarios z_0, z_1 y z_2, podemos plantear un enfoque de problema de contorno, esto es

$$\mathbb{F}(z_2)=\mathbf{p}_0^F\cdot\mathbb{F}(z_0)+\mathbf{p}_1^F\cdot\mathbb{F}(z_1) \tag{101}$$
$$\mathbb{A}(z_2)=\mathbf{p}_0^A\cdot\mathbb{F}(z_0)+\mathbf{p}_1^A\cdot\mathbb{F}(z_1)\ . \tag{102}$$

  A $\mathbf{p}_0^F,\mathbf{p}_1^F,\mathbf{p}_0^A$ y $\mathbf{p}_1^A$ le llamaremos Matrices de Poincaré.

El nombre de *Matriz de Stiffness* viene de la Elasticidad donde la tensión τ_{ij} -la LDF $\mathbb{A}$ de este problema- se pone en términos de la deformación u_{ij} -el campo $\mathbb{F}$ de este problema. Análogamente con la *Matriz de Compliance*.

No se suelen traducir estos términos al español. No obstante, cuando se hace, *Stiffness* se traduce como *Rigidez*. Con *Compliance* hay menos suerte; *Admitancia* pudiera ser una buena traducción.

Estudiemos a continuación, aunque sea brevemente, cada uno de estos enfoques.

6 Matriz de *Stiffness*

De manera simple se deducen las siguientes relaciones entre la matriz de stiffness y la ATM **T**:

$$\mathbf{E}_{11} = -\left[\mathbf{T}_{AD}\right]^{-1} \cdot \mathbf{T}_{AA} \tag{103}$$

$$\mathbf{E}_{12} = \left[\mathbf{T}_{AD}\right]^{-1} \tag{104}$$

$$\mathbf{E}_{21} = \mathbf{T}_{DA} - \mathbf{T}_{DD} \cdot \left[\mathbf{T}_{AD}\right]^{-1} \cdot \mathbf{T}_{AA} \tag{105}$$

$$\mathbf{E}_{22} = \mathbf{T}_{DD} \cdot \left[\mathbf{T}_{AD}\right]^{-1} \ . \tag{106}$$

Estas son las ecuaciones (15) de Rokhlin & Wang [51], aunque allí se denota **K** a la matriz de stiffness. Nosotros la denotamos **E** para no confundirla con nuestra CTM. En estas fórmulas tanto los bloques de **T** como los de **E** están evaluados en los mismos argumentos, (z, z_0) por ejemplo.

La matriz de stiffness tiene algunas propiedades generales interesantes; por ejemplo:

1. $\mathbf{E}(z_2, z_1)$ depende de dos *puntos*; no de intervalos como la CTM.
2. **E** es *única*. Al igual que la FTM y la ATM es una característica de la ecuación maestra. No conoce de las condiciones de contorno.
3. Determinante de **E**.

$$\begin{aligned} \mathrm{Det}\,[\mathbf{E}] &= \mathrm{Det}\,[\mathbf{E}_{11}]\ .\mathrm{Det}\,[\mathbf{E}_{22} - \mathbf{E}_{21} \cdot (\mathbf{E}_{11})^{-1} \cdot \mathbf{E}_{12}] \qquad (107) \\ &= \mathrm{Det}\,[-(\mathbf{T}_{AD})^{-1} \cdot \mathbf{T}_{AA}]\ . \\ &\quad \mathrm{Det}\,\Big[\mathbf{T}_{DD} \cdot (\mathbf{T}_{AD})^{-1} \\ &\quad -(\mathbf{T}_{DA} - \mathbf{T}_{DD} \cdot [\mathbf{T}_{AD}]^{-1} \cdot \mathbf{T}_{AA}) \cdot (-(\mathbf{T}_{AD})^{-1} \cdot \mathbf{T}_{AA})^{-1} \cdot (\mathbf{T}_{AD})^{-1}\Big] \\ &= (-1)^N \, \frac{\mathrm{Det}\,[\mathbf{T}_{DA}]}{\mathrm{Det}\,[\mathbf{T}_{AD}]}\ . \qquad (108) \end{aligned}$$

4. Regla de composición de matrices de *stiffness*.
   Ver ecuaciones (22) de Rokhlin & Wang en [51]. Notar que esta regla no es más que $\bigotimes$.

Ejemplo: Electrones en Teoría de Masa Efectiva; intervalo con potencial y masa constantes.

$$\mathbf{T} = \begin{pmatrix} \cos(kd) & \frac{m}{k}\sin(kd) \\ -\frac{k}{m}\sin(kd) & \cos(kd) \end{pmatrix} . \tag{109}$$

$$\mathbf{E} = -\frac{k}{m}\,\frac{1}{\sin(kd)}\,\begin{pmatrix} \cos(kd) & -1 \\ 1 & -\cos(kd) \end{pmatrix} . \tag{110}$$

$$\text{Det}\,[\mathbf{E}] = \left(\frac{k}{m}\right)^2 \tag{111}$$

$$= (-1)^1\,\frac{T_{DA}}{T_{AD}} . \tag{112}$$

7 Matriz de *Compliance*

De su misma definición resulta que la Matriz de Compliance $\mathbf{L}(z,z_0)$ es la inversa de la Matriz de Stiffness $\mathbf{E}(z,z_0)$,

$$\mathbf{L}(z,z_0) = [\mathbf{E}(z,z_0)]^{-1} \tag{113}$$

Y de una manera bien simple se puede deducir que

$$\mathbf{L}_{11} = -\,[\mathbf{T}_{DA}]^{-1}\cdot\mathbf{T}_{DD} \tag{114}$$

$$\mathbf{L}_{12} = [\mathbf{T}_{DA}]^{-1} \tag{115}$$

$$\mathbf{L}_{21} = \mathbf{T}_{AD} - \mathbf{T}_{AA}\cdot[\mathbf{T}_{DA}]^{-1}\cdot\mathbf{T}_{DD} \tag{116}$$

$$\mathbf{L}_{22} = \mathbf{T}_{AA}\cdot[\mathbf{T}_{DA}]^{-1} . \tag{117}$$

Para el caso de la ecuación de Schrödinger con masa y potencial constantes se tiene que:

$$\mathbf{L} = \begin{pmatrix} m\cot(kd) & -m\csc(kd) \\ -m\csc(kd) & -m\cot(kd) \end{pmatrix} . \tag{118}$$

8 Matriz de *Poincaré*

Las matrices $\mathbf{p}_0^F$, ..., se ponen de manera inmediata en términos de los bloques de las $\mathbf{T}$'s, y son las generalizaciones al caso matricial general de los coeficientes de Poincaré analizados por Monsivais y colaboradores en [52]. Empecemos por copiar aquí las fórmulas (95)-(96) para los puntos z_1 y z_2:

$$\mathbf{T}_{AA}(z_2,z_1)\cdot\mathbb{F}(z_1)+\mathbf{T}_{AD}(z_2,z_1)\cdot\mathbb{A}(z_1)=\mathbb{F}(z_2) \tag{119}$$
$$\mathbf{T}_{DA}(z_2,z_1)\cdot\mathbb{F}(z_1)+\mathbf{T}_{DD}(z_2,z_1)\cdot\mathbb{A}(z_1)=\mathbb{A}(z_2)\,. \tag{120}$$

Pero

$$\mathbb{F}(z_1)=\mathbf{T}_{AA}(z_1,z_0)\cdot\mathbb{F}(z_0)+\mathbf{T}_{AD}(z_1,z_0)\cdot\mathbb{A}(z_0) \tag{121}$$
$$\mathbb{A}(z_1)=\mathbf{T}_{DA}(z_1,z_0)\cdot\mathbb{F}(z_0)+\mathbf{T}_{DD}(z_1,z_0)\cdot\mathbb{A}(z_0)\,. \tag{122}$$

De (121) se tiene que

$$\mathbb{A}(z_0)=[\mathbf{T}_{AD}(z_1,z_0)]^{-1}\cdot\mathbb{F}(z_1)-[\mathbf{T}_{AD}(z_1,z_0)]^{-1}\cdot\mathbf{T}_{AA}(z_1,z_0)\cdot\mathbb{F}(z_0). \tag{123}$$

Y sustituyendo este resultado en (122) tendremos que

$$\begin{aligned}\mathbb{A}(z_1)=&\Big(\mathbf{T}_{DA}(z_1,z_0)-\mathbf{T}_{DD}(z_1,z_0)\cdot[\mathbf{T}_{AD}(z_1,z_0)]^{-1}\cdot\mathbf{T}_{AA}(z_1,z_0)\Big)\cdot\mathbb{F}(z_0)\\&+\mathbf{T}_{DD}(z_1,z_0)\cdot[\mathbf{T}_{AD}(z_1,z_0)]^{-1}\cdot\mathbb{F}(z_1)\,.\end{aligned} \tag{124}$$

Y por último, sustituyamos este resultado en (119) y (120):

$$\begin{aligned}\mathbb{F}(z_2)=&\mathbf{T}_{AD}(z_2,z_1)\cdot\Big(\mathbf{T}_{DA}(z_1,z_0)-\mathbf{T}_{DD}(z_1,z_0)\cdot[\mathbf{T}_{AD}(z_1,z_0)]^{-1}\cdot\mathbf{T}_{AA}(z_1,z_0)\Big)\cdot\mathbb{F}(z_0)\\&+\Big(\mathbf{T}_{AA}(z_2,z_1)+\mathbf{T}_{AD}(z_2,z_1)\cdot\mathbf{T}_{DD}(z_1,z_0)\cdot[\mathbf{T}_{AD}(z_1,z_0)]^{-1}\Big)\cdot\mathbb{F}(z_1)\end{aligned} \tag{125}$$
$$\begin{aligned}\mathbb{A}(z_2)=&\mathbf{T}_{DD}(z_2,z_1)\cdot\Big(\mathbf{T}_{DA}(z_1,z_0)-\mathbf{T}_{DD}(z_1,z_0)\cdot[\mathbf{T}_{AD}(z_1,z_0)]^{-1}\cdot\mathbf{T}_{AA}(z_1,z_0)\Big)\cdot\mathbb{F}(z_0)\\&+\Big(\mathbf{T}_{DA}(z_2,z_1)+\mathbf{T}_{DD}(z_2,z_1)\cdot\mathbf{T}_{DD}(z_1,z_0)\cdot[\mathbf{T}_{AD}(z_1,z_0)]^{-1}\Big)\cdot\mathbb{F}(z_1)\,.\end{aligned} \tag{126}$$

De aquí que

$$\mathbf{p}_0^F = \mathbf{T}_{AD}(z_2,z_1)\cdot\Big(\mathbf{T}_{DA}(z_1,z_0)-\mathbf{T}_{DD}(z_1,z_0)\cdot[\mathbf{T}_{AD}(z_1,z_0)]^{-1}\cdot\mathbf{T}_{AA}(z_1,z_0)\Big) \tag{127}$$

$$\mathbf{p}_1^F = \mathbf{T}_{AA}(z_2,z_1)+\mathbf{T}_{AD}(z_2,z_1)\cdot\mathbf{T}_{DD}(z_1,z_0)\cdot[\mathbf{T}_{AD}(z_1,z_0)]^{-1} \tag{128}$$

$$\mathbf{p}_0^A = \mathbf{T}_{DD}(z_2,z_1)\cdot\Big(\mathbf{T}_{DA}(z_1,z_0)-\mathbf{T}_{DD}(z_1,z_0)\cdot[\mathbf{T}_{AD}(z_1,z_0)]^{-1}\cdot\mathbf{T}_{AA}(z_1,z_0)\Big) \tag{129}$$

$$\mathbf{p}_1^A = \mathbf{T}_{DA}(z_2,z_1)+\mathbf{T}_{DD}(z_2,z_1)\cdot\mathbf{T}_{DD}(z_1,z_0)\cdot[\mathbf{T}_{AD}(z_1,z_0)]^{-1}\ . \tag{130}$$

Para escribir el caso más simple de la ecuación de Schrödinger con masa y potencial constantes pongamos

$$\ell_2 = z_2 - z_1 \tag{131}$$

$$\ell_1 = z_1 - z_0 \tag{132}$$

$$k = \sqrt{\frac{2m}{\hbar^2}(E-V)}\ . \tag{133}$$

Entonces

$$p_0^F = -\frac{\sin(k\ell_2)}{\sin(k\ell_1)} \tag{134}$$

$$p_1^F = \frac{\sin(k(\ell_1+\ell_2))}{\sin(k\ell_1)} \tag{135}$$

$$p_0^A = -\frac{1}{m}\frac{\cos(k\ell_2)}{\sin(k\ell_1)} \tag{136}$$

$$p_1^A = \frac{1}{m}\frac{\cos(k(\ell_1+\ell_2))}{\sin(k\ell_1)}\ . \tag{137}$$

Volviendo al caso general, notemos que si el campo es nulo en z_0 y z_1, la única manera en que tendremos campo y forma lineal no nulos en z_2 es que

$$\text{Det}\ [\mathbf{T}_{AD}(z_1,z_0)] = 0\ . \tag{138}$$

En el caso de Schrödinger esto es

$$\sin(k\ell_1) = 0 \tag{139}$$

$$\vdots$$

$$E_n = V + \frac{n^2\pi^2\hbar^2}{\ell_1^2} \, . \tag{140}$$

Para recuperar el pozo con extremos libres ($\mathbb{A}(z_0) = \mathbb{A}(z_1) = 0$) de manera sencilla habría que introducir matrices $\mathbf{u}$ tales que

$$\mathbb{F}(z_2) = \mathbf{u}_0^F \cdot \mathbb{A}(z_0) + \mathbf{u}_1^F \cdot \mathbb{A}(z_1) \tag{141}$$

$$\mathbb{A}(z_2) = \mathbf{u}_0^A \cdot \mathbb{A}(z_0) + \mathbf{u}_1^A \cdot \mathbb{A}(z_1) \, . \tag{142}$$

El álgebra y el razonamiento son similares al caso de las $\mathbf{p}$.

9 El problema $\omega - d$

El problema $\omega - d$ viene siendo estudiado desde mediados del siglo pasado. Vea por ejemplo las Refs. [36-38,47-51]. Para algún detalle sobre en qué consiste este escollo que por momentos es descomunal, el lector puede revisar la Ref. [7]. En general varios autores sostienen que esta dificultad se soslaya usando las matrices de scattering, pero ciertamente no hay prueba de semejante aseveración, y en todo caso esta tesis está sólo sostenida por una serie de experimentos numéricos aparentemente bien hechos.

Rodríguez-Ramos, Calás del Castillo y colaboradores [53,54] recientemente propusieron un procedimiento basado en el uso de la técnica de descomposición en valores singulares combinado con el método de la matriz global y una estrategia de múltiples reescalados.

En última instancia este problema está provocado porque nuestras ecuaciones tienen soluciones que explotan en el infinito. Los elementos matriciales de las distintas matrices ciertamente se expresan en términos de las soluciones de las ecuaciones maestras de diferentes maneras. Por eso no es descabellado pensar que el problema no se manifiesta de la misma manera cuando usamos una matriz u otra. El

paso de una de ellas a las otras pudiera darnos el detalle crucial para inferir la bondad de cada una de nuestras matrices.

10 Conclusiones y bibliografa

Aquí nos hemos limitado deliberadamente a los métodos de matrices de transferencia. En paralelo tenemos a las técnicas de Funciones de Green (vea la Ref. [23] y las citas que allí se dan). Se sigue trabajando arduamente en distintos campos de la Física para obtener las Funciones de Green de los operadores de Sturm-Liouville de las respectivas ecuaciones maestras. Vea, por ejemplo las Refs. [55,56].

Nuestra intención fue poner en el contexto general de la ecuación general (6) las distintas definiciones y obtener las relaciones entre las distintas matrices involucradas. En la tabla 1 se resumen las localizaciones de algunas de estas relaciones.

Como decíamos, existe otra temática muy cercana a la que aquí tratamos y cuyo estudio pudiera ser muy fructífero. Nos referimos a las relaciones de todas estas matrices con las Funciones de Green. Ya se han estudiado en detalle las relaciones de las Funciones de Green con las matrices **M** y **T** [7,23], pero mucho menos con las matrices de scattering **S** y aún en menor medida con las matrices de stiffness y compliance; pero resulta muy sugerente que la regla de composición $\otimes$ recuerde fuertemente al procedimiento para *componer* funciones de Green, más frecuentemente conocido como SGFM (*Surface Green Function Matching*) [23].

	M	**T**	**K**	**E**	**L**
M	**I**	Eq. (20)	Nota A	Nota B	Nota B
T	Eq. (20)	**I**	[**?**], pág. 29	Nota B	Nota B
K	Nota A	[7]	**I**	Nota C	Nota C
E	Nota B	Eq. (103)	Nota C	**I**	Eq. (113)
L	Nota B	Eq. (114)	Nota C	Eq. (113)	**I**

Table 1 Cuadro resumen de algunas de las distintas matrices estudiadas y las localizaciones respectivas de las relaciones entre ellas. Nota A: Estas relaciones se deducen de forma trivial de las respectivas relaciones entre **T** y **K** por un lado, y entre **M** y **T** por otro. Nota B: No conocemos que estén escritas en parte alguna, aunque la tarea de hallar estas relaciones parece ser de álgebra elemental. Nota C: No conocemos que hayan sido reportadas.

Agradecimientos

Buena parte de lo que hemos incluido en este reporte se hizo cuando aún trabajábamos con el hoy retirado Profesor Federico García Moliner; nuestro más profundo agradecimiento para Federico.

Varios colegas han investigado junto a nosotros sobre lo que aquí se expone: Víctor R Velasco Rodríguez, Leonor Chico Gómez, Marcelo Lago Izquierdo, María de la Luz Silba Vélez y aún otros. Vaya a todos ellos nuestros agradecimientos.

Bibliografía

1. L Esaki, *Advances in semiconductor superlattices, quantum wells and heterostructures*, J. Physique, Coloque C5, suplément au No. 4, **45**, 3-21 (1984).
2. G Bastard, *Electronic states in semiconductor heterostructures*, IEEE J of Quantum Electronics, QE-**22**:9, 1625-1644 (1986).
3. G Bastard, *Wave mechanics applied to semiconductor heterostructures*, Éditions de Physique, Paris (1989).
4. B Vinter and C Weisbuch, *Quantum Semiconductor Structures*, Academic Press, San Diego (1991).
5. C Trallero-Giner, R Pérez-Alvarez and F García-Moliner, *Long wave polar modes in semiconductor heterostructures*, Pergamon Elsevier Science, London (1998).
6. M E Mora-Ramos, R Pérez-Álvarez and L M Gaggero-Sager (editores), *Some current topics in condensed matter physics*, Universidad Autónoma del Estado de Morelos (2010).
7. R Pérez-Álvarez and F García-Moliner, *Transfer Matrix, Green Function and related techniques: Tools for the study of multilayer heterostructures*, ed. Universitat Jaume I, Castellón de la Plana, Spain (2004).
8. R Pérez-Alvarez and F García-Moliner, *The spectrum of quasiregular heterostructures*, invited chapter in "Some Contemporary Problems of Condensed Matter Physics", Nova Science Publishers, ed. by S. Vlaev and M. Gaggero-Sager (2000), pp. 1-37.

9. E Maciá and F Domínguez-Adame, *Electrons, phonons and excitons in low dimensional aperiodic systems*, Madrid, Editorial Complutense (2000).
10. D J BenDaniel and C B Duke, *Space-Charge Effects on Electron Tunneling*, Phys. Rev **152**:2, 683-692 (1966).
11. L C Lew Yan Voon, *Discontinuities in the effective-mass equation*, Superlattices and Microstructures **31**:6, 269-276 (2002).
12. N Ashcroft and N D Mermin, *Solid state physics*, Holt, Rinehart and Winston (1976).
13. Ch Kittel, *Introduction to solid state physics*, 5th edition, John Wiley & Sons (1976).
14. C Weisbuch, *Applications of MBE-grown heterostructures and quantum wells in fundamental research and in advanced semiconductor devices*, J. Crystal Growth **127**, 742-751 (1993).
15. M R Geller and W Kohn, *Theory of generalized Wannier functions for nearly periodic potentials*, Phys. Rev. B **48**:19, 14085-14088 (1993).
16. M R Geller and W Kohn, *Quantum mechanics of electrons in crystals with graded composition*, Phys. Rev. Lett. **70**:20, 3103-3106 (1993).
17. S J Vlaev and L M Gaggero-Sager, *Quasi-Bound Hole States in δ-Doped Quantum Wells*, Physica Status Solidi (b) **220**:1, 147-151 (2000).
18. L M Gaggero-Sager and M E Mora-Ramos, *Hole Energy Levels in p-Type δ-Doped Si Quantum Wells: Influence of the Split-Off Band*, Physica Status Solidi (b) **220**:1, 163-166 (2000).
19. L Chico, F García-Moliner and V R Velasco, *Electronic structure of periodically δ-doped GaAs:Si*, Phys. Rev. **B48**:15, 11427-11430 (1993).
20. F Capasso, HM Cox, AL Hutchinson, NA Olsson and SG Hummel, *Pseudo-quaternary GaInAsP semiconductors: A new Ga0.47In0.53As/InP graded gap superlattice and its applications to avalanche photodiodes*, Appl. Phys. Lett. **45**, 1193-1195 (1984);
21. S Vlaev, F García-Moliner and VR Velasco, *Electronic states of digital versus analog graded quantum wells*, Phys. Rev. B **52**:19, 13784-13787 (1995).
22. Akio Sasaki, *Effective-mass superlattice*, Phys. Rev. B **30**:12, 7016-7020 (1984).

23. F García-Moliner and VR Velasco, *Theory of Single and Multiple Interfaces*, World Scientific, Singapore (1992).
24. V Hurewicz, *Lectures on ordinary differential equations*, The MIT Press (1958).
25. Yu N Bibikov, *Curso General de Ecuaciones Diferenciales Ordinarias* (en ruso), Editorial de la Universidad de Leningrado (1981). Yu N Bibikov, *Obshchii kurs obyknovennykh differentsialnykh uravnenii: uchebnoe posobie* / IU.N. Bibikov. Published by Leningrad: Izd-vo Leningradskogo universiteta, (1981).
26. S Barnett, *Matrices. Methods and Applications*, Oxford Applied Mathematics and Computing Sciences Series, Clarendon Press, Oxford (1990).
27. F R Gantmakher, *Teoría de Matrices* (en ruso), editorial Nauka (1988). F R Gantmakher, *Applications of the theory of matrices*; translated and revised by J.L. Brenner, with the assistance of D.W. Bushaw and S. Evanusa, New York, Interscience Publishers (1959).
28. L Schwartz, *Méthodes mathématiques pour les sciences physiques*, Hermann, Paris (1965).
29. J Mathews and R L Walker, *Mathematical methods of physics*, WA Benjamin, New York (1965).
30. B Friedman, *Principles and techniques of applied mathematics*, J Wiley, New York (1956).
31. S Datta, M Cahay and M McLennan, *Scatter-matrix approach to quantum transport*, Phys. Rev. **B36**:10, 5655-5658 (1987).
32. Z Wang and A N Norris, *Waves in cylindrical shells with circumferential submembers: a matrix approach*, Journal of Sound and Vibration **181**:3, 457-484 (1995).
    Usa las matrices de coeficientes y de scattering y proclama claramente que *The loss of computational accuracy due to the inevitable exponentially growing terms in a propagator matrix is completely avoided by using the* **S***-matrix*. Hace referencia a varios artículos de los años 50, 60 y 70 donde se definen y usan las matrices de transferencia y las de scattering en el campo de las ondas elásticas, Sismología y Geofísica en general, y de trabajos algo más recientes en esta misma dirección. En particular [33-45].
33. W T Thomson, *Transmission of elastic waves through a stratified solid medium*, Journal of Applied Physics **21**, 89-93 (1950).

34. N A Haskell, *Dispersion of surface waves on multilayered media*, Bull. Seism. Soc. Am. **43**, 17-34 (1953).
35. R Redheffer, *Modern Mathematics for Engineers*, New York: McGraw-Hill (1961). Capítulo 12.
36. L Knopoff, *A matrix method for elastic wave problem*, Bull. Seism. Soc. Amer. **54**, 431-438 (1964).
37. J W Dunkin, *Computation of modal solution in layered elastic media at high frequencies*, Bull. Seismol. Soc. Am. 55, 335-358 (1965).
38. Y K Lin and B K Donaldson, *A brief survey of transfer matrix technique with special reference to the analysis of aircraft panels*, Journal of Sound and Vibration **10**, 103-143 (1969).
39. B L N Kennett, *Reflection, rays and reverberations*, Bull. of the Seismological Society of America **64**, 1685-1969 (1974).
40. B L N Kennett and N J Kerry, *Seismic waves in a stratified half space*, Geophysical Journal of the Royal Astronomical Society **57**, 557-583 (1979).
41. B L N Kennett, *Seismic Wave Propagation in Stratified Media*, Cambridge: Cambridge University Press (1983).
42. B R Mace, *Wave reflection and transmission in beams*, Journal of Sound and Vibration **97**, 237-246 (1984).
43. A H von Flotow, *Disturbance propagation in structural networks*, Journal of Sound and Vibration **106**, 433-450 (1986).
44. Y Yong and Y K Lin, *Dynamic of complex truss-type space structures*, American Institute of Aeronautics and Astronautics Journal **28**, 1250-1258 (1990).
45. Y Yong and Y K Lin, *Dynamic response analysis of truss-type structural networks: a wave propagation approach*, Journal of Sound and Vibration **156**, 27-45 (1992).
46. P Pereyra, *Symmetries, parametrization and group structure of transfer matrices in quantum scattering theory*, J. Math. Phys. **36**:3, 1166-1176 (1995).
    La **M** de la fórmula (3) es la **K** nuestra.
47. W-D Sheng and J-B Xia, *A transfer matrix approach to conductance in quantum waveguides*, Journal of Physics: Condensed Matter **8**, 3635-3645 (1996).
    Tunelaje multicanal al estilo de [46]. La matriz **M** de Sheng en este artículo es la inversa de nuestra **K** pues pone los coeficientes

de la parte izquierda (L) en términos de los de la parte derecha (R) ($\mathbf{a}(L) = \mathbf{M}_{Sheng} \cdot \mathbf{a}(R)$; fórmula (4) en [47]).

48. W-D Sheng, *Calculation of the band structure of semiconductor quantum wells using scattering matrices*, Journal of Physics: Condensed Matter **8**, 10347-10352 (1996).
    Dice que con las matrices de scattering se evitan los problemas numéricos. Ver [47] y [49].
49. W-D Sheng, *The scattering matrix method for quantum waveguides*, Journal of Physics: Condensed Matter **9**, 8369-8380 (1997).
50. A Khalil and M B Steer, *A generalized scattering matrix method using the method of moments for electromagnetic analysis of multilayered structures in waveguide*, IEEE Transactions on microwave theory and techniques **47**:11, 2151-2157 (1999).
51. S I Rokhlin and L Wang, *Stable recursive algorithm for elastic wave propagation in layered anisotropic media: Stiffness matrix method*, J. Acoust. Soc. Am. 112, 822-834 (2002).
    Vale la pena copiar el resumen del artículo literalmente:
    An efficient recursive algorithm, the stiffness matrix method, has been developed for wave propagation in multilayered generally anisotropic media. This algorithm has the computational efficiency and simplicity of the standard transfer matrix method and is unconditionally computationally stable for high frequency and layer thickness. In this algorithm, the stiffness (compliance) matrix is calculated for each layer and recursively applied to generate a stiffness (compliance) matrix for a layered system. Next, reflection and transmission coefficients are calculated for layered media bounded by liquid or solid semispaces. The results show that the method is stable for arbitrary number and thickness of layers and the computation time is proportional to the number of layers. It is shown both numerically and analytically that for a thick structure the solution approaches the solution for a semispace. This algorithm is easily adaptable to laminates with periodicity, such as multiangle lay-up composites. The repetition and symmetry of the unit cell are naturally incorporated in the recursive scheme. As an example the angle beam time domain pulse reflections from fluid-loaded multilayered composites have been computed and compared with experiment. Based on this method, characteristic equations for Lamb waves and Floquet waves in periodic media have also been determined.

52. G Monsivais, F García-Moliner and V R Velasco, *Unified description of quantum particles and electromagnetic and elastic waves in multilayers*, J. Phys.: Condens. Matter **7**, 5491-5506 (1995).
53. H Calás, R Rodriguez-Ramos, J A Otero, L Leija, A Ramos and G Monsivais, *Dispersion curves of shear horizontal wave surface velocities in multilayer piezoelectric systems*, Journal of Applied Physics **107**:4, 044511 (2010).
54. R Rodríguez-Ramos, H Calás, J A Otero, V Guerra, A Ramos and Y S Wang, *Shear horizontal wave in multilayered piezoelectric structures: Effect of frequency, incidence angle and constructive parameters*, International Journal of Solids and Structures **48**:20, 2941-2947 (2011).
55. Xiangyong Li and Minzhong Wang, *Three-dimensional Green's functions for infinite anisotropic piezoelectric media*, International Journal of Solids and Structures **44**:5, 1680-1684 (2007).
56. G Bonnet, *Orthotropic elastic media having a closed form expression of the Green tensor*, International Journal of Solids and Structures **46**:5, 1240-1250 (2009).

Plasmon-polariton spectra in one-dimensional Rudin-Shapiro photonic lattices

H. A. Gómez-Urrea, E. Reyes-Gómez, M. E. Mora-Ramos

Abstract

Numerical experiments concerning the Rudin-Shapiro (RS) aperiodic sequence show fractality in associated electronic spectra of RS semiconducting multilayers. However, for such quasiregular structures there are still uncertainties regarding the possible fractal properties. The present work intends to shed some light onto this problem by investigating the features of the plasmon-polariton frequency spectrum in one-dimensional photonic superlattices with Rudin-Shapiro dielectric layered unit cell. The outcome of the study shows that the reduced plasmon-polariton dispersion relation obtained within a Drude-like dielectric model exhibits a self-similar character. However, the inclusion of optical loses via absorption damping seems to destroy the self-similarity in the frequency spectrum. Therefore, a practical realization of actual fractal-like photonic RS systems might not be achievable.

H. A. Gómez-Urrea Universidad Autónoma del Estado de Morelos. Facultad de Ciencias. Cuernavaca, Morelos, Mexico
e-mail: hagu@uaem.mx

E. Reyes-Gómez
Insituto de Física. Universidad de Antioquia. Medellín. Colombia
e-mail: ereyesgomez@gmail.com

M. E. Mora-Ramos
Universidad Autónoma del Estado de Morelos. Facultad de Ciencias.
e-mail: memora@uaem.m

1 Introduction and posing of the problem

In the most recent decades there has opened a whole branch of research that assumes the feasibility of controlling the optical properties of materials. A large amount of new technological and fundamental developments would be put forward if one is able to produce –for instance– systems that respond to the incidence of electromagnetic waves with signals restricted to a given range of frequencies. Or, perhaps, just allowing their propagation along certain specific directions. Another desirable property could be the confinement of some particular radiation modes within a chosen spatial region; thus making possible to amplify the optical intensity, in a search for some kind of lasing regime.

Many of this kind of systems have come true thanks to the design and fabrication of the so-called photonic crystals. These are structures obtained from a regular disposition of materials with different indices of refraction. The basic aspects associated with a photonic crystal (PC) were presented for the first time in the reports by Yablonovitch [1] and John [2]. In their works it is established that the PCs have the property of controlling and inhibiting the spontaneous emission. This has a significant impact in solid state physics, particularly in the study of the semiconductor laser [1]. Besides, it is pointed out that the disorder in dielectric superlattices may bring about a localization of light. Summing up, the structures with periodic variations of the dielectric properties can affect the nature of the electromagnetic radiation in the crystal. This happens in such a way that the PCs show, for the electromagnetic radiation, the same distribution of allowed and forbidden frequency bands typical of the electron energy spectrum in a crystalline solid [2].

It is worth noticing at this point that the scientific literature contains some antecedents of the formulation of PCs. For instance, there is a review article by R. A. Silin [9]. The review focuses on artificial dielectrics formed as various periodic arrangements of conductive and dielectric elements. Optical propagation properties are explained in terms iso-frequency surfaces. In addition, it is stated that flat parallel slabs of artificial dielectrics may convert a divergent beam into convergent one, total reflection may appear at small incidence angles and at larger incidence angles partial reflection, increasing incidence angle

may result in decreasing refraction angle. Also, depending on the incidence angle, birefringence may occur. The work also refers to earlier experimental and theoretical research on the subject by the renowned soviet physicist L.I. Mandel'shtam [**?**], dated as back as 1947.

The existence of a photonic bandgap (PBG) implies that there is a range of frequencies for which the propagation of the light inside the system is forbidden. For example, once a PBG is present it is possible to introduce a defect within the crystal in order to trap or localize the light inside it. The introduction of a line of defects may lead to the guidance of the light from one localization to another. Then, an electromagnetic wave whose frequency lies within the PBG can propagate through such kind of waveguide. The light is kept confined and can be directed along the guide precisely because its frequency cannot propagate in the crystal [3].

The use of dielectric PCs overcomes an important problem found in metallic waveguides and cavities: the strong dissipation of visible light inside the metallic components. The consequence of this is the impossibility of an effective optical control beyond the microwave regime. The fabrication of those optical devices using PCs would allow for the desired control by means of the appropriate choice of waveguide geometry and size. Millimetric dimensions permit a control in the microwave region whereas a micrometer size makes possible to obtain such control but in the infrared part of the spectrum [3].

In this work we focus our attention on one-dimensional PCs. According to the above comments the presence of a PBG is of the utmost importance. For this reason, it is necessary to investigate the different influences or phenomena that may affect the properties of the optical bandgap.

It is a well known fact that PCs made of ordinary or right-handed materials (RHM), which are those having positive values of the refractive index, exhibit a forbidden bandgap due to the Bragg dispersion. This phenomenon is highly sensitive to the variations in the lattice constant, the angle of incidence, as well as the disorder in the crystal. This could limit the use of the PBGs in the control of the optical transmission. To overcome these limitations, a quite radical proposal is being the subject of debate and study by physicists in the recent years. This idea consists of including the so-called metamaterials in the fabrication of PCs.

The metamaterials are artificial optical structures presenting negative values of the dielectric permittivity,ε, and the magnetic permeability, μ, over some specific frequency ranges [4, 16, 6, 7]. A medium that exhibits both negative ε and negative μ within the same range of frequencies behaves as if it is a system with a negative index of refraction.

It is widely recognized that the possibility of existence of the metamaterials was theoretically formulated in 1968 by the Russian physicist Victor G. Veselago [8]. However, the scientific literature already contained some previous communications in relation with the analysis of wave propagation in a medium with negative refractive index [11, 12]. On the other hand, various artificial dielectrics composed of periodically spaced lattices of metallic rods had been intensively studied in fifties and early sixties of the last century. Although they do not possess a negative index of refraction, they exhibit a plasma-like behavior [13], and their index of refraction can be less than unity [14].

The ideas posed by Veselago remained mostly as an academic curiosity for almost thirty years. Only more recently there has been a revival of theoretical proposals on structures in which ε y μ are negative within the same interval of the optical frequency. This initiates with the work by Pendry et al. [15], and has seen a first experimental realization thanks to modern technological advances [16]. As a consequence, a new field of physics related with the materials of negative refractive index [or left-handed materials (LHM)] has made way.

In a one-dimensional PC composed of alternated RHM and LHM, unusual optical phenomena such as imaginary modes with complex frequencies as well as discrete modes come about. There appear some electromagnetic properties different to those present in dielectric structures made of only ordinary materials. In fact, a new kind of band structure appears in these systems when the average value of the index of refractive over a period of the one-dimensional PC vanishes (zeroth-order gap) [17]. Besides, once the situation of oblique incidence is considered one may detect the appearance of a plasmon-polariton gap [18]. This gap is caused by the interference between the incident light and the wave that is newly radiated by the LHM as a result of the interaction of the electromagnetic field with the material, along the growth direction.

There has also been an intense research activity regarding optical transport, dispersion and emission properties of aperiodic –or quasi-

regular– systems, specially quasi-periodic PCs. These efforts have revealed the connection between the spectral properties of the aperiodic sequences and the complex optical behavior of the resulting structures, thus giving rise to new concepts in the optical design and control of one-dimensional dielectric layered systems [19, 20, 21, 22].

The fractality in the dimensions of the spectra has been analyzed in several quasi-regular heterostructure orderings. Among these non-periodic sequences we can mention: the Fibonacci sequence, the Thue-Morse sequence, the Rudin-Shapiro (RS) sequence, etc. [23, 25, 26]. For some of these sequences the mathematicians have proved useful theorems (see, for example, those proven by Bovier and Ghez [27, 28]). But, for the time being, these exact results are limited to the so-called elementary excitations; i.e., excitations obeying a master equation which is isomorphic with the one-dimensional Schrödinger equation. Among these isomorphic excitations one finds transversal horizontal elastic modes, transversal horizontal optical modes, electromagnetic TE and TM modes, etc. However, numerical experiments performed for non-isomorphic excitations reveal that the key point of the fractal character of the spectra would be the geometric ordering, and not necessarily the complexity of the master equation [23]. This is particularly valid for the case of the RS-based heterostructures.

The RS quasi-regular sequence was initially –and independently– proposed by M. Golay (1951) [29], H. S. Shapiro (1951) [30], and W. Rudin (1957) [31]. A RS heterostructure can be generated using a four letter alphabet and their corresponding substitution rules. Then, starting with letter A, the RS sequence expands by substituting $A \to AC$, $B \to DC$, $C \to AB$, and $D \to DB$ in successive generations. Although it is a quaternary structure, the n-th generation contains only 2^n letters, just like the binary Thue-Morse and Period-Doubling sequences. Another important property of this sequence is that the same letter never appears consecutively repeated. This makes it of interest for the design of optical layered structures provided that it always keeps a dielectric contrast on both sides of a given interface, should each constituting block is set to have distinct values of ε and μ.

A numerical experiment performed by Pérez-Álvarez et al. [32] calculates the spectrum of the electron energy levels in a RS GaAs-AlGaAs semiconducting heterostructure. The outcome of the calculation is that, depending on the chosen values of layer widths and potential barrier heights the set of eigenenergies in the structure may or may

not have a fractal dimension. Since the Bovier-Ghez theorem does not fulfill for Krönig-Penney-like RS systems, the main conclusion arising from such an experiment is that the fractality of the spectrum of elementary excitations in this kind of quasi-regular structures is closely connected with the very geometry of the system.

The simple Cantor set is a paradigmatic example of fractal system. In fact, its fractal dimension is $D = \log 2/\log \approx 0.6309$. But the Cantor set has another interesting property which is called *self-similarity*.

Let us assume that the set of values corresponding to certain "spectrum" of elementary excitations has the Cantor structure. Then, if we take a fragment of the spectrum and make a zoom magnification the result will reproduce the entire spectrum, and so it happens when – using the same magnification factor– we perform the same zooming process within an arbitrary portion of the originally selected fragment. This is the property of self-similarity, and it has been proved that self-similar sets have fractal dimension [33].

Then, if some kind of self-similarity manifests during the calculation of the optical spectrum of a RS-based dielectric layered heterostructure, one would be able to support the existence of a fractality associated with this particular quasi-regular sequence in a physical system. For this reason, the present work deals with an investigation of the properties of plasmon-polariton modes in one-dimensional photonic crystals with RS unit cell, under oblique light incidence.

The RS basis will consist of passive layers with positive indices of refraction, together with active layers showing a Drude-like response both the dielectric permittivity and magnetic permeability. These layers may behave as metamaterials for certain values of the frequency. The study takes into account both the presence and absence of optical absorption effects in the structure.

2 Preliminary theoretical concepts

2.1 Maxwell equations and the Drude Model

2.1.1 Maxwell equations

The study of light propagation in a PC implies the solution of the Maxwell equations governing the behavior of the electromagnetic field in the substance. If no free charge densities are present in the material system, these equations have the form;

$$\nabla \cdot \mathbf{B} = \mathbf{0}, \tag{1}$$

$$\nabla \cdot \mathbf{D} = \mathbf{0}, \tag{2}$$

$$\nabla \times \mathbf{E} = -\frac{\mathbf{1}}{\mathbf{c}} \frac{\partial \mathbf{B}}{\partial \mathbf{t}}, \tag{3}$$

and

$$\nabla \times \mathbf{H} = \frac{\mathbf{1}}{\mathbf{c}} \frac{\partial \mathbf{D}}{\partial \mathbf{t}}. \tag{4}$$

Vectors **D** y **H** connect with vectors **E** y **B**, respectively, by means of constitutive relations. In the case of linear media

$$\mathbf{D} = \varepsilon(\mathbf{r})\mathbf{E}, \tag{5}$$

and

$$\mathbf{B} = \mu(\mathbf{r})\mathbf{H}, \tag{6}$$

being ε and μ the dielectric permittivity and the magnetic permeability of the medium, respectively. The electromagnetic field may also be described with the use of vector and scalar potential functions: **A**, ϕ. This fact exploits the important property of the Maxwell equations known as gauge invariance. Then, we may write

$$\mathbf{E} = -\nabla\phi - \frac{\mathbf{1}}{\mathbf{c}} \frac{\partial \mathbf{A}}{\partial \mathbf{t}}, \tag{7}$$

$$\mathbf{B} = \nabla \times \mathbf{A}. \tag{8}$$

and using the so-called Coulomb gauge we set $\phi = 0$. Therefore,

$$\mathbf{E} = -\frac{\mathbf{1}}{\mathbf{c}}\frac{\partial \mathbf{A}}{\partial \mathbf{t}}, \tag{9}$$

$$\mathbf{B} = \nabla \times \mathbf{A}. \tag{10}$$

According to the equations (2), (5), y (9)

$$0 = \nabla \cdot \mathbf{D} = \nabla \cdot (\varepsilon \mathbf{E}) = -\nabla \cdot \left[\varepsilon \frac{\mathbf{1}}{\mathbf{c}}\frac{\partial \mathbf{A}}{\partial \mathbf{t}}\right] = -\frac{\mathbf{1}}{\mathbf{c}}\frac{\partial}{\partial \mathbf{t}}\nabla \cdot (\varepsilon \mathbf{A})$$

and we obtain

$$\nabla \cdot [\varepsilon \mathbf{A}] = \mathbf{0}. \tag{11}$$

2.1.2 The Drude Model

The optical properties of metals can be explained, over a wide interval of frequencies, with the use of the Drude model (P. Drude (1900) [34]). In order to guarantee the electrical neutrality, the model assumes the metal as a collection of electrons and positively charged heavy particles (ions or nuclei). The electron subsystem behaves as an ideal classical –charged– gas whilst the heavy particles remain motionless. The motion of electrons in the gas under the effect of an external electric field is described within the kinetic theory of gases.

An estimation of number of electrons per unit volume in a real monatomic metal, n, gives

$$n = 0,6022 * 10^{23}\frac{Z\rho_m}{A}, \tag{12}$$

where Z is the number of valence electrons in the atom, and A is the atomic mass of the metallic element. ρ_m is the mass density in g/cm^3. Typically, this electron density is of the order of 10^{22} conduction electrons per cubic centimeter. Such a value is three orders of magnitude above the volume density of a classical ideal gas under normal pressure and temperature conditions. In spite of this fact and the existence of strong electron-electron and electron-ion Coulombic interactions

in the system, Drude used the kinetic theory for electrons in a metal, with only a few modifications:

- The gas reaches the thermodynamical equilibrium with its surrounds through a scattering mechanism associated to electron-ion collisions.
- The collisions constitute a sort of instant events which abruptly change the electron velocity. These changes are attributed to rebounds of the electrons after hitting the rigid shell of the ionic cores. The electron-electron collisions are neglected.
- Between collisions, the electrons behave as free particles and move along a straight line in absence of an external electromagnetic field. When external fields are applied, the electron motion obeys the Newtonian laws, but ignoring all the additional interactions with other electrons and the ions.
- One electron suffers a collision with a probability per unit time of $\frac{1}{\tau}$. The quantity τ is known as mean free time or *relaxation time*. An electron will travel freely in the gas during a time period equals to τ before its next collision. Under normal conditions the value of the relaxation time in a metal is of $10^{-15} - 10^{-14}$ s.

Using this ideas we should be able to derive the constitutive relations for a metal. The equation of motion for the k-th electron (with charge e and mass m) in the presence of an external electric field is:

$$\begin{aligned} m\frac{d}{dt}\mathbf{v_k}(\mathbf{t}) &= -m\gamma\mathbf{v_k}(\mathbf{t}) + \mathbf{eE}(\mathbf{t}), \quad \gamma = \frac{\mathbf{1}}{\tau} \\ \frac{d}{dt}\mathbf{v_k}(\mathbf{t}) &= -\gamma\mathbf{v_k}(\mathbf{t}) + \frac{\mathbf{e}}{\mathbf{m}}\mathbf{E}(\mathbf{t}) \end{aligned} \tag{13}$$

This equation contains the accelerating part proportional to the electric field as well as a braking effect associated to collisions which is proportional and opposite to the electron velocity. The model neglects the local variations in the electric field given that the velocities of interest are much smaller than the speed of light, c. Besides, the atomic-scale variations are not significant within a classical approach like the Drude one. The physical interpretation of the friction term is inferred directly from the equation of motion for the electron velocity in absence of the external field;

$$\frac{d}{dt}\mathbf{v_k}(\mathbf{t}) = -\gamma \mathbf{v_k}(\mathbf{t}) \Longrightarrow \mathbf{v_k}(\mathbf{t}) = \mathbf{v_{0k}} \exp(-\gamma \mathbf{t}). \tag{14}$$

That is, any initial velocity $\mathbf{v_0}$ decreases its magnitude exponentially as a function of the time due to the electron-ion collision-related scattering. In this case, $\tau = \frac{1}{\gamma}$ is the characteristic time of decay; the relaxation time. By rewriting the equation of motion as

$$\frac{d}{dt}\left[\exp(\gamma t)\mathbf{v_k}(\mathbf{t})\right] = -\frac{e}{m}\exp(\gamma t)\mathbf{E}(\mathbf{t}), \tag{15}$$

and considering the time variation of the applied field in the form $\mathbf{E_k} = \mathbf{E_{0k}}\exp(-\mathbf{i}\omega\mathbf{t})$ –with the additional assumption that the wavelength of the incident radiation is large compared with the average distance of electron free traveling–, we have

$$\frac{d}{dt}\left[\exp(\gamma t)\mathbf{v_k}(\mathbf{t})\right] = -\frac{e}{m}\exp(\gamma t)\mathbf{E_0}\exp(-\mathbf{i}\omega\mathbf{t}), \tag{16}$$

and the solution is

$$\mathbf{v_k}(\mathbf{t}) = -\frac{\mathbf{e}}{\mathbf{m}}\mathbf{E_{0k}}\int_{-\infty}^{\mathbf{t}} \mathbf{dt}' \exp(-\omega \mathbf{t}')\exp\left[\gamma(\mathbf{t}-\mathbf{t}')\right]. \tag{17}$$

In this expression, the upper and lower limits of integration define a time t', previous to the application of the external field and the time of observation, respectively. The response of the metal to the applied electric field is nonlocal in time. That is, the electron velocity at a given time depends on the values taken by the electric field at earlier instants. The larger contribution to the integral (17) comes from the region in which the time differences are of the order of $\frac{1}{\gamma}$, $\mathbf{v_k}(\mathbf{t}) = -\frac{\mathbf{e}}{\mathbf{m}}\mathbf{E_0}\int_{-\infty}^{\mathbf{t}} \mathbf{dt}' \exp(-\mathbf{i}\omega\mathbf{t}')$.

Solving the integral (17) leads to,

$$\frac{d}{dt}\mathbf{r_k}(\mathbf{t}) = -\frac{\mathbf{e}}{\mathbf{m}}\frac{\mathbf{E_0}\exp(-\mathbf{i}\omega\mathbf{t})}{\gamma - \mathbf{i}\omega}, \tag{18}$$

and then;

$$\mathbf{r_k}(\mathbf{t}) = -\frac{\left(\frac{\mathbf{e}}{\mathbf{m}}\right)\mathbf{E}}{\omega(\omega + \mathbf{i}\gamma)}. \tag{19}$$

The assumptions made in the formulation of the model imply that the only contribution to the electric polarization in the system comes

form the electrons. The polarization, defined as the dipole moment per unit volume is given by

$$\mathbf{P} = (\varepsilon - \mathbf{1})\varepsilon_{\mathbf{0}}\mathbf{E} = -\mathbf{Ner(t)} = -\frac{\frac{\mathbf{Ne^2}}{\mathbf{m}}\mathbf{E}}{\omega(\omega + \mathbf{i}\gamma)}, \tag{20}$$

where N is the conduction electron density, with each electron contributing independently to the polarization. The relative dielectric permittivity is then expressed as;

$$\varepsilon(\omega) = 1 - \frac{\frac{Ne^2}{\varepsilon_0 m}}{\omega(\omega + i\gamma)} = 1 - \frac{\omega_p}{\omega(\omega + i\gamma)}, \tag{21}$$

where we have defined the plasma frequency, $\omega_p \equiv \sqrt{\frac{Ne^2}{\varepsilon_0 m}}$. From the above equation it is noticed that the real part of the dielectric permittivity is negative in the interval of frequencies $\omega < \omega_p$. For frequencies below ω_p the charges can move fast enough such as the electromagnetic radiation remains inside the medium. If, on the other hand, the frequencies are larger than the plasma frequency, the system behaves as an ordinary dielectric medium.

The physical meaning of the quantity ω_p is to be the natural frequency of a collective excitation in the electron gas. Let us consider a small displacement (Δ) of the whole electron gas with respect to the fixed ions. As a consequence, there is an accumulation of negative charge towards one side of the system and also there will be an accumulation of positive charge on the opposite side. Due to this charge separation, an electric field of intensity $E = Ne\Delta/\varepsilon_0$ appears, oriented along the displacement direction. The force acting over a single electron is $F = -Ne^2/\varepsilon_0\Delta$. This means that the electrons are influenced by a restoring force which is proportional to the displacement. The resulting electron motion is of oscillatory type and its frequency is $\omega_p \equiv \sqrt{\frac{Ne^2}{\varepsilon_0 m}}$; that is, the plasma frequency. The plasma (charged gas) oscillations are named plasmonic modes. These modes are dispersionless.

2.2 Left-handed materials

The Drude model predicts frequency regions of negative ε and μ, provided the loses in the medium are small enough [35]. Although loses can prevent the observation of this property, it is possible to find media that exhibit negative permittivity in nature (plasmas, metals and, under certain conditions, semiconductors). Media with negative magnetic permeability are much less common. Only the ferromagnetic materials have revealed the possibility of presenting regions negative μ, given the larger strength of the magnetic interactions in them. Here, we will briefly describe some properties of the light propagation in LHM.

2.2.1 Propagation of electromagnetic waves in left-handed materials

To analyze the propagation of an electromagnetic wave in a LHM, let us consider the equation

$$\left(\nabla^2 - \frac{n^2}{c^2}\frac{\partial^2}{\partial t^2}\right)\psi = 0, \tag{22}$$

where n is the refractive index, c is the speed of light in vacuum, and $\frac{n^2}{c^2} = \varepsilon\mu$. Since the squared refractive index is not affected by simultaneous changes in sign, one might think that the solutions of the equation (22) would remain unaltered after a simultaneous change in the sign of ε y μ. However, when the Maxwell equations are explicitly considered;

$$\nabla \times \mathbf{E} = -\mathbf{i}\omega\mu\mathbf{H} \tag{23}$$

$$\nabla \times \mathbf{H} = -\mathbf{i}\omega\varepsilon\mathbf{E}, \tag{24}$$

it becomes evident that these solutions are quite different. In fact, for a plane wave of the type $\mathbf{E} = \mathbf{E_0}\mathbf{e}^{(-\mathbf{i}\mathbf{K}\cdot\mathbf{r}+\mathbf{i}\omega\mathbf{t})}$ y $\mathbf{H} = \mathbf{H_0}\mathbf{e}^{(-\mathbf{i}\mathbf{K}\cdot\mathbf{r}+\mathbf{i}\omega\mathbf{t})}$, the former equations reduce to

$$\mathbf{k} \times \mathbf{E} = \omega\mu\mathbf{H} \tag{25}$$

$$\mathbf{k} \times \mathbf{H} = -\omega\varepsilon\mathbf{E}. \tag{26}$$

Therefore, in the case of positive ε and μ, $\mathbf{E}$, $\mathbf{H}$, and $\mathbf{k}$ form a right-handed orthogonal system. But, if $\varepsilon < 0$ and $\mu < 0$, then the equations (25) and (26) can be written as

$$\mathbf{k} \times \mathbf{E} = -\omega|\mu|\mathbf{H} \tag{27}$$

$$\mathbf{k} \times \mathbf{H} = \omega|\varepsilon|\mathbf{E}, \tag{28}$$

from which it is revealed that $\mathbf{E}$, $\mathbf{H}$, and $\mathbf{k}$ form a left-handed orthogonal system.

The main physical implication of the former analysis is the so-called *backward propagation* [**?**]. In fact, the direction of the average energy flux is determined by the real part of the Poynting vector

$$\mathbf{S} = \frac{\mathbf{1}}{\mathbf{2}}\mathbf{E} \times \mathbf{H}^*, \tag{29}$$

which is not affected by the simultaneous change in the sign of ε and μ. Thus, the vectors $\mathbf{E}$, $\mathbf{H}$, and $\mathbf{S}$ keep forming a right-handed triplet in a left-handed medium. This means that is such media the energy and the wavefronts travel in opposite directions –the backward wave propagation. It is possible to observe the phenomenon of backward propagation in the case of non-uniform waveguides [**?**, **?**].

In the former discussion we did not take into account the loses. Nonetheless, loses are unavoidable in any practical material. To include such an effect, let us consider a finite medium consisting of an homogeneous LHM. In the steady state, and whenever no sources are found within the region, there must be some kind of power flux in order to compensate the loses. So, from the complex Poynting theorem [36];

$$\nabla \cdot (\mathbf{E} \times \mathbf{H}^*) = i\omega \left(\mathbf{E} \cdot \mathbf{D}^* - \mathbf{B} \cdot \mathbf{H}^*\right), \tag{30}$$

with which

$$\Re\left[\oint \mathbf{E} \times \mathbf{H}^* \cdot \mathbf{ndS}\right] = \omega\Im\left[\int \left(\mu|\mathbf{H}|^{\mathbf{2}} - \varepsilon^*|\mathbf{E}|^{\mathbf{2}}\right) dV\right] \quad < 0, \tag{31}$$

where the integration is performed on the mentioned region. Thus, we have,

$$\Im(\varepsilon) < 0; \qquad \Re(\mu) < 0. \tag{32}$$

Let us consider now a plane wave with squared wavenumber $k^2 = \omega^2 \mu \varepsilon$, that propagates in a LHM with dielectric loses in which $\Re(\varepsilon) < 0$ and $\Re(\mu) < 0$. From the expression (32), it follows that $\Im(k^2) > 0$. Therefore

$$[\Re(k) > 0 \quad y \quad \Im(k) > 0] \quad o \quad [\Re(k) < 0 \quad y \quad \Im(k) < 0] \tag{33}$$

That is, the oscillations grow along the propagation direction of the wavefronts. This fact is in agreement with the previously mentioned backward wave propagation.

2.2.2 Energy density and group velocity

When negative values of ε are μ are introduced in the usual expression for the average energy density of a non-dispersive transparent medium,

$$U_{nd} = \frac{1}{4}\left(\varepsilon |\mathbf{E}|^2 + \mu |\mathbf{H}|^2\right), \tag{34}$$

they produce a physically meaningless negative energy density. However, as it is well known, any non-vacuum physical medium must be a dispersive one, and the equation (34) is, in such case, only a very simple approximation. The correct approach for a monochromatic wavepacket propagating along a dispersive medium is [37]

$$U = \frac{1}{4}\left(\frac{\partial(\omega\varepsilon)}{\partial\omega}|\mathbf{E}|^2 + \frac{\partial(\omega\mu)}{\partial\omega}|\mathbf{H}|^2\right), \tag{35}$$

where the derivatives are evaluated at the central frequency of the wavepacket. Hence, the physical requirement for a positive density of energy implies that

$$\frac{\partial(\omega\varepsilon)}{\partial\omega} > 0 \quad y \quad \frac{\partial(\omega\mu)}{\partial\omega} > 0, \tag{36}$$

which is compatible with the fact that $\varepsilon < 0$ and $\mu < 0$ when the conditions $\frac{\partial \varepsilon}{\partial \omega} > |\varepsilon|/\omega$ and $\frac{\partial \mu}{\partial \omega} > |\mu|/\omega$ fulfill. Thus, a LHM must be a highly dispersive medium. This is in accordance with the Drude model, which predicts negative values of ε and/or μ in highly dispersive regions, just above the resonance. It is also important to mention that the interpretation related with the imaginary part of the complex Poynting theorem –that relates the flux of reative power through a closed surface [38]–, can not be applied in the case of highly dispersive media, in which the equation (35) is replaced by 36).

The backward wave propagation implies that the signs of the phase and group velocities are opposite. In fact,

$$\frac{\partial k^2}{\partial \omega} = 2k\frac{\partial k}{\partial \omega} \equiv 2\frac{\omega}{v_p v_g}, \tag{37}$$

where $v_p = \omega/k$ and $v_g = \partial\omega/\partial k$, are, the phase and group velocity, respectively. Besides from $k^2 = \omega^2\varepsilon\mu$ and the equation (36),

$$\frac{\partial k^2}{\partial \omega} = \omega\varepsilon\frac{\partial(\omega\mu)}{\partial \omega} + \omega\mu\frac{\partial(\omega\varepsilon)}{\partial \omega} < 0. \tag{38}$$

Finally, from equations (37) and (38) we obtain

$$v_p v_g < 0. \tag{39}$$

This property means that the wavepacket and the wavefront travel along opposite directions, and can be considered as an additional proof of the wave backward propagation in a LHM.

2.3 Negative refraction

We will consider now the refraction of an incident light ray at the interface between an ordinary medium ($\varepsilon > 0$ and $\mu > 0$) and a LHM. The boundary conditions imply the continuity of the tangential component of the wavevector all along the interface. Due to the above mentioned backward propagation in a LHM region it follows immediately that, contrary to the ordinary refraction case, the angles of incidence and refraction must have opposite signs. The figure 1 illustrates such effect.

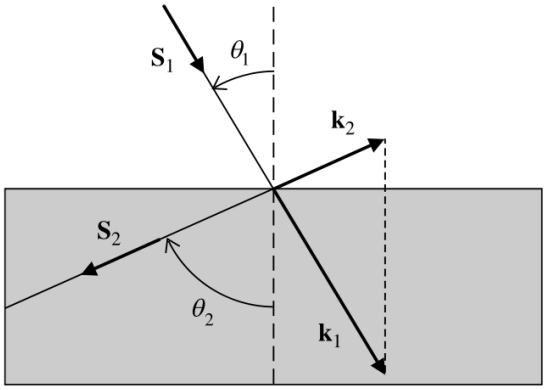

Fig. 1 Graphical demonstration of negative refraction between an ordinary medium (upper part) and a LHM (lower part). The Poynting vector and the wavevector for each medium are respectively labeled as $\mathbf{S}_1$, $\mathbf{S}_2$, $\mathbf{k}_1$, and $\mathbf{k}_2$. The negative refraction comes from the continuity of the wavevector components, $\mathbf{k}_1$ and $\mathbf{k}_2$, parallel to the interface, and from the fact that the rays propagate along the direction of propagation of the energy flux. That is, they would have to be parallel to the corresponding Poynting vectors $\mathbf{S}_1$ y $\mathbf{S}_2$.

From the continuity of the tangential components of the wavevector, the incident ray and the refracted ray it follows that

$$\frac{\sin\theta_i}{\sin\theta_r} = \frac{-|\mathbf{k}_2|}{|\mathbf{k}_1|} \equiv \frac{n_2}{n_1} < 0, \tag{40}$$

which is –well– known as Snell law. In this expression n_1 and n_2 are the refractive indices of the ordinary medium and the LHM respectively. Assuming that $n_1 > 0$, from equation (40) follows that $n_2 < 0$. In other words, the sign in front of the square root should be the negative one [8]

$$n \equiv -c\sqrt{\varepsilon\mu} < 0. \tag{41}$$

For this reason, the LHM are also called as negative refraction index materials or negative refraction media.

The geometrical optics of systems containing LHM is dominated by the equation (41). By tracing the rays's paths throughout conventional lenses made of LHM it is possible to show that concave lenses behave as convergent lenses whereas convex lenses behave as divergent lenses [8]. However, the most interesting feature of the LHM that can be derived within the geometrical optics is the concentration of the energy coming from a point source [8]. This effect is shown in the figure 2.

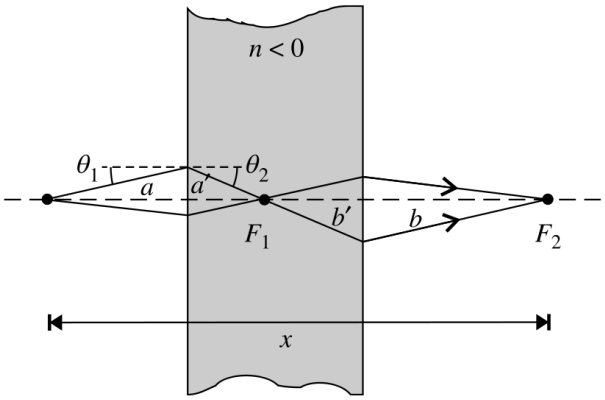

Fig. 2 Graphical illustration of the concentration of paraxial rays coming from a point source by a LHM. The light focuses in two points, F_1 and F_2, inside and outside the material.

In the case of paraxial rays

$$|n| = \frac{|\sin\theta_1|}{|\sin\theta_2|} \simeq \frac{|\tan\theta_1|}{|\tan\theta_2|} = \frac{a^{'}}{a} = \frac{b^{'}}{b}, \tag{42}$$

where n is the index of refraction of the LHM, relative to the surrounding media. In consequence, as it can observed from Fig. 2, the electromagnetic energy coming from a point source concentrates in two points. One of them lies within the LHM and the other locates outside of the LHM layer, at a distance

$$x = a + a^{'} + b + b^{'} = d + \frac{d}{|n|} \tag{43}$$

from the source; where d is the width of the LHM layer. If $n = -1$ the aforementioned effect does not restrict only to paraxial rays because, in such case, $|\theta_1| = |\theta_2|$ for some angle of incidence. In fact, when $n = -1$ all rays coming from a source are concentrated in two points, one inside and one outside the layer; the latter being at a distance equals to $2d$ from the source.

3 The plasmon-polariton problem

As we mentioned above, the plasma frequency can be physically interpreted as a collective excitation of a free electron gas. The small oscil-

lations of such gas when it is slightly departed from its original position in a metal characterize by a frequency ω_p. Then, one may define a plasmon to be the quantum of the plasma oscillation whose frequency is precisely the plasma frequency ω_p. Then a plasmon mode occurs when the frequency ω becomes equal to the plasmon frequency.

The metal surface can also contain surface plasmons. These are basically electromagnetic modes that propagate on the surface of the metal and originate in the process of interaction of the light with the free electrons in the metal. An important feature of these modes is that they allow for a significant light concentration in the metallic surfaces of volumes with dimensions much smaller that the incident light wavelength.

3.1 Surface plasmon-polaritons

The surface plasmon-polaritons (SPP) are electromagnetic excitations that propagate in the interface between a dielectric and a conductor. They are confined in the perpendicular direction and originate from the coupling of the electromagnetic field with the plasma oscillations of the electrons in the conductor.

To study the properties of the SPP it is necessary to apply the Maxwell equations (1), (2), (3), and (4) to the case of a plane interface separating a conducting and a dielectric media. In absence of external charges and current densities, the equations (2) y (4) can be combined to obtain

$$\nabla \times \nabla \times \mathbf{E} = -\mu_0 \frac{\partial^2 \mathbf{D}}{\partial t^2}. \tag{44}$$

Using the identities $\nabla \times \nabla \times \mathbf{E} \equiv \nabla(\nabla \cdot \mathbf{E}) - \nabla^2 \mathbf{E}$, and $\nabla \cdot (\varepsilon \mathbf{E}) \equiv \mathbf{E} \cdot \nabla \varepsilon + \varepsilon \nabla \cdot \mathbf{E}$, and keeping in mind that, due to the absence of any external influence, $\nabla \cdot \mathbf{D} = 0$, the equation (44) can be put as

$$\nabla \left(-\frac{1}{\varepsilon} \mathbf{E} \cdot \nabla \varepsilon \right) - \nabla^2 \mathbf{E} = -\mu_0 \varepsilon_0 \varepsilon \frac{\partial^2 \mathbf{E}}{\partial t^2}. \tag{45}$$

For negligible variations of the dielectric permittivity $\varepsilon = \varepsilon(\mathbf{r})$ along distance of the order of the optical wavelength, the equation 45) becomes

$$\nabla^2\mathbf{E} - \frac{\varepsilon}{c^2}\frac{\partial^2\mathbf{E}}{\partial t^2} = 0. \tag{46}$$

A suitable solution of this equation that can explain the propagation of surface waves is reached in two steps. First, a harmonic dependence of the electric field, $\mathbf{E}(\mathbf{R},t) = \mathbf{E}(\mathbf{r})e^{-i\omega t}$, is assumed. The substitution in (46) gives

$$\nabla^2\mathbf{E} + k_0^2\varepsilon\mathbf{E} = 0, \tag{47}$$

where $k_0 = \omega/c$ is the wavevector propagating in vacuum. The equation (47) is known as Helmholtz equation. The next step involves defining the geometry. We assume for simplicity a one-dimensional problem; that is ε is taken to depend only on one spatial coordinate. More specifically, the waves will propagate along the x-axis direction. NO spatial variation along the y-axis is present (see Fig. 3). Therefore, $\varepsilon = \varepsilon(z)$. We are considering the $z = 0$ plane to coincide with the interface bearing the wave propagation. The solution can now be put in the form $\mathbf{E}(x,y,z) = \mathbf{E}(z)e^{i\beta x}$. The parameter $\beta = k_x$ is called the *travel wave propagation constant* and corresponds to the components of the wavevector in the direction of propagation. Inserting this expression in the equation (47) one may reach to the desired wave equation

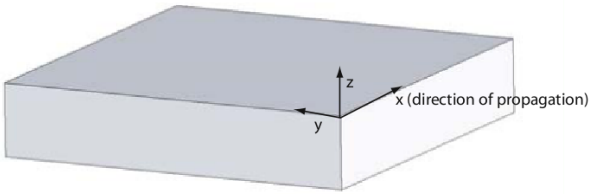

Fig. 3 The geometry of a plane waveguide. The waves propagate along the x-axis direction.

$$\frac{\partial^2\mathbf{E}(z)}{\partial z^2} + \left(k_0^2\varepsilon - \beta^2\right)\mathbf{E} = 0. \tag{48}$$

Naturally, a totally equivalent equation exists for the magnetic field $\mathbf{H}$.

Equation (48) is the starting point for the analysis of the electromagnetic modes in a waveguide. The use of this equation to determine the spatial field profile will need to have explicit expressions for the components of $\mathbf{E}$ y $\mathbf{H}$. This can be achieved in a simple manner with

the use of the equations (2) and (4). For a harmonic time dependence $\left(\frac{\partial}{\partial t} = -i\omega\right)$, we arrive to the following set of coupled equations

$$\frac{\partial E_z}{\partial y} - \frac{\partial E_y}{\partial z} = i\omega\mu_0 H_x, \tag{49}$$

$$\frac{\partial E_x}{\partial z} - \frac{\partial E_z}{\partial x} = i\omega\mu_0 H_y, \tag{50}$$

$$\frac{\partial E_y}{\partial x} - \frac{\partial E_x}{\partial y} = i\omega\mu_0 H_z, \tag{51}$$

$$\frac{\partial H_z}{\partial y} - \frac{\partial H_y}{\partial z} = -i\omega\varepsilon_0\varepsilon E_x, \tag{52}$$

$$\frac{\partial H_x}{\partial z} - \frac{\partial H_z}{\partial x} = -i\omega\varepsilon_0\varepsilon E_y, \tag{53}$$

$$\frac{\partial H_y}{\partial x} - \frac{\partial H_x}{\partial y} = -i\omega\varepsilon_0\varepsilon E_z. \tag{54}$$

This group of equations simplifies if one considers a propagation along x, $\left(\frac{\partial}{\partial x} = i\beta\right)$, homogeneous in the y-direction, $\left(\frac{\partial}{\partial y} = 0\right)$. The system then becomes

$$\frac{\partial E_z}{\partial y} = i\omega\mu_0 H_x, \tag{55}$$

$$\frac{\partial E_x}{\partial z} - i\beta E_z = i\omega\mu_0 H_y, \tag{56}$$

$$i\beta E_y = i\omega\mu_0 H_z, \tag{57}$$

$$\frac{\partial H_y}{\partial z} = i\omega\varepsilon_0\varepsilon E_x, \tag{58}$$

$$\frac{\partial H_x}{\partial z} - i\beta H_z = -i\omega\varepsilon_0\varepsilon E_y, \tag{59}$$

$$i\beta H_y = -i\omega\varepsilon_0\varepsilon E_z; \tag{60}$$

and has two sets of self-consistent solutions with different wave polarization properties. The first set are the so-called *transverse magnetic modes* (TM or P), in which only the components E_x, E_z and H_y are different from zero. The second set of solutions are the transverse electrical modes (TE or S), with only the components H_x, H_z y E_y different from zero.

The equations for the TM modes reduce to

$$E_x = -i\frac{1}{\omega\varepsilon_0\varepsilon}\frac{\partial H_y}{\partial z} \tag{61}$$

$$E_z = -\frac{\beta}{\omega\varepsilon_0\varepsilon}H_y, \tag{62}$$

and the TM equation of motion is

$$\frac{\partial^2 H_y}{\partial z^2} + \left(k_0^2\varepsilon - \beta^2\right)H_y = 0. \tag{63}$$

The analogous for the TE case is the set

$$H_x = i\frac{1}{\omega\mu_0}\frac{\partial E_y}{\partial z} \tag{64}$$

$$H_z = -\frac{\beta}{\omega\mu_0\varepsilon}E_y, \tag{65}$$

with the TE wave equation to be of the form

$$\frac{\partial^2 E_y}{\partial z^2} + \left(k_0^2\varepsilon - \beta^2\right)E_y = 0. \tag{66}$$

Then, the surface plasmon-polariton modes can be described with the use of these previous equations.

3.2 Interface surface plasmon-polaritons

The most simple geometry that can bear a SPP is the plane interface (see figure 4): A region $z > 0$ with a real and positive value of the dielectric constant ε_2, and a region $z < 0$ taken to be conducting and described through a dielectric function $\varepsilon_1(\omega)$. The requirement of a

metallic character implies that $\mathrm{Re}[\varepsilon] < 0$. This condition fulfills when the frequencies are below ω_p. We want to find the solutions for the propagation of the wave confined at the interface. Let us examine first the solutions for the TM case, using the set of equations (61) to (63)

$$H_y(z) = A_2 e^{i\beta x} e^{-k_2 z}, \tag{67}$$

$$E_x(z) = iA_2 \frac{1}{\omega\varepsilon_0\varepsilon_2} k_2 e^{i\beta x} e^{-k_2 z}, \tag{68}$$

and

$$E_z(z) = -A_1 \frac{\beta}{\omega\varepsilon_0\varepsilon_2} e^{i\beta x} e^{-k_2 z}; \tag{69}$$

for $z > 0$ and

$$H_y(z) = A_1 e^{i\beta x} e^{k_1 z}, \tag{70}$$

$$E_x(z) = -iA_1 \frac{1}{\omega\varepsilon_0\varepsilon_1} k_1 e^{i\beta x} e^{k_1 z}, \tag{71}$$

and

$$E_z(z) = -A_1 \frac{\beta}{\omega\varepsilon_0\varepsilon_1} e^{i\beta x} e^{k_1 z}. \tag{72}$$

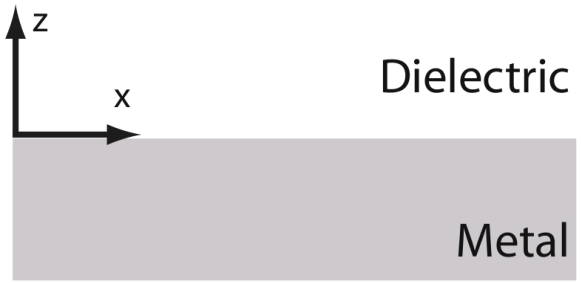

Fig. 4 Geomatry of the surface plasmon-polariton propagation at an interface between a dielectric and a metal.

when $z < 0$. $k_i \equiv k_{zi}$ $(i = 1,2)$ is the component of the wavevector perpendicular to the interface between the two media. Its reciprocal

value, $\hat{z} = 1/|k_z|$, defines the decay length of the field perpendicular to the interface and quantifies the wave confinement. The continuity of H_y and $\varepsilon_i E_z$ at the interface requires that $A_1 = A_2$ and

$$\frac{k_2}{k_1} = \frac{\varepsilon_2}{\varepsilon_1}. \tag{73}$$

Notice that in the convention of signs adopted for the set of equations (61) to (63) and (54) to (65), the confinement at the surface demands that $\mathrm{Re}[\varepsilon_1] < 0$ if $\varepsilon_2 > 0$. In such a way, the surface waves only exist at the interfaces between materials with opposite signs of the real part of their dielectric permittivities. That is, when they are a conductor and an insulator. Besides, the expression for H_y must obey the wave equation (69) leading to

$$k_1^2 = \beta^2 - k_0^2 \varepsilon_1 \tag{74}$$

$$k_2^2 = \beta^2 - k_0^2 \varepsilon_2. \tag{75}$$

By combining these equations with (73) we reach to the dispersion relation for the SPP modes propagating between the two spaces,

$$\beta = k_0 \sqrt{\frac{\varepsilon_1 \varepsilon_2}{\varepsilon_1 + \varepsilon_2}}. \tag{76}$$

This expression is valid both for real and complex permittivity ε_1. That is to say, for conductors with and without attenuation.

Let us analyze now the possibility of surface TE modes. Using the set of equations (64) to (66) we obtain the respective expressions for the field components,

$$E_y(z) = A_2 e^{i\beta x} e^{-k_2 z}, \tag{77}$$

$$H_x(z) = -iA_2 \frac{1}{\omega \mu_0} k_2 e^{i\beta x} e^{-k_2 z}, \tag{78}$$

and

$$H_z(z) = A_2 \frac{\beta}{\omega \mu_0} k_2 e^{i\beta x} e^{-k_2 z}; \tag{79}$$

for $z > 0$ and

$$E_y(z) = A_1 e^{i\beta x} e^{k_1 z}, \tag{80}$$

$$H_x(z) = iA_1 \frac{1}{\omega\mu_0} k_1 e^{i\beta x} e^{k_1 z}, \tag{81}$$

and

$$H_z(z) = A_1 \frac{\beta}{\omega\mu_0} e^{i\beta x} e^{k_1 z}; \tag{82}$$

in the case of $z < 0$. The continuity of E_y and H_x at the interface leads to the condition

$$A_1(k_1 + k_2) = 0. \tag{83}$$

Given that the surface confinement requires that $\mathrm{Re}[k_1] > 0$ y $\mathrm{Re}[k_2] > 0$, the previous condition only fulfills if $A_1 = 0$. This also means that $A_2 = A_1 = 0$. Then, no surface modes exist for the TE polarization. The SPP modes only appear for the TM case.

4 Electric and magnetic transverse modes in a one-dimensional photonic crystal

In this section we shall work out the procedure for the obtention of the dispersion relations in a one-dimensional photonic crystal (1DPC). With this goal, the equations for the propagation of the TE and TM modes in this kind of systems are derived. On the other hand, we describe the transfer matrix method that allows to calculate the transmission coefficient (TC) and the reflection coefficient (RC) of the wave, taking into account the conditions of continuity of the field at the interfaces between the different layers in the crystal.

A transverse mode of an electromagnetic wave is the profile of the field in a plane perpendicular (transversal) to the propagation direction. To obtain this kind of modes in the problem under study we are going to find the equations describing the field by taking the rotational in the equation (3), taking into account the expressions (4), (5), and (6). The general equation for the electric field is

$$-\nabla^2\mathbf{E}-\nabla\left[\frac{\nabla(\mu\varepsilon)}{\mu\varepsilon}\cdot\mathbf{E}\right]+(\mathbf{E}\cdot\nabla)\left(\frac{\nabla\mu}{\mu}\right)+\left[\left(\frac{\nabla\mu}{\mu}\right)\cdot\nabla\right]\mathbf{E}-\frac{\mu\varepsilon}{c^2}\omega^2\mathbf{E}=0. \tag{84}$$

Analogously, taking the rotational of the equation (4) and considering (4), (5), and (6) we are able to obtain the general equation for the magnetic field

$$-\nabla^2\mathbf{H}-\nabla\left[\frac{\nabla(\mu\varepsilon)}{\mu\varepsilon}\cdot\mathbf{H}\right]+[\mathbf{H}\cdot\nabla]\left(\frac{\nabla\varepsilon}{\varepsilon}\right)+\left[\left(\frac{\nabla\varepsilon}{\varepsilon}\right)\cdot\nabla\right]\mathbf{H}-\frac{\mu\varepsilon}{c^2}\omega^2\mathbf{H}=0. \tag{85}$$

Equations (84) and (85) contain all the necessary information about the vectors **E** and **H** respectively. Accordingly, for a structure with a given permittivity, the solution of the equation (85) gives the modes for $\mathbf{H}(\mathbf{r})$ with their corresponding frequencies. To later determine the electric field, we must use equation (4). It is also possible to find **H** by solving (84), to find the modes of **E** with the corresponding frequencies, to determine **H** with the equation (3), subsequently.

Then, applying symmetry arguments it is possible to describe the allowed electromagnetic modes in the PC. The system is taken to be periodic along the z direction, and homogeneous in the xy plane. Thus, we obtain the field modes with the k vector in the direction of the z-axis.

4.1 Transverse electric modes

For the TE modes the vector **E** is perpendicular to the plane of incidence. Here we consider the physical situation depicted in the figure **??**, where xz is the plane of incidence and θ is the angle of incidence ($\theta = 0 \rightarrow$ normal incidence). Let us assume that z is the growth direction of the metamaterial formed by the periodic deposition of a layer 1 with refractive index n_1, dielectric constant ε_1 and magnetic permeability μ_1, followed by the layer 2 with parameters n_2, ε_2, and μ_2. In this particular situation

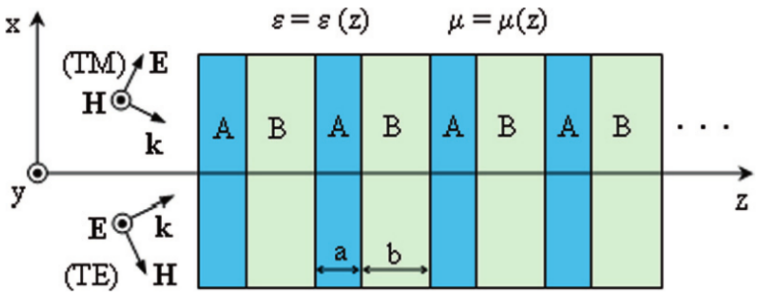

Fig. 5 Transverse electric modes (TE)

$$\mu(\mathbf{r}) = \mu(z), \tag{86}$$

$$\varepsilon(\mathbf{r}) = \varepsilon(z), \tag{87}$$

and

$$\mathbf{E}(\mathbf{r}) = E(z)e^{iqx}\mathbf{e}_y = E_y\mathbf{e}_y. \tag{88}$$

In the equation (88) $\mathbf{e}_y$ is the unit vector in the direction of the y-axis, and q is the wavevector component in the x direction. Then

$$\nabla^2\mathbf{E} = \mathbf{e}_y\left[-q^2 + \frac{\partial^2}{\partial z^2}\right]E(z)e^{iqx}. \tag{89}$$

Furthermore, we have that

$$\frac{\nabla(\mu\varepsilon)}{\mu\varepsilon}\cdot\mathbf{E} = \frac{1}{\mu\varepsilon}\left[\frac{\partial}{\partial y}(\mu\varepsilon)\right]E(z)e^{iqx} = 0.$$

So, by virtue of the equations (86) and (87), μ and ε turn out to be functions of z, only. Likewise,

$$(\mathbf{E}\cdot\nabla)\left(\frac{\nabla\mu}{\mu}\right) = \left[E_x\frac{\partial}{\partial x} + E_y\frac{\partial}{\partial y} + E_z\frac{\partial}{\partial z}\right]\frac{\nabla\mu}{\mu} = E_y\frac{\partial}{\partial y}\left(\frac{\nabla\mu}{\mu}\right) = 0.$$

On the other hand,

$$\left[\frac{\partial\mu}{\mu}\cdot\nabla\right]\mathbf{E}=\frac{1}{\mu}\left[\left(\frac{\partial}{\partial x}\mu,\frac{\partial}{\partial y}\mu,\frac{\partial}{\partial z}\mu\right)\cdot\left(\frac{\partial}{\partial x},\frac{\partial}{\partial y},\frac{\partial}{\partial z}\right)\right]\mathbf{E}$$

$$\left[\frac{\nabla\mu}{\mu}\cdot\nabla\right]\mathbf{E}=\frac{1}{\mu}\left(\frac{d}{dz}\mu\right)\left(\frac{\partial}{\partial z}\mathbf{E}\right)=\mathbf{e}_y\frac{e^{iqx}}{\mu}\left(\frac{d}{dz}\mu\right)\left(\frac{d}{dz}E_z\right) \quad (90)$$

The substitution of the equations (89),(90) in (**??**) gives

$$-\frac{1}{\varepsilon(z)}\left[\frac{1}{\mu(z)}\frac{d}{dz}E(z)+\frac{q^2}{\mu(z)\varepsilon(z)}E(z)\right]=\left(\frac{\omega}{c}\right)^2E(z). \quad (91)$$

This is the differential equation for the electric field associated to the TE modes. According to the equations (1), (**??**), (**??**);

$$\frac{i\omega}{c}\mathbf{B}(\mathbf{r})=e^{iqx}\left[-\frac{d}{dz}E(z)\mathbf{e}_x+iqE(z)\mathbf{e}_z\right]. \quad (92)$$

Or, in accordance with the equation (9) it is obtained that

$$\frac{i\omega}{c}\mu(z)\mathbf{H}(\mathbf{r})=e^{iqx}\left[-\frac{d}{dz}E(z)\mathbf{e}_x+iqE(z)\mathbf{e}_z\right], \quad (93)$$

which is the equation useful to determine the magnetic field once the electric field is known.

4.2 The magnetic field in the case of the transverse magnetic modes

Dealing with the TM modes, one notices that the electric field lies on the plane of incidence whilst the magnetic field is perpendicular to it. Assuming that

$$\mathbf{H}(\mathbf{r})=H(z)e^{iqx}\mathbf{e}_y=H_y\mathbf{e}_y, \quad (94)$$

we then have

$$-\nabla^2\mathbf{H}=\left[-q^2+\frac{\partial^2}{\partial z^2}\right]H(z)e^{iqx}\mathbf{e}_y. \quad (95)$$

If we now take into account that $\mu=\mu(z)$ and $\varepsilon=\varepsilon(z)$

$$\frac{\nabla(\mu\varepsilon)}{\mu\varepsilon}\cdot\mathbf{H}=\frac{1}{c}\left(\frac{\partial}{\partial y}\mu\varepsilon\right)H_y,$$

$$(\mathbf{H}\cdot\nabla)\left(\frac{\nabla\varepsilon}{\varepsilon}\right)=H_y\frac{\partial}{\partial y}\left(\frac{\nabla\varepsilon}{\varepsilon}\right)=0,$$

$$\left[\left(\frac{\nabla\varepsilon}{\varepsilon}\right)\cdot\nabla\right]\mathbf{H}=\frac{1}{\varepsilon}\left[\frac{d}{dz}\varepsilon\right]\frac{\partial}{\partial z}\mathbf{H}=\frac{1}{\varepsilon}\frac{d\varepsilon}{dz}\frac{dH(z)}{dz}e^{iqx}\mathbf{e}_y. \tag{96}$$

As well, by substituting the equations (95) y (96) in (**??**), we get

$$-\frac{1}{\mu(z)}\frac{d}{dz}\frac{1}{\varepsilon(z)}\frac{d}{dz}H(z)+\frac{q^2}{\mu\varepsilon}H(z)=\left(\frac{\omega}{c}\right)^2H(z); \tag{97}$$

and this is the equation for the TM modes. After obtaining the magnetic field from (152), the electric field can be calculated from the Maxwell equations in the form

$$-i\frac{\omega}{c}\varepsilon(z)\mathbf{E}(\mathbf{r})=e^{iqx}\left[-\frac{d}{dz}H(z)\mathbf{e}_x+iqH(z)\mathbf{e}_z\right]. \tag{98}$$

5 The transfer matrix method

The main idea behind all definitions of the transfer matrix is that one may know what happens at some point by having the information of what happens at another one. At the basis of this idea lies the theorem of uniqueness and existence of a solution of a system of linear differential equations with given initial conditions [39]. In the case of the equation (151) which describes the electric field of the TE modes, we have

$$-\frac{1}{\varepsilon(z)}\frac{d}{dz}\frac{1}{\mu(z)}\frac{d}{dz}E(z)+\frac{q^2}{\mu(z)\varepsilon(z)}E(z)=\left(\frac{\omega}{c}\right)^2$$

either

$$-\frac{d}{dz}\frac{1}{\mu(z)}\frac{d}{dz}E(z)=-\varepsilon(z)\left[\left(\frac{\omega}{c}\right)^2-\frac{q^2}{\mu(z)\varepsilon(z)}\right]E(z). \tag{99}$$

Defining the refractive index as

$$n(z) = \sqrt{\mu(z)}\sqrt{\varepsilon(z)}, \tag{100}$$

we have

$$-\frac{d}{dz}\frac{1}{\mu(z)}\frac{d}{dz}E(z) = -\varepsilon(z)\left[\left(\frac{\omega}{c}\right)^2 - \frac{q^2}{n^2(z)}\right]E(z).$$

Let $z_0 \in \Re$ and $\delta > 0$, and assume that the right hand side of the expression above is integrable in the open interval $(z_0-\delta, z_0+\delta)$. Then,

$$\int_{z_0-\delta}^{z_0+\delta} \frac{d}{dz}\frac{1}{\mu(z)}\frac{d}{dz}E(z)dz = -\int_{z_0-\delta}^{z_0+\delta} \varepsilon(z)\left[\left(\frac{\omega}{c}\right)^2 - \frac{q^2}{n^2(z)}\right]E(z)dz,$$

$$\frac{1}{\mu(z)}\frac{d}{dz}E(z)|_{z_0-\delta}^{z_0+\delta} = -\int_{Z_0-\delta}^{Z_0+\delta} \varepsilon(z)\left[\left(\frac{\omega}{c}\right)^2 - \frac{q^2}{n^2(z)}\right]E(z)dz.$$

Taking the limit when $\delta \to 0$ it is found that

$$\frac{1}{\mu(z)}\frac{d}{dz}E(z)|_{z_0^-} = \frac{1}{\mu(z)}\frac{d}{dz}E(z)|_{Z_0^+}. \tag{101}$$

That is, the function $\frac{1}{\mu(z)}\frac{d}{dz}E(z)$ is continuous in $\Re$. With the additional assumption that $E(z)$ is a continuous function (according to the continuity boundary conditions of $\mathbf{E}$ at the interface between two media), and if μ and ε do not depend on the position, the equation (99) rewrites as

$$\frac{d^2}{d^2z}E(z) + \left[\left(\frac{n\omega}{c}\right)^2 - q^2\right]E(z) = 0. \tag{102}$$

Considering the continuity boundary conditions for the electric field, it is possible to choose that:

$$E(z_0) = A, \tag{103}$$

$$\frac{1}{\mu}\frac{dE}{dz}|_{z_0} = B, \tag{104}$$

in such a way that we can propose the solution of (102) in the form:

$$E(z) = A\cos\left[Q(z-z_0)\right] + \frac{\mu}{Q}B\sin\left[Q(z-z_0)\right] \tag{105}$$

Here, Q represents the component of the wavevector along the growth direction and

$$Q^2 = \left[\left(\frac{n\omega}{c}\right)^2 - q^2\right]. \tag{106}$$

Let us write now,

$$\Psi(z) = \begin{bmatrix} E(z) \\ \frac{1}{\mu}\frac{dE}{dz} \end{bmatrix}. \tag{107}$$

We see that, in this case,

$$\Psi(0) = \begin{bmatrix} A \\ B \end{bmatrix}. \tag{108}$$

According with the equations (103) and (104), we will have;

$$\Psi(z) = \begin{bmatrix} A\cos\left[Q(z-z_0)\right] + \left(\frac{1}{\mu}\right)B\sin\left[Q(z-z_0)\right] \\ -A\left(\frac{Q}{\mu}\right)\sin\left[Q(z-z_0)\right] + B\cos\left[Q(z-z_0)\right] \end{bmatrix}. \tag{109}$$

Which can be written as

$$\Psi(z) = \mathbf{M}(z-z_0)\Psi(z_0), \tag{110}$$

with

$$\mathbf{M}(z-z_0) = \begin{bmatrix} \cos\left[Q(z-z_0)\right] & \left(\frac{\mu}{Q}\right)\sin\left[Q(z-z_0)\right] \\ -\left(\frac{Q}{\mu}\right)\sin\left[Q(z-z_0)\right] & \cos\left[Q(z-z_0)\right] \end{bmatrix}. \tag{111}$$

From the equation (111) we readily notice that,

$$\det|\mathbf{M}(z-z_0)| = 1; \tag{112}$$

where $\mathbf{M}$ is the transfer matrix associated with the system under study.

5.1 Equations for a periodic system

We study here a periodic system like the one shown in the figure 6; in which it is assumed that $n_1 > 0$, whereas n_2 may be a real positive, a real negative or a pure imaginary number. In the figure, we have labeled as "a" the width of the layers of index n_1, and as "b" the width of the layers of index n_2, with $d = a + b$.

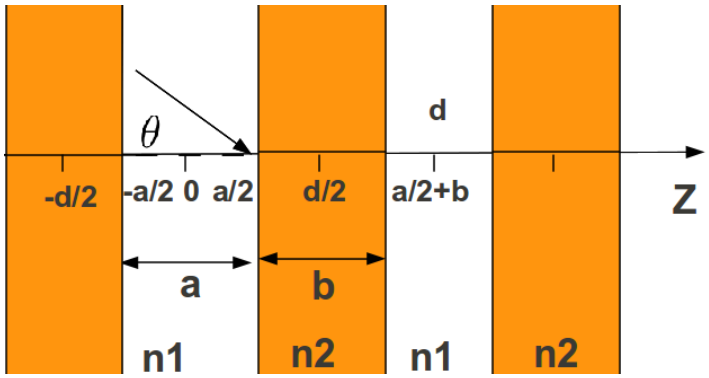

Fig. 6 Periodic layered system.

taking into account the Snell law we may write

$$q = n_1 \frac{\omega}{c} \sin(\theta), \tag{113}$$

with θ being the angle of incidence. Let $z_0 = 0$ and $z = \frac{a}{2}$, so that in the medium 1 we will have

$$\Psi\left(\frac{a}{2}\right) = \mathbf{M}_1\left(\frac{a}{2}\right)\Psi(0), \tag{114}$$

$$\mathbf{M}_1\left(\frac{a}{2}\right) = \begin{bmatrix} \cos\left[Q_1\left(\frac{a}{2}\right)\right] & \left(\frac{\mu_1}{Q_1}\right)\sin\left[Q_1\left(\frac{a}{2}\right)\right] \\ -\left(\frac{Q_1}{\mu_1}\right)\sin\left[Q_1\left(\frac{a}{2}\right)\right] & \cos\left[Q_1\left(\frac{a}{2}\right)\right] \end{bmatrix}, \tag{115}$$

with $Q_1 = \frac{n_1\omega}{c}|\cos\theta|$.

Now we are going to analyze the possibilities for the medium 2, setting $z_0 = \frac{a}{2}$ and $z = \frac{a+b}{2}$, it is obtained that

$$\Psi\left(\frac{a+b}{2}\right) = \mathbf{M}_2\left(\frac{b}{2}\right)\Psi\left(\frac{a}{2}\right), \tag{116}$$

$$\mathbf{M}_2\left(\frac{a+b}{2}\right) = \begin{bmatrix} \cos\left[Q_2\left(\frac{b}{2}\right)\right] & \left(\frac{\mu_2}{Q_2}\right)\sin\left[Q_2\left(\frac{b}{2}\right)\right] \\ -\left(\frac{Q_2}{\mu_2}\right)\sin\left[Q_2\left(\frac{b}{2}\right)\right] & \cos\left[Q_2\left(\frac{b}{2}\right)\right] \end{bmatrix}, \tag{117}$$

$$Q_2 = \frac{\omega}{c}\sqrt{n_2^2 - n_1^2 Sen^2\theta}. \tag{118}$$

With which, we have,

$$\Psi\left(\frac{a+b}{2}\right) = \mathbf{M}_2\left(\frac{b}{2}\right)\mathbf{M}_1\left(\frac{a}{2}\right)\Psi(0) = \mathbf{M}_T(a,b)\,\Psi(0), \tag{119}$$

and

$$\mathbf{M}_T(a,b) = \mathbf{M}_2\left(\frac{b}{2}\right)\mathbf{M}_1\left(\frac{a}{2}\right). \tag{120}$$

$\mathbf{M}_T(a,b)$ connects the vector Ψ of the medium 1 withe the vector Ψ of the medium labeled as 2. Explicitly;

$$\mathbf{M}_T(a,b) = \begin{bmatrix} p & q \\ r & s \end{bmatrix} \tag{121}$$

with

$$p = \cos\left(Q_2\frac{b}{2}\right)\cos\left(Q_1\frac{b}{2}\right) - \frac{\mu_2}{\mu_1}\frac{Q_1}{Q_2}\sin\left(Q_2\frac{b}{2}\right)\sin\left(Q_1\frac{b}{2}\right), \tag{122}$$

$$q = \frac{\mu_1}{Q_1}\cos\left(Q_2\frac{b}{2}\right)\sin\left(Q_1\frac{b}{2}\right) - \frac{\mu_2}{Q_2}\frac{Q_2}{Q_1}\sin\left(Q_2\frac{b}{2}\right)\cos\left(Q_1\frac{b}{2}\right), \tag{123}$$

$$r = -\frac{Q_2}{\mu_2}\sin\left(Q_1\frac{b}{2}\right)\cos\left(Q_1\frac{a}{2}\right) - \frac{Q_1}{\mu_1}\cos\left(Q_2\frac{b}{2}\right)\cos\left(Q_1\frac{b}{2}\right), \tag{124}$$

$$p = -\frac{\mu_1}{\mu_2}\frac{Q_2}{Q_1}\sin\left(Q_2\frac{b}{2}\right)\sin\left(Q_1\frac{b}{2}\right) + \cos\left(Q_2\frac{b}{2}\right)\cos\left(Q_1\frac{b}{2}\right). \tag{125}$$

Let $\mathbf{T}_d$ to be the translation operator in a period d. Applying $\mathbf{T}_d$ on equation (99) results in

$$\mathbf{T}_d\left[-\frac{1}{\varepsilon(z)}\frac{d}{dz}\frac{1}{\mu(z)}\frac{d}{dz}E(z)+\frac{q^2}{\mu(z)\varepsilon(z)}E(z)\right]=\left(\frac{\omega}{c}\right)^2\mathbf{T}_dE(z)$$

Given that the system under study is periodic (with period d), we have that $\mu(z+d)=\mu(z)$ and $\varepsilon(z+d)=\varepsilon(z)$. Consequently,

$$-\frac{1}{\varepsilon(z)}\frac{d}{dz}\frac{1}{\mu(z)}\frac{d}{dz}\mathbf{T}_dE(z)+\frac{q^2}{\mu(z)\varepsilon(z)}\mathbf{T}_dE(z)=\left(\frac{\omega}{c}\right)^2\mathbf{T}_dE(z)$$

All this tells us that $\mathbf{T}_d$ and $E(z)$ satisfy the same differential equation. So, they must differ –at most– in a constant that is equal to the eigenvalue of $\mathbf{T}_d$. In accordance;

$$\mathbf{T}_dE(z)=E(z+d)=\lambda E(z). \tag{126}$$

Moreover, $E(z)$ must be the solution for the TE modes, and also an eigenfunction of the translation operator. This implies that

$$\mathbf{T}_d\left[\frac{1}{\mu(z)}\frac{d}{dz}E(z)\right]=\lambda\frac{1}{\mu(z)}\frac{d}{dz}E(z) \tag{127}$$

Therefore,

$$\mathbf{T}_d\Psi(z)=\lambda\Psi(z)=\Psi(z+d).$$

Since a translation over a period should not change the field amplitude, the quantity λ must necessarily be a phase factor of unit modulus. That is,

$$\lambda=e^{i\phi}, \tag{128}$$

and the magnitude of ϕ will be a function of the period d, $\phi=\phi(d)$, by which;

$$\mathbf{T}_{d+d'}\Psi(z)=e^{i\phi(d+d')}\Psi(z)=\mathbf{T}_d\mathbf{T}_{d'}\Psi(z)=e^{i\phi(d)}e^{i\phi(d')}\Phi.$$

This means that $\phi(d)+\phi(d')=\phi(d+d')$ or, in other words, that ϕ is a linear function of d. The usual thing is to propose $\phi(d)=kd$, with k being a complex constant that turns to a real one if one makes use of the periodicity. For integer N it is generally obtained that

$$\Psi(z+Nd) = \Psi(z) = e^{iNkd}\Psi(z), \tag{129}$$

from which we have that $Nkd = 2m\pi$, and m is also an integer. Making $N = 1$ and $z = -\frac{a+b}{2} = -\frac{d}{2}$ in equation (129) one has

$$\Psi\left(\frac{a+b}{2}\right) = e^{ikd}\Psi\left(-\frac{a+b}{2}\right), \tag{130}$$

or, equivalently,

$$\begin{bmatrix} p & q \\ r & s \end{bmatrix} \Psi(0) = \lambda \begin{bmatrix} p & -q \\ -r & s \end{bmatrix} \Psi(0), \tag{131}$$

from which

$$\begin{bmatrix} p(1-\lambda) & q(1+\lambda) \\ r(1+\lambda) & s(1-\lambda) \end{bmatrix} \Psi(0) = 0. \tag{132}$$

The system (133) has a solution only if

$$\det \begin{vmatrix} p(1-\lambda) & q(1+\lambda) \\ r(1+\lambda) & s(1-\lambda) \end{vmatrix} = 0, \tag{133}$$

then

$$(ps-qr)(1+\lambda^2) = 2\lambda(ps+qr); \tag{134}$$

but $ps - qr = det\,|\mathbf{M}_T| = 1$, leading to

$$\cos(kd) = ps + qr. \tag{135}$$

This is the equation needed to calculate the dispersion relation $\omega = \omega(k)$ corresponding to the TE modes.

6 Transmission and reflection coefficients under oblique incidence in one-dimensional photonic crystals

We assume an electromagnetic wave that impacts with oblique angle of incidence, θ on a 1DPC of finite length L grown along the z direction (see figure **??**).

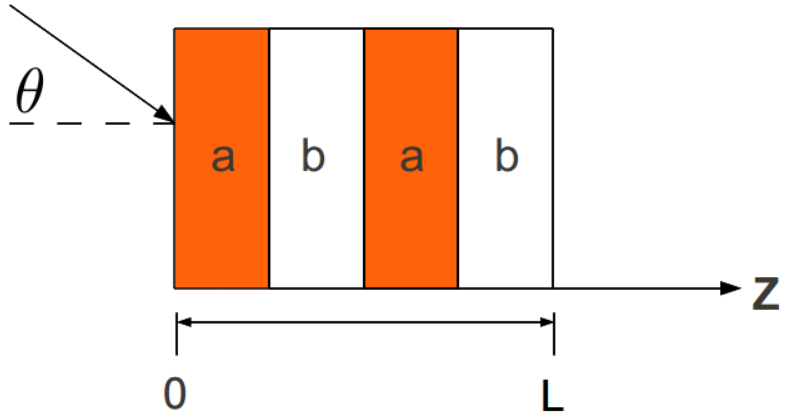

Fig. 7 One-dimensional photonic crystal

In the case of the TE modes, the vector **E** of the incident radiation is perpendicular to the plane of incidence. In such a way,

$$\mathbf{E}(\mathbf{r}) = E(z)e^{iqx}\mathbf{e}_y, \tag{136}$$

$\mathbf{e}_y$ being the unit vector along the direction of the y-axis, and q the wavevector along the x-axis direction. Usually, it is proposed,

$$E(z) = \begin{cases} a_0 e^{iQ_0 z} + b_0 e^{-iQ_0 z} & z < 0 \\ E_z & 0 \le z \le L \\ c_0 e^{iQ_0(z-L)} & z > L \end{cases} \tag{137}$$

The functions $E(z)$ and $\frac{1}{\mu(z)}\frac{d}{dz}E(z)$ are continuous in z, and $Q_0 = \sqrt{\frac{n_0^2\omega^2}{c^2} - q^2}$, with $q = \left(\frac{\omega}{c}n_0\right)\sin\theta$. At the interface $z = 0$,

$$\begin{aligned} a_0 + b_0 &= E(0), \\ i\frac{Q_0}{\mu_0}a_0 - i\frac{Q_0}{\mu_0}b_0 &= \frac{1}{\mu(z)}\frac{d}{dz}E(z)|_{z=0}. \end{aligned}$$

Here μ_0 is the magnetic permeability of the media at $z < 0$ and $z > L$. In matrix terms we have:

$$\begin{bmatrix} 1 & 1 \\ i\frac{Q_0}{\mu_0} & -i\frac{Q_0}{\mu_0} \end{bmatrix} \begin{bmatrix} a_0 \\ b_0 \end{bmatrix} = \Psi(0) \tag{138}$$

where

$$\Psi(z) = \begin{bmatrix} E(z) \\ \frac{1}{\mu(z)} \frac{d}{dz} E(z) \end{bmatrix} \tag{139}$$

On the other hand, at the interface $z = L$,

$$\begin{aligned} c_0 &= E(L), \\ i\frac{Q_0}{\mu_0} c_0 &= \frac{1}{\mu(z)} \frac{d}{dz} E(z)|_{z=L}, \end{aligned}$$

which in matrix form reads

$$\begin{bmatrix} 1 & 1 \\ i\frac{Q_0}{\mu_0} & -i\frac{Q_0}{\mu_0} \end{bmatrix} \begin{bmatrix} c_0 \\ 0 \end{bmatrix} = \Psi(L) \tag{140}$$

With the use of (110) we may write

$$\Psi(L) = \mathbf{M}\Psi(0), \tag{141}$$

Which results in

$$\begin{bmatrix} 1 & 1 \\ i\frac{Q_0}{\mu_0} & -i\frac{Q_0}{\mu_0} \end{bmatrix} \begin{bmatrix} c_0 \\ 0 \end{bmatrix} = \mathbf{M} \begin{bmatrix} 1 & 1 \\ i\frac{Q_0}{\mu_0} & -i\frac{Q_0}{\mu_0} \end{bmatrix} \begin{bmatrix} a_0 \\ b_0 \end{bmatrix}, \tag{142}$$

$$\begin{bmatrix} a_0 \\ b_0 \end{bmatrix} = \begin{bmatrix} -i\frac{Q_0}{\mu_0} M_{22} + M_{21} - \frac{Q_0^2}{\mu_0^2} M_{12} - i\frac{Q_0}{\mu_0} M_{11} & -i\frac{Q_0}{\mu_0} M_{22} + M_{21} + \frac{Q_0^2}{\mu_0^2} M_{12} + i\frac{Q_0}{\mu_0} M_{11} \\ 0 - i\frac{Q_0}{\mu_0} M_{22} + M_{21} - \frac{Q_0^2}{\mu_0^2} M_{12} + i\frac{Q_0}{\mu_0} M_{11} & -i\frac{Q_0}{\mu_0} M_{22} - M_{21} + \frac{Q_0^2}{\mu_0^2} M_{12} - i\frac{Q_0}{\mu_0} M_{11} \end{bmatrix} \begin{bmatrix} c_0 \\ 0 \end{bmatrix}.$$

Thus obtaining,

$$\frac{c_0}{a_0} = \frac{2}{M_{11} + M_{22} + i\left[\frac{\mu_0}{Q_0} M_{21} - \frac{Q_0}{\mu_0} M_{12}\right]}, \tag{143}$$

$$\frac{b_0}{a_0} = \frac{M_{22} - M_{11} - i\left[\frac{\mu_0}{Q_0} M_{21} + \frac{Q_0}{\mu_0} M_{12}\right]}{M_{11} + M_{22} + i\left[\frac{\mu_0}{Q_0} M_{21} - \frac{Q_0}{\mu_0} M_{12}\right]}. \tag{144}$$

If we define

$$t = \frac{c_0}{a_0} \tag{145}$$

and

$$t = \frac{b_0}{a_0} \tag{146}$$

the transmission and reflection coefficients of the wave will be

$$T = |t|^2, \tag{147}$$

$$R = |r|^2. \tag{148}$$

7 The plasmon-polariton modes in a one-dimensional Rudin-Shapiro photonic superlattice

Here we will theoretically study the problem of the SPP in a 1DPC. The numerical experiment will consider an ideal system. This is a one-dimensional superlattice whose basis will consist of passive layers with positive indices of refraction, together with active layers showing a Drude-like response in the dielectric permittivity and magnetic permeability. These layers may behave as metamaterials for certain values of the frequency [19]. The figure 8 contains a schematic representation of the structure that considers a third-order RS basis. The layers A and D are chosen to have positive refractive indices with $\varepsilon_A = 1$, $\mu_A = 1$, and $\varepsilon_D = 3$, $\mu_D = 1$. For the active layers B and C we use, in each case, the frequency-dependent expressions:

$$\varepsilon(\omega) = \varepsilon_0 - \frac{\omega_e^2}{\omega(\omega + i\gamma_e)}, \tag{149}$$

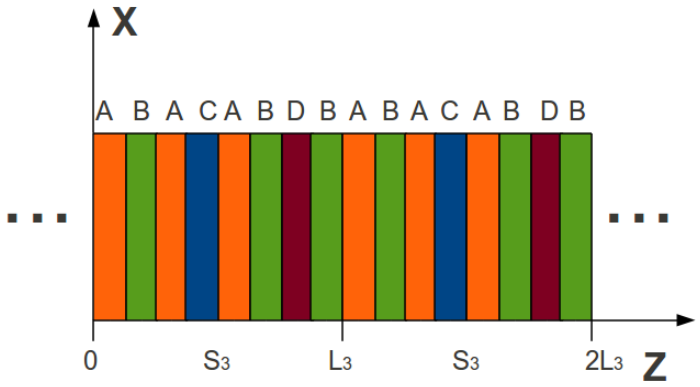

Fig. 8 One-dimensional photonic crystal with a unit cell consisting of a $m = 3$ Rudin-Shapiro layer sequence.

$$\mu(\omega) = \mu_0 - \frac{\omega_m^2}{\omega(\omega + i\gamma_m)}. \tag{150}$$

As mentioned, the basic equations of the model are those for the TE and TM modes [18]:

$$-\frac{1}{\varepsilon(z)}\frac{d}{dz}\frac{1}{\mu(z)}\frac{d}{dz}E(z) + \frac{q^2}{\mu(z)\varepsilon(z)}E(z) = \left(\frac{\omega}{c}\right)^2 E(z). \tag{151}$$

$$-\frac{1}{\mu(z)}\frac{d}{dz}\frac{1}{\varepsilon(z)}\frac{d}{dz}H(z) + \frac{q^2}{\mu(z)\varepsilon(z)}H(z) = \left(\frac{\omega}{c}\right)^2 H(z). \tag{152}$$

In order to obtain the photonic spectrum of the heterostructure we apply the transfer matrix method. The total transfer matrix $\mathbf{M}$ results from the product of the transfer matrices corresponding to each of the layers included according with the RS sequence. The general form of these constituent matrices is;

$$\mathbf{M}_j^{\alpha} = \begin{pmatrix} \cos(q_\alpha \alpha) & i\sin(q_\alpha \alpha)/f_\alpha \\ if_\alpha \sin(q_\alpha \alpha) & \cos(q_\alpha \alpha) \end{pmatrix}, \tag{153}$$

where $\alpha = A, B, C, D$ and $q_\alpha = \frac{\omega}{c}\sqrt{\varepsilon_\alpha(\omega)\mu_\alpha(\omega) - \sin^2\theta}$; θ being the angle of incidence of the light. For incident waves with TE and TM polarizations, the coefficients f_α are, respectively:

$$f_{\alpha}^{TE} = \frac{1}{\mu_{\alpha}(\omega)}\sqrt{\varepsilon_{\alpha}(\omega)\mu_{\alpha}(\omega) - \sin^2\theta}, \tag{154}$$

$$f_{\alpha}^{TM} = \frac{1}{\varepsilon_{\alpha}(\omega)}\sqrt{\varepsilon_{\alpha}(\omega)\mu_{\alpha}(\omega) - \sin^2\theta}. \tag{155}$$

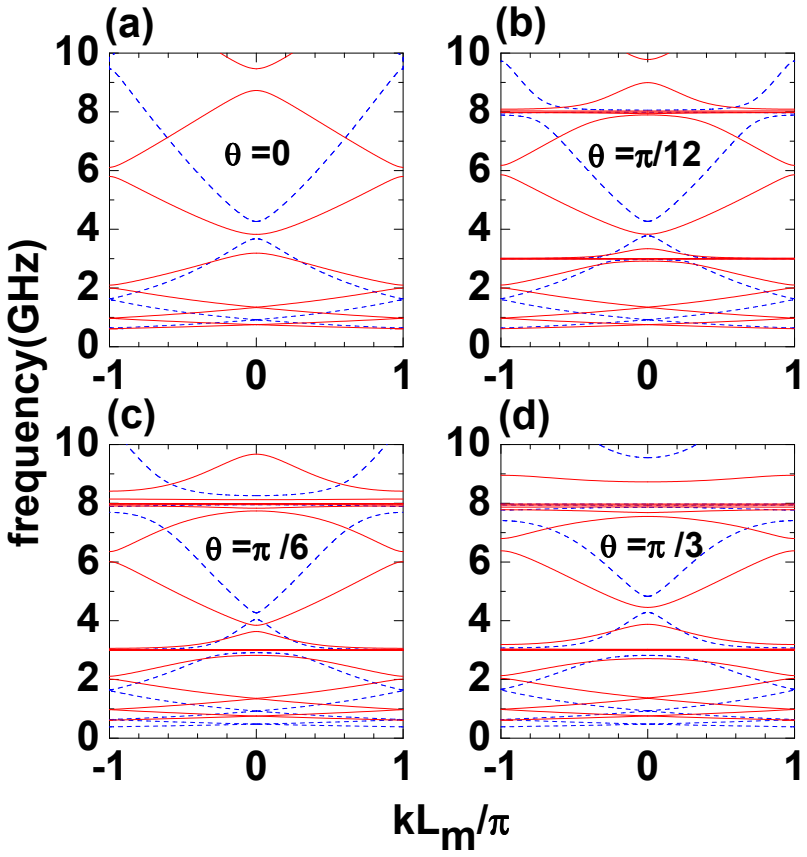

Fig. 9 (Color online) The dispersion relation of TE modes without absorption loss in a RS photonic superlattice for different values of the incidence angle. The dashed line corresponds to the RS generation of order $m = 4$, whereas the solid line represents the modes of an order $m = 5$ RS photonic superlattice. The results are obtained using the values $\omega_e/2\pi = \omega_m/2\pi = 3\,\text{GHz}$ for layer-type B, and $\omega_e/2\pi = \omega_m/2\pi = 8\,\text{GHz}$ for layer-type C.

Then, the dispersion relation for the allowed modes in the m-th order RS-based superlattice is evaluated from the total transfer matrix in the form [40]:

$$\cos\left(kL_m\right) = \frac{1}{2}Tr\left(M_T\right). \tag{156}$$

We shall first consider the non-dispersive case with $\gamma_0 = 0$. Then, the figure 9 contains the distribution of allowed TE modes in the cases of photonic superlattices with the unit cell given by the RS sequence, for generations $m = 4$ and $m = 5$. The widths of all the involved layers are consider to be equal to 2 mm, and the values of the Drude frequencies corresponding to layers B and C are $\omega_e/2\pi = \omega_m/2\pi = 3\,\text{GHz}$ and $\omega_e/2\pi = \omega_m/2\pi = 8\,\text{GHz}$, respectively. The dispersion relations, $\nu = \nu(k)$, are shown for different values of the angle of incidence, θ. The dashed and solid lines correspond, respectively, to the cases with RS generation orders $m = 4$ y $m = 5$.

As expected, when $\theta = 0$ (normal incidence) there are no plasmon-polariton modes in the photonic spectrum. The lowest photonic bandgap (PBG) observed under that condition is a zeroth-order one at the superlattice Brillouin zone boundary, associated with the vanishing of the average quantity [18, 41],

$$\langle n(\omega)\rangle = \frac{1}{d}\int n(z,\omega)dz. \tag{157}$$

It is necessary to mention that this $\langle n\rangle = 0$ gap is present in all cases of oblique incidence as well, because it is inherent to the distribution of layers with alternate positive and negative refractive indices [42].

Above the zeroth-order gap, at normal incidence, one also notices the presence of Bragg-type PBGs. Particularly, we have a zone-center main PBG located between $\nu \simeq 3\,\text{GHz}$ and $\nu \simeq 4\,\text{GHz}$ when the RS generation order is $m = 5$ –which is found shifted upwards in the case of the lower RS generation–, as well as a secondary Bragg-PBG above, at the boundary.

In the situation, in which an electromagnetic wave comes into contact with the photonic crystal with an oblique angle of incidence, the magnetic field of the wave (in the case of the TE modes) has a longitudinal component –along the superlattice growth direction– that interacts with the dipole moments in the material, which oscillate with the plasma frequency. Such an interaction gives rise to an elementary excitation in the system, making the dipole moments to radiate. The superposition of the incident and radiated waves produces a new kind of electromagnetic wave known as plasmon-polariton. When the electromagnetic wave resonates with the magnetic dipole moments, these do not radiate back. Instead, the resonance mode is absorbed by the system. This also happens for those modes whose frequencies

are closed to the plasma one. As a consequence, there will appear a plasmon-polariton bandgap (PPBG), as one observes from figures 9(b)-9(d) around the values of $\omega_{e,m}$ for the layers B and C. The modes that are able to propagate through the system can be of both electric and magnetic nature. Besides the magnetic ones already discussed, those with electric nature are coupled modes arising from the interaction of the incident electromagnetic waves, with transversal magnetic polarization, with the free electrons and electric dipole moments in the material [18].

We better notice the presence of the Bragg and plasmon gaps by observing the Fig. 10. It contains the photonic dispersion relation for the fifth-order RS superlattice in the situation of an oblique incidence of $\theta = \pi/12$ (left column), together with its corresponding calculated transmission coefficient, T, (right column). The figures 10(a) and 10(b) represent, respectively, the photonic structure and T in the case in which we make layers B and C in the RS sequence to be equal in geometric and dielectric properties, with $\omega_e/2\pi = \omega_m/2\pi = 3\,\mathrm{GHz}$. In the lowest row we present the dispersion relation [Fig. 10(c)], and the transmission coefficient [Fig. 10(d)] in the situation in which both B and C layers are different, with the parameters used to generate the photonic spectra presented in the figure 9 above.

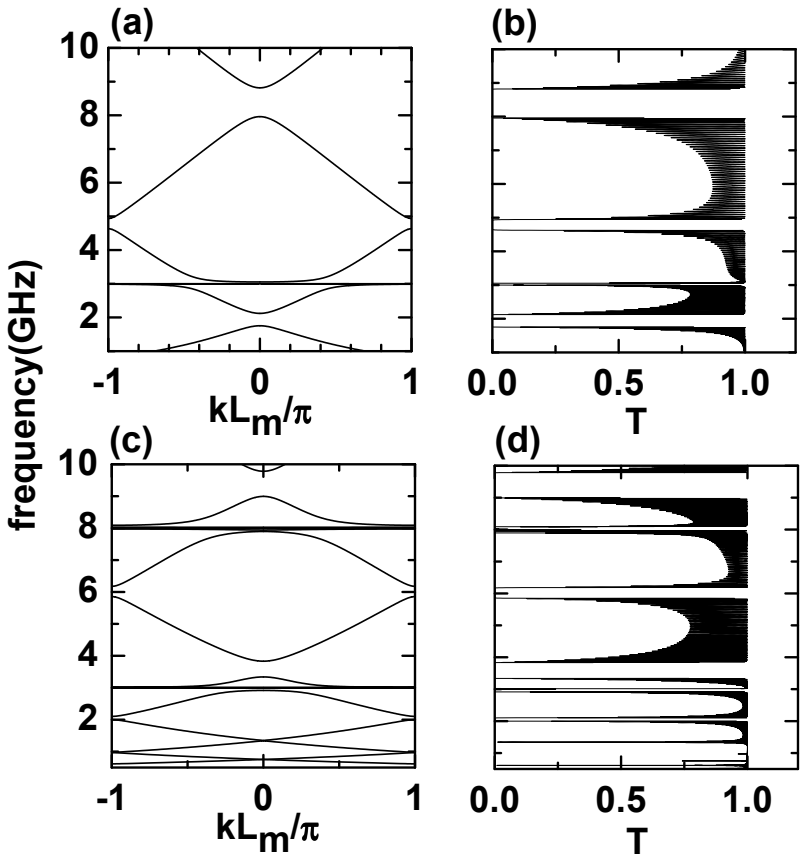

Fig. 10 Photonic dispersion relation and the associated transmittance of a dielectric superlattice with fifth-order Rudin-Shapiro unit cell for oblique incidence $\theta = \pi/12$. Graphs (a) and (b) correspond to a RS unit cell in which we have made $B = C$ in the quasiregular sequence, with $\omega_e/2\pi = \omega_m/2\pi = 3\,\text{GHz}$. Graphs (c) and (d) correspond to the more general situation with nonequal B and C layers, calculated using the parameters chosen to generate the dispersion relations in figure 9.

It is possible to see the coincidence of the PBGs in Fig. 10(a) with the intervals on the vertical axis of Fig. 10(b) that correspond to zero values of the transmission coefficient. Then, looking at these zero T intervals we have, from bottom to top: the zeroth-order gap, the first PPBG, the fundamental Bragg-PBG at the Brillouin zone center, the Bragg-PBG at the zone boundary, the second PPBG, and the second zone-center Bragg-PBG.

In addition, from the observation of the figure 9 we realize that the positions and the widths of these photonic gaps depend on the magnitude of the angle of incidence in both superlattices under study. Accordingly, the figure 11 presents, for the sake of illustration, the

particular example of the variations of the three lowest bangaps in the photonic structure of a $m = 4$ RS-superlattice with equal dispersive B and C layers as discussed above. The figures located on the left column [11(a), (c), (e)] contain the variations of the widths of such gaps as functions of θ. On the other

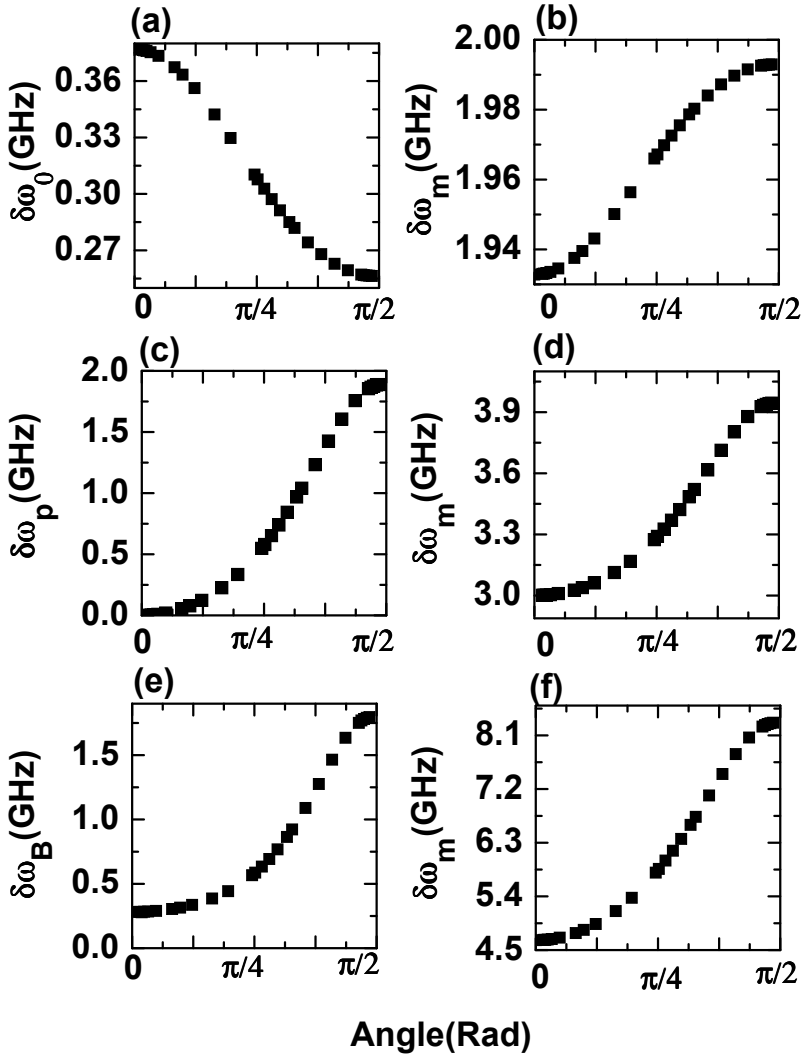

Fig. 11 The variation of the width (left column) and the central frequency position (ω_m) as functions of the angle of incidence, for the three lowest frequency photonic bandgaps in the case of a $m = 5$ Rudin-Shapiro photonic superlattice whose dispersion relation is shown in the Fig. 10(a). The upper row corresponds to the zeroth-order gap, the middle row contains the variations associated to the plasmon-polariton bandgap, and in the lowest row we are presenting the angular dependencies of the zone-boundary Bragg gap appearing above 4 GHz.

hand, the figures on the right column depict the change in the frequency position of the midpoint (ω_m) of each of the gaps considered [Figs. 11(b), (d), (f)] as a result of the increase in the angle of incidence. One straightforward conclusion in this case is that the three gaps shift upwards in frequency as long as the incidence goes from normal to transversal. But the rates of displacement are quite different between them. One notices that the center of the zeroth-order gap suffers only a slight increase in its position, whilst in the case of the zone-boundary Bragg gap, when the angle of incidence is of about 88 degrees (the limit chosen in the calculation) ω_m displaces to a frequency value that is almost the double of that corresponding to normal incidence. The position of the plasmon-polariton gap middle frequency raises in the frequency scale as well, with an increment of approximately 1 GHz in the process. This change in the gap frequency positions relates with the θ-related variation in the dielectric contrast seen by the longitudinally propagating wave as a consequence of the Snell-type refractions at each interface. Such alteration in the refractive index contrast also leads to a slight narrowing of the frequency interval for which the condition (157) fulfills, as can be seen in the reduction of the zeroth-order gap width reported in Fig. 11(a). However, the larger the angle of incidence, the wider the zone-boundary photonic and plasmon-polariton bandgaps considered, as one observes from the figures 11(c) and 11(e), respectively. As expected, the plasmon-polariton PBG is the one that becomes more affected by the increase in the incident light inclination. The width of this gap goes from zero at normal incidence to approximately 2 GHz when θ is just slightly below $\pi/2$. The Bragg-type zone-boundary gap has its width augmenting in about 1.5 GHz.

Within the PPBGs there are a number of excited plasmon modes. In the figure 5 we are showing the zooming of the dispersion relation for the case of a $S = 4$ RS generation superlattice near the plasma frequencies at 3 and 8 GHz. It can be readily seen that around $\omega = 3$ GHz there are four coupled plasmon modes that correspond to the number of dispersive B layers. Likewise, there are also four coupled excited plasmon modes around the frequency value of 8 GHz which correspond to the four dispersive C layers found within the superlattice period (consisting, in this specific order, of 2^4 layers). In each case, there is a single plasmon mode that exhibits a stronger dispersion,

whilst the remaining three are much less dispersive. The value of the angle of incidence considered is $\theta = \pi/12$.

Let us discuss now the influence of including a non-zero imaginary part in the denominators of equations (149) and (150). That is, the incorporation of optical absorption in the system. As it was discussed in reference [43], in this situation the equation (156) becomes a complex one, and one must solve it for both the real and imaginary part of the superlattice wave vector $k = k_1 + ik_2$. This can be done by separating the transcendental equation into a system of two coupled equations or by solving (156) directly, using the inverse cosine function and then taking the real and imaginary parts of the obtained value for each input frequency.

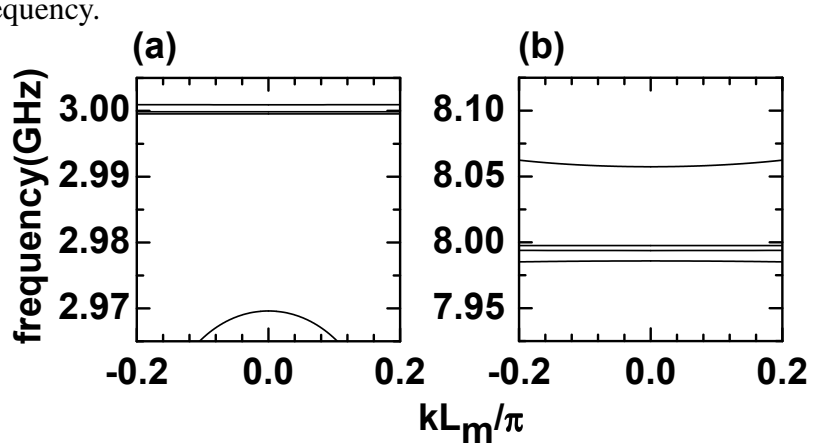

Fig. 12 Augmentation of the photonic dispersion relation around the lower and upper plasmon-polariton frequencies showing the number of excited plasmon-polariton states in a $m = 4$ Rudin-Shapiro superlattice with two different dispersive layers, B and C, for the same case represented in the figure 9(b). The total number of modes, 8, equals the number of dispersive layers included in a superlattice unit cell for such generation order in the Rudin-Shapiro sequence.

The presence of absorption strongly modifies the frequency band structure of 1D photonic superlattices. A detailed discussion on its effects in the case of system made of quasiregular layered metamaterials is given in reference [43]. The figure 13 shows an example –for the sake of illustration– of the effect of the of optical absorption in the calculation of the photonic structure in RS-superlattices. Again, we take $\omega_e/2\pi = \omega_m/2\pi = 3\,\mathrm{GHz}$ for the dispersive B and C layers. The RS order of generation is $m = 4$ and set $\theta = \pi/12$. The absorption parameter is taken to be $\gamma_e = \gamma_m = \gamma_0 = 0.001$. This value of the damping constant corresponds to a low level of absorption. We have chosen to plot the real solutions of equation (156), to show the disper-

sion relations near the frequency of 3 GHz. It is possible to see that the plasmon-polariton structure is drastically modified by the influence of the optical absorption. The first thing to notice is that, even for such small absorption, the gap structure is simply washed out. However, following the analysis put forward in [43], when γ_0 is very small, as in the example here shown, there still remains a quasi-gap structure which reflects in the form of sharp —but not divergent— peaks in the two-dimensional density of states (DOS). By observing the figure 13(b) and 13(c), one notices that, inside the frequency regions corresponding to the plasmon-polariton gap and the $\langle n \rangle = 0$ gap, respectively, there are points for which the group velocity becomes infinite. The DOS, which is inversely proportional to the group velocity, should then vanish for these values of frequency. The figure 13(d) contains the plot of the real part of the half-trace of the total transfer matrix for the interval around the plasma frequency. Then, it would be more easy to understand the features of the dispersion relation in the plasmon-polariton region around the Brillouin zone center [Fig. 13(b)].

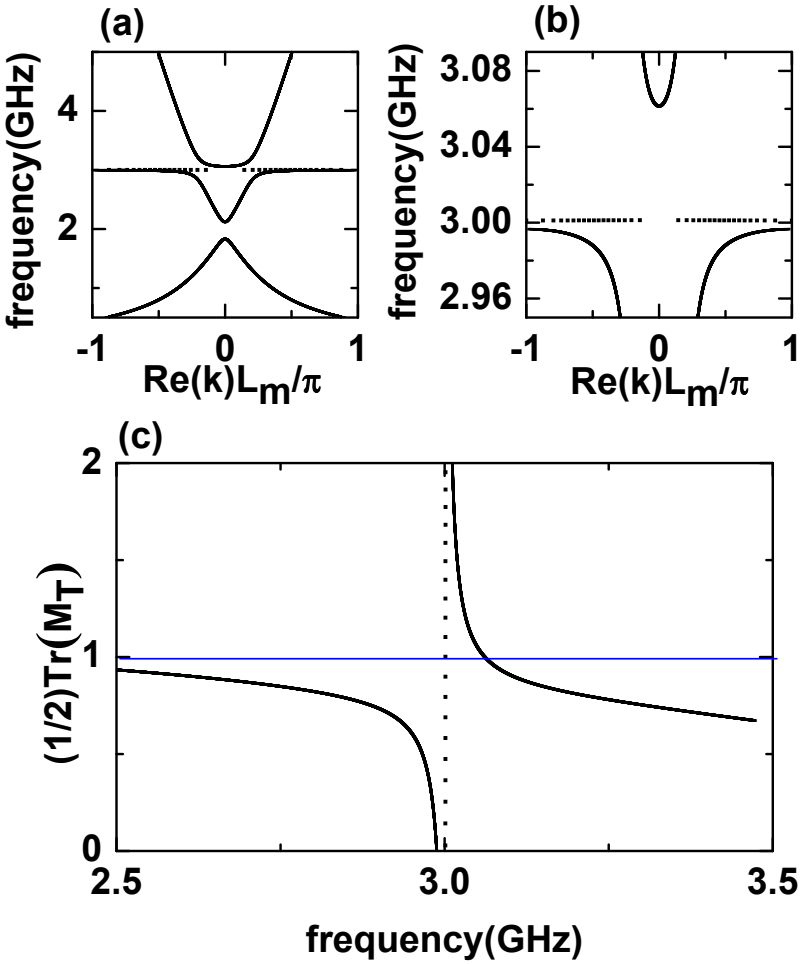

Fig. 13 [(a) and (b)] Two different views of the dispersion relation corresponding to a fourth-order Rudin-Shapiro superlattice, with dispersive B and C layers of equal Drude-like dielectric functions ($\omega_e/2\pi = \omega_m/2\pi = 3\,\text{GHz}$) calculated for oblique incidence of $\theta = \pi/12$ and with the inclusion of light absorption via the choice of $\gamma_0 = \gamma_e = \gamma_m = 0.001$. (c) Graphical representation of the real part of the transcendental equation (8) in the case of $k = 0$ around 3 GHz for same value of γ_0. The curved lines correspond to the calculated trace whilst the horizontal line corresponds to the evaluation of the left hand side in (156) at the zone center point.

7.1 Self-similarity in the plasmon-polariton spectrum of Rudin-Shapiro photonic superlattices

Reached this point in the chapter, it is time to say something regarding self-similarity. As mentioned in the introduction, the possibility of a fractal nature asso-

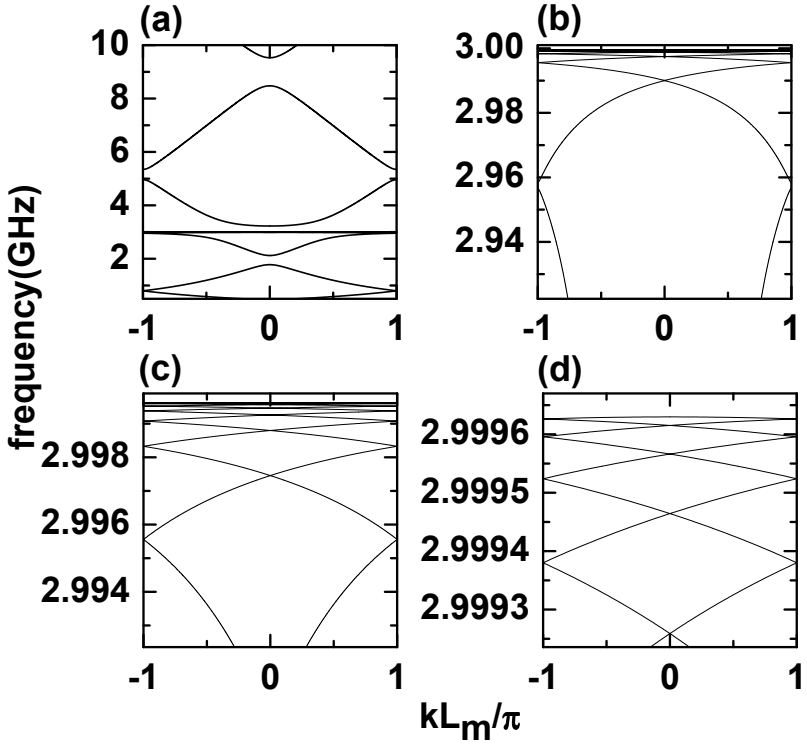

Fig. 14 Different views [normal (a) and zoomings around the plasma frequency (b)-(d)] of the dispersion relation for a fifth-order generation Rudin-Shapiro superlattice with dispersive B and C layers of equal Drude-like dielectric functions ($\omega_e/2\pi = \omega_m/2\pi = 3\,\mathrm{GHz}$) calculated for oblique incidence of $\theta = \pi/6$. The figures (c) and (d) allow to observe the self-similarity in the plasmon-polariton spectrum.

ciated to the RS sequence is, by far, the most intriguing part of the present study. Although not completely conclusive, the results that will be shown below constitute a new point of view in the quest for clarifying this matter.

In our numerical experiments we have detected the appearance of this phenomenon in the case when the dielectric features of the dispersive layers B and C are taken to be equal, with the specific superlattice dimensions and parameters mentioned above. This does not

mean that a configuration in which the dispersive layers have different ω_e, ω_m is excluded from presenting this property. As it has been pointed out by Perez-Alvarez et al. [24, 25], the fractal character in the spectrum of RS-based heterostructures greatly depends on the particular geometry –that is, the layer widths and the generation order– and, in our case, the combination of dielectric and magnetic properties of the constituent layers.

If the absence of absorption, a process of zooming into the plasmon-polariton mode region close to 3 GHz, leads to the results shown in the figures 14 and 15, for the $m = 5$ and $m = 8$ Rudin-Shapiro superlattices, respectively, when the angle of incidence is equal to $\pi/6$. It is possible to observe the reproduction of the dispersi-

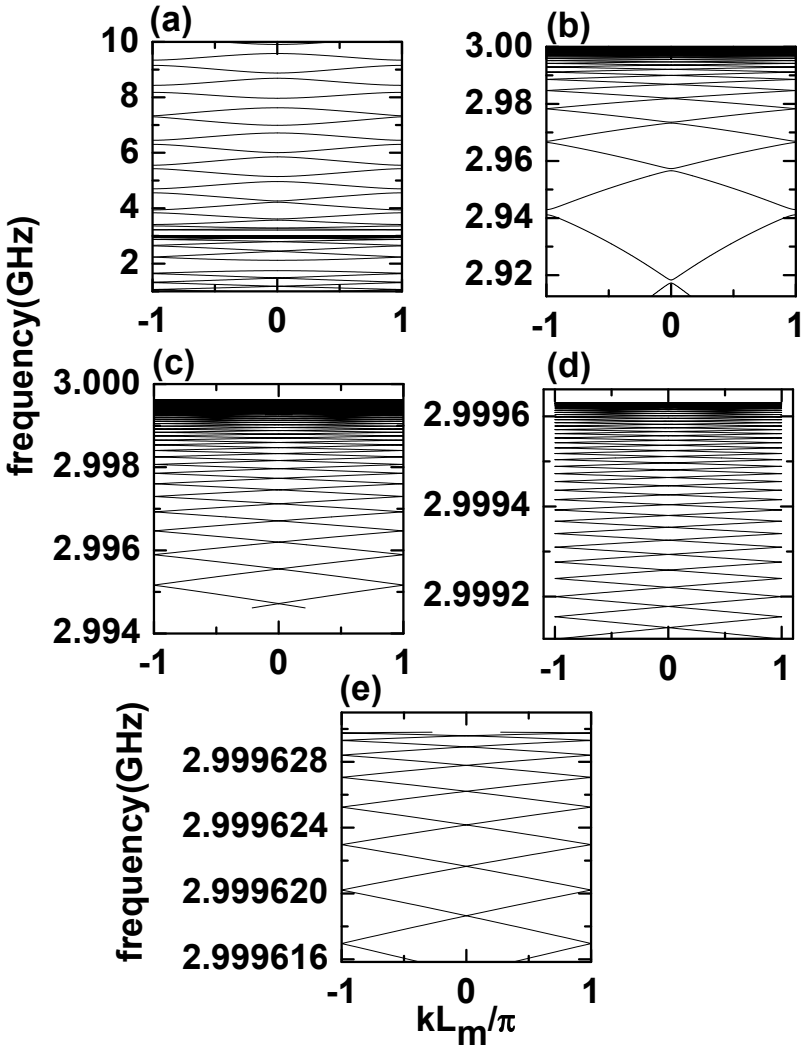

Fig. 15 The same as in figure 7 but for the case of superlattice with an eighth-order generation Rudin-Shapiro unit cell. In this case, the self-similar character of the plasmon-polariton states is directly observed from figures (b)-(e).

on pattern as long as the partition of the frequency interval becomes narrower. Of course, this effect is more pronounced in the case of the higher RS-generation, as it should be expected. In principle, the fractality is a feature of the quasiregular sequence as a whole; that is, an infinity non-periodic array of letters (layers). That the self-similarity can manifest for a quasiregular sequence in a generation order as low as the fifth one would be, in this case, a consequence of the periodic rep-

etition of the corresponding RS unit cell, associated to the superlattice structure. Of course, the use of higher-order generations will surely lead to a much more defined self-similar sets of plasmon-polariton branches thus allowing for the estimation of the fractal dimension of, let us say, the set of points corresponding to $k = 0$ solutions of (8), which would provide information on the fractal nature of these RS-based systems.

The numerical experiment that allows to discover the self-similarity in the plasmon-polariton spectrum of this particular RS sequence, with equal B and C layers, resembles that of ref. [25]; in which the parameters of the four letter (layers) were chosen to be equal in two pairs, as mention in the introduction. The fact of making $B = C$ in our RS-sequences reinforces, in some way, the quasiregular distribution of this particular dispersive layer in the structure. Then, there is a greater chance of revealing a fractal-related property like self-similarity in the spectrum of this kind of elementary excitations, as it happens in the example under discussion.

All this makes more necessary to continue the calculation of the plasmon-polariton modes in RS-based superlattices with different choices of the geometry and dielectric and magnetic properties. Then, it would be possible to assert that, despite the non-applicability of the Bovier-Ghez theorem, the RS quasiregular sequence has an associated fractal nature. The example reported here undoubtedly contributes to clarify this possibility for the spectrum of elementary excitations in RS-based one-dimensional structures. It also shows a way to study this problem in depth. Some work in this direction is still on progress.

8 Conclusions

We have studied the problem of the excitation of plasmon-polariton modes in Rudin-Shapiro photonic superlattices made of non-dispersive and dispersive dielectric layers, with the possibility of having frequency intervals of right-handed and left-handed behaviors in different layers. The discussion of the main features of the photonic structure shows the particular dependence of zeroth-order, Bragg and polariton frequency bandgaps with the value of the angle of incidence.

The work reveals the negative effect of the optical absorption in the sense that even very small values of the damping in the dielectric function of the layers result in the loss of physically meaningful solutions for the characteristic superlattice dispersion relation in the optical range around the plasmon frequency.

When there are plasmon-polariton modes we found that, in a particular configuration, the property of self-similarity appears in the plasmon-polariton branches of the photonic spectrum. This is one of the few examples that highlight the presence of a fractal-related property in one-dimensional heterostructures made under the Rudin-Shapiro sequence.

Acknowledgments

M.E. Mora-Ramos acknowledges support from Mexican CONACYT through grant 101777 (CB-2008).

References

1. E. Yablonovitch, Phys. Rev. Lett. **58**, 2059 (1987).
2. S. John, Phys. Rev. Lett. **58**, 2486 (1987).
3. J. D. Joannopoulos, *Photonic Cristals, Molding the flow of light. 2nd. Edn.* (Princeton University Press, 2007).
4. A. A. Houck, J. B. Brock, and I. L. Chuang, Phys. Rev. Lett. 90, 137401 (2003).
5. D. R. Smith and N. Kroll, Phys. Rev. Lett. 85, 2933 (2000).
6. Z. M. Zhang and C. J. Fu, Appl. Phys. Rev. Lett. 80, 1097 (2002).
7. J. Li. L. Zhou, C. T Chan, and P. Sheng, Phys. Rev. Lett. 90, 083901 (2003).
8. V. G. Veselago, "*The Electrodynamics of Substances with Simultaneously Negative Values of* ε *and* μ", Sov. Phys. Usp. **10**, 509 (1968).
9. R.A. Silin, "*Optical properties of artificial dielectrics*", Izv. VUZ Radiofiz. **15**, 809-820 (1972).
10. L.I. Mandel'shtam, "*Group velocity in crystalline arrays*", Zh. Eksp. Teor. Fiz. **15**, 475-478 (1945).
11. G.D. Malyuzhinets, "*A note on the radiation principle*", Zh. Tekh. Fiz. **21**, 940-942 (1951).
12. D.V. Sivukhin, "T*he energy of electromagnetic waves in dispersive media*", Opt. Spektrosk. **3**, 308-312 (1957).
13. W. Rotman, "*Plasma simulation by artificial dielectrics and parallel-plate media*", IEEE Trans. Antennas Propag. **10**, 82-95 (1962).
14. J. Brown, "*Artificial dielectrics having refractive indices less than unity*", Proc. IEEE, Monograph no. 62R, **100**, pp. 51-62 (1953).
15. J. B. Pendry, A. J. Holden, W. J. Stewart, and I Youngs, Phys. Rev. Lett. **76**, 4773 (1996).
16. D. R. Smith and N. Kroll, Phys. Rev. Lett. 85, 2933 (2000).
17. L. Wu, S. He, and L. Shen, Phys. Rev. B. 67,235103 (2003).

18. E. Reyes-Gómez, D. Mogilevtsev, S. B: Cavalcanti, C. A. A. De Carvalho and L. E. Oliveira "*Plasmon polaritons in photonic superlattices containing a left-handed material*", Eur. Phys. Lett. **88**, 24002 (2009).
19. E. Reyes-Gómez, N Raigoza, S. B. Cavalcanti, C. A. A. de Carvalho, L.E. Oliveira, Phys. Rev.B. 81 , 153101.
20. M. Dulea, M. Johansson, and R. Riklund, "*Localization of electrons and electromagnetic waves in a deterministic aperiodic system*", Phys. Rev. B **45**, 105114 (1992).
21. W. Gellermann, M. Kohmoto, B. Southerland, and P. C. Taylor, "*Localization of light waves in Fibonacci dielectric multilayers*", Phys. Rev. Lett. **72**, 633 (1993).
22. V. Agarwal and M.E. Mora-Ramos, "*Optical characterization of polytype Fibonacci and ThueMorse quasiregular dielectric structures made of porous silicon multilayers*", J. Phys. D: Appl. Phys. **40**, 3203-3211 (2007).
23. R. Pérez-Alvarez, F. García-Moliner, C. Trallero-Giner and V.R. Velasco, "*Polar optical modes in Fibonacci heterostructures*", Journal of Raman Spectroscopy, **31**:5, 421-425 (2000).
24. R. Pérez-Alvarez, F. García-Moliner, and V.R. Velasco, *"Some elementary questions in the theory of quasiperiodic heterostructures*", J. Phys.: Cond. Matt. **13**, 3689-3698 (2001).
25. R. Pérez-Alvarez and F. García-Moliner, "*The spectrum of quasiregular heterostructures*", invited chapter in "*Some Contemporary Problems of Condensed Matter Physics*", Nova Science Publishers, ed. by S. Vlaev and M. Gaggero-Sager (2000), pp. 1-37.
26. V.R. Velasco, R. Pérez-Alvarez and F. García-Moliner, "*Some properties of the elastic waves in quasiregular heterostructures*", J. Phys.: Cond. Matt. **14**, 5933-5957 (2002).
27. A. Bovier and J.M. Ghez, "*Spectral properties of one-dimensional Schrödinger operators with potentials generated by substitutions*", Commun. Math. Phys. **158**(1), 45-66 (1993).
28. A. Bovier and J.M. Ghez, "*Remarks on the spectral properties of tight-binding and Kronig-Penney models with substitution sequences*", J. Phys. A: Math. Gen. **28**:8, 2313-2324 (1995).
29. M. J. E. Golay, "*Static multislit spectrometry and its application to the panoramic display of infrared spectra*", J. Opt. Soc. Am. **41**, 468-472 (1951).
30. H. S. Shapiro, "*Extremal problems for polynomials and power series*", Master's Thesis, M.I.T., (Cambridge, Mass., 1951).
31. W. Rudin, "*Some theorems on Fourier coefficients*", Proc. Am. Math. Soc. **10** 855-859 (1959).
32. R. Pérez-Álvarez and F. García-Moliner "The spectrum of quasi-regular heterostructures", Nova Scientia (to be published).
33. R. C. Hilborn, "Chaos and nonlinear dynamics", (Oxford University Press, 1994).
34. P. Drude, "*Zur Elektronentheorie der Metalle*", Annalen der Physik 1, 566 (1900).
35. J. D. Jackson, *Classical Electrodynamics*. Wiley, New York, 1999 (3rd ed.).
36. R. F. Harrington, *Time-harmonic Electromagnetic Fields*. McGraw-Hill, New York, 1961.
37. L. D. Landau, E. M. Lifshitz, and L. P. Pitaevskii, *Electrodynamics of Continuous Media*. Pergamon, New York, 1984.
38. D. R. Smith, D. Schurig, and J. B. Pendry *Negative refraction of modulated electromagnetic waves*, Appl. Phys. Lett., vol. 81, pp. 27132715, 2002.
39. Rolando Prez-Alvarez, *Matrices de Transferencia y Funciones de Green en el estudio de heteroestructuras multicapas*, Tesis en opcin al ttulo de Doctor en Ciencias, La Habana, Cuba, 2005.
40. M.E. Mora, R. Pérez-Álvarez and C. Sommers, *"Transer matrix in one dimensional problems"*, J. Physique **46**:7, 1021-1026 (1985).
41. D. Moglievtsev, E. Reyes-Gómez, S. B. Cavalcanti, C. A. A. de Carvalho, L. E. Oliveira, Phys. Rev. E **81**, 047601 (2010).
42. C. A. A. de Carvalho, S. B. Cavalcanti, E. Reyes-Gómez, and L. E. Oliveira, Phys. Rev. B **83**, 081408 (2011).
43. E. Reyes-Gómez, N. Raigoza, S. B. Cavalcanti, C. A. A. de Carvalho, and L E Oliveira, J. Phys.:Condens. Matter **22**, 385901 (2010).

Transmission for a finite superlattice with a linear modulation of the barriers height

K. A. Rodríguez-Magdaleno, J. C. Martínez Orozco, D. A. Contreras-Solorio

Abstract

We use the transfer matrix method and the Ben Daniel-Duke equation for electrons with variable mass for calculating the transmittance for a finite superlattice where the potential barriers height has a linear modulation like that of an inverted "V" letter. The energy dependence of the transmittance presents intervals of stopbands and nearly flat passbands. We calculate the transmission for several numbers of barriers as well as for different barrier and wells widths and make a comparison with the transmission obtained for a regular superlattice.

1 Introduction

The subject of propagation of any kind of waves in layered structures is very important and interesting. One of their important applications is as reflector structures and as filters. The search for energy, electronic, optical and acoustic filters is an interesting and active field. There have been proposals of energy passband filters using quantum superlattices with a Gaussian potential profile [1, 2]. These layered structures allow the incident electrons to be nearly totally transmitted when the impinging electron energy is in the passband energy region. Also, a complete reflection occurs when the impinging energy is in the stopband energy region. The idea behind using these types of structures is that a Gaussian profile provides a slowly varying potential for the layers, which can improve the transmission of electrons through the multilayer system. Following the idea of the superlattices with

Unidad Académica de Física de la Universidad Autónoma de Zacatecas. Apartado Postal C-580, 98060 Zacatecas, Zac., Mexico. e-mail: D. A. C. S.: dacs10@yahoo.com.mx

a Gaussian potential profile, layered omnidirectional optical mirrors have been proposed where the refractive index varies according to the envelope of a Gaussian function, using only normal materials [3] and using also metamaterials [4]. These systems were proposed only as omnidirectional mirrors but their properties as optical filters were not investigated. However, there is a proposal of a multilayer optical filter where the refractive index of the layers is modulated by a Gaussian function [5]. Likewise, there is a proposal of a layered acoustic filter where the characteristic acoustic impedance of the layers is modulated by a Gaussian distribution [6]. In this work we propose a structure where the height of the potential barriers follows a linear profile like that of an inverted V letter. The spectrum of eigenenergies for this type of structure consists of quasibands or passbands separated by energy gaps or stopbands. For the calculations we use the transfer matrix method and the Ben Daniel-Duke equation for variable mass electrons [7]. The spectrum of transmittance of the structure presents stopbands and nearly flat transmission bands of energy. In the next section we introduce the theoretical background, then we present some of our results and discussion of the behavior of the transmittance and finally we give some conclusions.

2 Theoretical model and calculation method

The propagation of the electrons in the structure is described by the Ben Daniel-Duke equation, appropriate for electrons with variable effective mass m^*

$$-\frac{\hbar^2}{2}\frac{d}{dz}\left\{\frac{1}{m^*(z)}\frac{d\psi(z)}{dz}\right\}+V(z)\psi(z)=E\psi(z) \tag{1}$$

The boundary conditions are the continuity of ψ and $\frac{1}{m*}\frac{d\psi(z)}{dz}$.

In order to solve the previous equation we use the theory for transfer matrix of Reference [8].We consider a system of n coupled differential equations of second order with variable coefficients,

$$A(z)\frac{d^2f}{dz^2}+B(z)\frac{df}{dz}\{D(z)-EI\}f=0 \tag{2}$$

with

$$f = \begin{pmatrix} f_1(z) \\ f_2(z) \\ f_3(z) \\ \cdot \\ \cdot \\ \cdot \\ f_n(z) \end{pmatrix}, \tag{3}$$

and A, B y D are $n \times n$ matrices, I is the identity matrix, $f_i(z)$ are the n unknown functions of the system. We also use the notation

$$f'' = \frac{d^2}{dz^2} \qquad f' = \frac{d}{dz}, \tag{4}$$

The system can be changed to another system of 2n equations of first order $F' = PF$ where

$$P = \begin{pmatrix} 0 & I \\ A^{-1}(EI - D) & -A^{-1}B \end{pmatrix} \tag{5}$$

$$F = \begin{pmatrix} f \\ f' \end{pmatrix}, \tag{6}$$

F is a column vector of $2n$ components, and P is a $2n \times 2n$ matrix. The system $F' = PF$ has $2n$ independent solutions F_j, with $j = 1, 2, 3, ...2n$. Every solution F of the system can be expressed as a lineal combination

$$F = \sum_{j=1}^{2n} c_j F_j. \tag{7}$$

The matrix M of complete transfer is defined as

$$F(z) = M(z, z_0) F(z_0), \tag{8}$$

or also

$$\begin{pmatrix} f(z) \\ f'(z) \end{pmatrix} = \begin{pmatrix} M_{AA}\ M_{AD} \\ M_{DA}\ M_{DD} \end{pmatrix} = \begin{pmatrix} f(z_0) \\ f'(z_0) \end{pmatrix}, \tag{9}$$

where the $M_{\alpha\beta}$ are *nxn* blocks of the transfer matrix $M(z,z_0)$. This matrix transfer the solution at z_0 to another point z. M is called a complete transfer matrix because it transfers f and also f', in order to distinguish it from the matrix that transfers only f.

We consider electrons as plane waves. The transmittance T is given by by the ratio of the transmitted probability current density to that of the incident one, and is given in terms of the transfer matrix by

$$T = \frac{4k^2}{[(k^2 M_{AD} - M_{DA})^2 + k^2 (M_{AA} + M_{DD})^2]}, \tag{10}$$

where k is the wave vector in $GaAs$ for $V = 0$.

3 Results

We consider a structure made with the materials $GaAs/Al_xGa_{1-x}As$ with a profile like that shown schematically in Figure. 1. The height of the barriers follows a linear variation like an inverted "V" letter. The gallium arsenide gap is $1.42eV$. We consider an $AlAs$ concentration until $x = 0.45$ for which $AlGaAs$ has still a direct gap. At this concentration we take a gap of $1.98eV$ for $AlGaAs$. The conduction band offset for the $GaAs/AlGaAs$ interface is 0.6. Then the maximum height which can be taken for the central barrier is 0.33 eV corresponding to a concentration $x = 0.45$. All the barriers have the same width and similarly, all the wells have the same width, different in general from that of the barriers. The width is given in monolayers, one monolayer has a thickness of 2.825Å.

We follow the virtual crystal approximation (VCA), taking a linear variation of the potential barrier V(x) for $0 \leq x \leq 0.45$ We take the

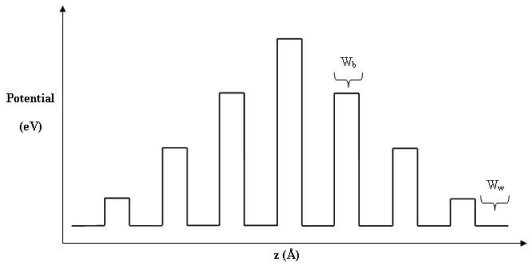

Fig. 1 Schematic potential profile of the structure. The barriers have width Wb and the wells width Ww.

electron effective mass for AlAs as that of the gamma point of the Brillouin zone, $m_A = 0.15$. Similarly for GaAs, $m_G = 0.067$. The effective mass for $Al_xGa_{1-x}As$ (m_i) is calculated using the VCA formula [9].

$$\frac{1}{m_i} = \frac{x_i}{m_A} + \frac{1-x_i}{m_G} \tag{11}$$

We perform the computations for the electronic transmittance for normal incidence of the electrons within the transfer matrix formalism solving the Ben Daniel-Duke equation that takes into account the dependence of the effective mass for the ternary alloy through the VCA approximation. We take a maximum height of 0.25 eV for the central barrier and a minimum height of $0.25/((N_b+1)/2)eV$ for the height of the end barriers, where N_b is the total number of potential barriers. We denote with W_b and W_w the barrier and well width, respectively. In Figure 2 we present the transmittance versus energy of the incident electrons for a structure with 15 barriers of width 5 ML and a well width of 30 ML. The flat passbands are outstanding. In Figure 3 we show the transmittance for 11, 13 and 15 barriers, W_b is 5 ML and W_w is 22 ML. The black curve corresponds to the case of 11 barriers, the red one to 13 barriers and finally the blue line to 15 barriers. We can observe that the passband becomes narrower as the number of barriers increase, but in the three cases the passbands can be considered nearly flat. In Figure 4 we compare the transmittance spectrum for a structure with an inverted "V" linear profile with that of a regular structure where all the barriers have the same height of 0.25 eV. In both cases the barrier and well width have the same values which

correspond to those of Figure 3. We see that for the regular structure we cannot obtain flat passbands. We argue that the physical reason which causes flat transmission bands is that the reduction of the barriers height from the center to the borders of the structure, causes that the lifetime of the eigenstates decreases because the electrons in the wells tunnel more easily to the outer sides. By the Uncertainty Principle, the bandwidth of the corresponding resonance curves increases. Since the passbands of the structure are the envelope of the resonance curves, then this type of profile can improve the transmission in the passbands. When the number of barriers is higher, the total thickness of the superlattice increases and the lifetime of the eigenstates raises, and the bandwidth of the resonance curves decreases. This causes a reduction of the passband width and that the transition from stopbands and passbands is sharper.

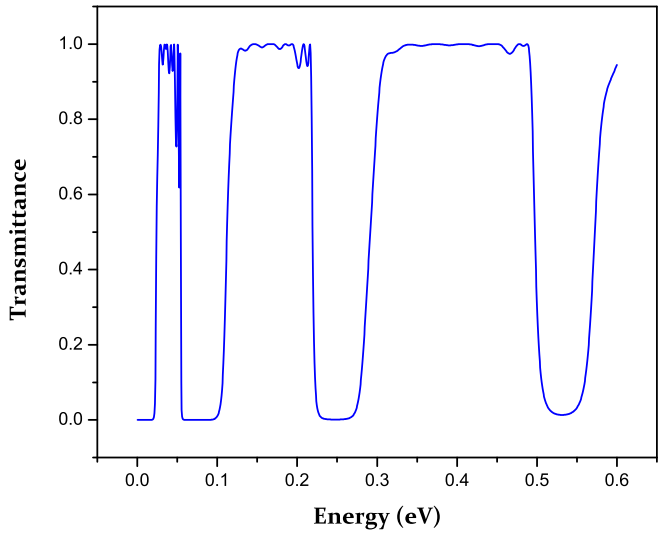

Fig. 2 Transmittance as a function of energy for an inverted "V" like potential barrier height lineal dependency for a 5 ML barrier width and a 30 ML wells width for 15 barriers. We observe three rather well defined passbands for energies within the intervals (0.028 - 0.054) eV, (0.127 - 0.215) eV and (0.310 - 0.489) eV.

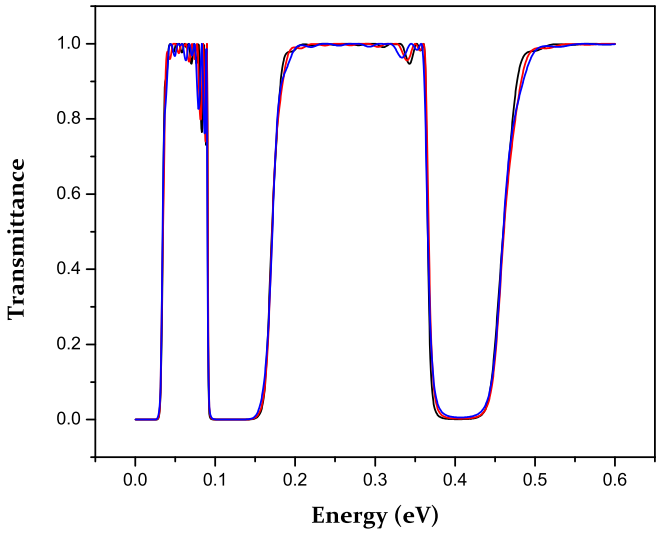

Fig. 3 Transmittance as a function of energy. We compare the transmittance of the superlattices formed by 15, 13 and 11 barriers, taking the width of the barriers 5ML and the width of the wells 22ML. The blue curve corresponds to the superlattice of 15 barriers, the red curve of 13 barriers and the black curve of 11 barriers.

4 Conclusions

We have made a study of the electrons transmittance for a finite superlattice where the height of the potential barriers follows an inverted "V" like potential profile. The transmittance presents flat transmission and reflection bands. This type of structure could have applications as energy filters for electrons, investigating a design which could eliminate unsuitable bands, allowing electrons of a selected energy interval to pass through. This superlattice could also be suitable for quantum wells solar cells. For this purpose we plan to do calculations for this structure subject to an electric field.

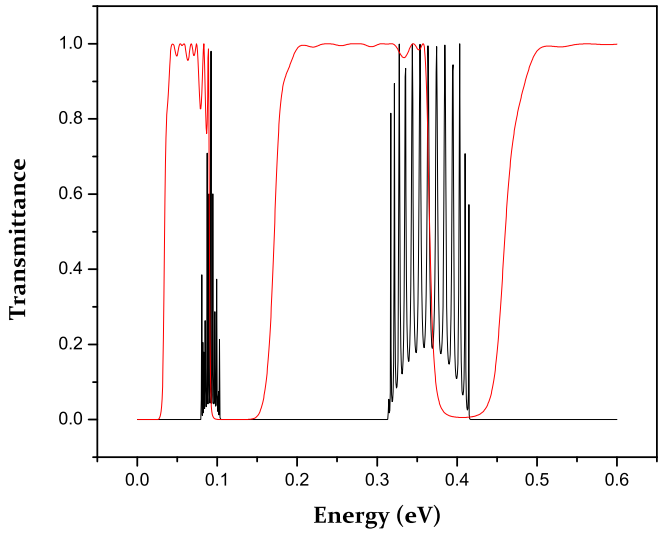

Fig. 4 Transmittance as a function of energy. In this figure we compare the transmittance of a superlattice for an inverted "V" potential profile (red line) and a regular superlattice (black line), where the width barriers is 5ML and the width wells is 22ML

ACKNOWLEDGEMENTS

This work has been supported partially by Universidad Autónoma de Zacatecas and Consejo Zacatecano de Ciencia y Tecnología (COZCyT).

References

1. H. H. Tung and C. P. Lee, *An energy band-pass filter using superlattice structures*, IEEE J. Quantum Electron. 32, 507-512 (1996).
2. I. Gómez, F. Domínguez-Adame, E. Diez, and V. Bellani, *Electron transport across a Gaussian superlattice*, J. Appl. Phys. 85(7), 3916-3918 (1999).
3. J. Arriaga and X. Saldaña, *Band structure and reflectivity of omnidirectional Si-based mirrors with a Gaussian profile refractive index*, J. Appl. Phys. 100(4), 044911 (2006).
4. X. I. Saldaña, D. A. Contreras Solorio, and A. Enciso Muñoz, *Reflectancia de una estructura multicapas con intercalado de materiales izquierdos*, 20 Encuentro Nal. De Inv. Cient. y Tec. del Golfo de México, Cd. Victoria, Tam., México (2008).
5. J. Madrigal Melchor, Agustín Enciso Muñoz, X. I. Saldaña, D. A. Contreras-Solorio, *Filtro óptico multicapas con variación gaussiana del índice refractivo*, LII Congreso Nacional de

Física, Acapulco, Guerrero, Mxico (2009).
6. J. Madrigal-Melchor, R. A. Reyes-Villagrana, X. Saldaña, S. Jelev-Vlaev, and D. A. Contreras-Solorio, *Acoustic layered filter with a Gaussian distribution of impedances*, SLAFES, Book of Abstracts. Iguazú, Argentina (2008).
7. D. J. Ben Daniel and C. B. Duke, Phys. Rev. 152, 683-692 (1966).
8. R. Pérez-Álvarez, F. García-Moliner, Transfer matrix, *Green functions and related techniques* (Universitat Jaume I, Spain, 2004).
9. J. Singh, *Physics of semiconductors and their heterostructures* (McGraw-Hill, 1993).

Recent Progress in the codes implementing Density Functional Theory

J.A. Camargo-Martínez, R. Baquero

Abstract

It is known that one of the traditional short comes of the codes based on Density Functional Theory is its impossibility to account for the band gap of semiconductors. This is the case of several known codes as Abinit, Siesta, Hamilt, and others. It is also the case for Wien 2K. Very recently, in the so call code Wien 2011, this difficulty was overcome. In this paper, we report our analysis of this recent progress. We have calculated, using this code, the band structure of several semiconductors and found an important improvement in the overall agreement with experiment which remains nevertheless in some very few cases as big as 20% off. In spite of it, this new progress opens the possibility for surface and interface calculations involving semiconductors which were not possible with the necessary accuracy using the former versions of any code implementing Density functional Theory and therefore some important findings remained uncertain. Further, the recommendation to optimize within the Local Density Approximation and to use the lattice constant found in this way into the new code to proceed with a calculation is analyzed in detail and found appropriate, It remains, nevertheless, according to us, as a point to fix in more detail in the future.
PACS: 71.15.Mb;71.20.Mq;71.20.Nr;71.20.Be
Keywords: TB-MBJLDA potential; semiconductors, band gap; Wien2k 2011

J. Flores-Méndez and R. Baquero
Departamento de Física, CINVESTAV-IPN, Av. IPN 2508, 07360 México

1 Introduction

Density Functional Theory (*DFT*) is nowadays the most used method to calculate band structures. It is implemented in several codes. One very well known is the Wien2k code. It has evolved in several versions. A friendly interaction was produced already in the 2000 version. Nevertheless, a long standing problem of all the codes based on *DFT* was that the band structure of semiconductors, although giving a reasonable account of the dispersion of the bands, was systematically unable to reproduce the experimental values of the gap, This problem could be solved by hand using a trick but this kind of solution is not what we expect from an *ab initio* calculation. The removal of this problem in the new version (*Wien2k 2011*) is the subject of the analysis that we present in this work. The new ability to reproduce the gap value of semiconducting materials, allows confirming results for semiconductor/metal and semiconductor/semiconductor interfaces and to calculate new ones. These results are of technological interest and per se. For example, the *YBCO7/GaAs*(001) interface was calculated [1] using the previous version of the *Wien2k* code (2008 version) and two atomic planes in the GaAs side of the interface were found to be metallic. This result could, nevertheless, be influenced by the inability of the previous version of the code to properly account for the gap of the semiconductor. Since the trick mentioned above could not be used in an interface calculation, the result remained questionable because of the uncertainties in the *GaAs* side results around the very important gap region. The rest of the paper is organized as follows. In the next section II, we deal very briefly with Density Functional theory (*DFT*) to point to a detail important to this work. In section III, we briefly present a few of our calculated results for the band structure of metals to check that the accuracy of the new version remains the same also in this case. Section IV is devoted to semiconductors. We recalculate the results from references [2] and [3] and present new results for some other semiconductors which we compare to experiment. In a final section V, we analyze the results with the new code and present our conclusions.

2 Density Functional Theory

In solids, ions and electrons constitute a many body interacting system described by a Schrödinger equation with too many particle coordinates to be numerically treatable nowadays, as it is very well known. During the last decade, several codes were developed based on *DFT* and this method became the most used, precise and practical way to calculate the band structure of solids. The development of practical approximations to the correlation and interchange potential lead to a remarkable degree of accuracy to describe even complicated metallic systems. At the basis of *DFT* is the celebrated Hohenberg-Kohn theorem which shows that the density of the ground state contains all the possible information on a system and its knowledge is equivalent to the wave function itself. So, the expectation value [4] of any observable can be calculated from a unique functional of the ground state density, $\rho(r)$, which minimizes the energy functional, E[ρ]. Further, Kohn and Sham [5] transformed the many-body problem into a one-body problem and showed that the density of states calculated from the solution of the so-called Kohn-Sham equations ((1)) is equal to the one of the real ground state density of the many-body system,

$$[T + V_H + V_{xc}]\varphi_i(r) = \varepsilon_i \varphi_i \tag{1}$$

Where the density is calculated taking into account the occupied states only. In eq. (1), T is the kinetic energy operator, V_H is the Hartree potential and V_{xc} is the exchange and correlation potential which is calculated from the exchange and correlation energy functional,$V_{xc}(r) = \frac{\delta E_{xc}[\rho]}{\delta \rho}$. To solve the Kohn-Sham equations (1), an explicit expression for $E_{xc}[\rho]$ is needed. The exact expression is unknown since it includes all kind of correlations between all the particles in the system. So an approximation is needed. The first and best known approximation is Local Density Approximation, *LDA* [6], which was followed by the Generalized Gradient Approximation (*GGA*)[6] and the *meta-GGA* [7] among other approximations. These potentials reproduce rather well the band structure of even complicated metallic systems but fail in reproducing the gap in semiconductors. A recent progress has been made. Blaha et al. [2] have reported the so-called *TB-MBJLDA* potential which is a modification of the exchange and correlation potential of Becker and Johnson (*BJ*) [8]. The new potential reproduces the

experimental gaps with accuracy several orders of magnitude better than the former existing potentials. The modified *TB-MBJLDA* is

$$V_{x,\sigma}^{MBJ}(r) = cV_{x,\sigma}^{BR}(r) + (3c-2)\frac{1}{\pi}\frac{\sqrt{5}}{12}\frac{\sqrt{2t_\sigma(r)}}{\rho_\sigma(r)} \tag{2}$$

Where $\rho_\sigma(r)$ is the density of states, $t_\sigma(r)$ is the kinetic energy density and $V_{x,\sigma}^{BJ}(r)$ is the Becker-Roussel potential (*BR*) [9]. The c stands for,

$$c = \alpha + \left(\beta\frac{1}{V_{cell}}\int d^3r\frac{|\nabla\rho(r)|}{\rho(r)}\right)^{1/2} \tag{3}$$

α and β are free parameters. Within the *Wien2k 2011* code $\alpha = -0.012$ and $\beta = 1.023$ $Bohr^{1/2}$. We now proceed to present our results using the new *Wien2k 2011* code.

3 Metal calculations

We present here our result for Nb, V and Ta, just to check whether differences arise between the old code and the new one for the case of metals. We have calculated these band structures, first, using the Full Potential-Linearized Plane Waves plus local orbitals (*FP-LAPW + lo*) approximation as implemented in the *Wien2k* code [10] and then we redid the same calculation using the new *MBJLDA* potential [2] implemented in the Wien 2011 code. Some of the relevant parameters are presented in Table 1.

Table 1 The lattice parameter, a, in Angstrom; the Fermi energy, E_F, in Rydbergs; the density of states at E_F, $N(E_F)$ in states per Rydberg for Nb, V and Ta calculated with LDA and with MBJLDA. The experimental values were taken from reference [11].

	Experiment	LDA			MBJLDA		
Element	a	a	E_F	$N(E_F)$	a	E_F	$N(E_F)$
Nb	3.30059	3.2487	0.78890	24	3.2746	0.7535	23
V	3.02487	2.9273	0.67200	28.28	2.9574	0.6362	30.54
Ta	3.30280	3.2500	0.84131	21.20	3.3114	0.7950	21.95

We have made the corresponding optimization of the lattice parameter, a, using the same potential as to calculate the band structure and

the density of states. As it can be appreciated from the table, some small but not negligible differences occur. This illustrates the need to follow the following procedure. To optimize the lattice parameter in a consistent way it is recommended [2] to use *LDA* (*GGA*) first and to use further the optimized lattice parameter obtained in this way to compute with the *MBJLDA* new potential. If we follow this method, we find a better agreement between *LDA* and *MBJLDA* for all the three metals calculated as it can be checked from Table 2.

Table 2 Result of the new calculation optimizing both with LDA. The symbols and the units are the same as in Table 1. Here we use the lattice parameter optimize with LDA for both calculations (see Table 1).

	LDA		MBJLDA	
Element	E_F	$N(E_F)$	E_F	$N(E_F)$
Nb	0.78890	24	0.7785	22.15
V	0.67200	28.28	0.6734	29.24
Ta	0.84131	21.20	0.8572	20.78

Indeed, the Fermi energy for *Nb*, differs 0.01 Ry which represents 1.3% with respect to the *LDA* value which improves the 4.5% difference from Table I. For *V* and Ta these values are 0.2% and 1.8% which improve the 5.3% and 5.5% difference from Table I, respectively. So, we conclude that the recommendation given should be followed in any case, not only when dealing with semiconductor systems, to get better results when the use of the *MBJLDA* potential is compulsory as in the case of a metal/semiconductor interface, for example. The argument to it was given by Blaha et al. [2] in the sense that since there is no exchange functional, E_x, from which an exchange potential can be obtained, $V_{xc}(r) = \frac{\delta E_{xc}[\rho]}{\delta \rho}$, the procedure is justified. We omit the plot of the band structure and the density of states obtained in the different ways mentioned here since the overall agreement is such that the details just discussed do not show explicitly enough and these band structures are very well known. For *Nb* we have compared our results with references [12, 13, 14], *V* with references [14, 15] and for *Ta* with reference [16].

4 Semiconductor calculations

In Table 3, we present the gap value obtained from our band structure calculations for several semiconductors using *LDA* and the new *MBJLDA* as in the *Wien2k 2011* code and compare our results with the ones reported by Blaha et al. [2], with the ones obtained using the hybridized exchange potential of *Heyd-Scuseria-Ernzerhof* (*HSE*) reported in reference [3] and to the experimental values reported in references [2, 3, 17, 18].

Table 3 The gap is in eV, the crystal structure is indicated in the second column, the data are from Blaha et al. [2], from HSE [3] and the experimental ones from references [2, 3, 17, 18].

		This work		Blaha et al.			
Element	Structure	LDA	MBJLDA	LDA	MBJLDA	HSE	Expt.
Si	A1	0.48	1.18	0.47	1.17	1.28	1.17
Ge	A1	0.00	0.86	0.00	0.85	0.56	0.74
MgO	B1	4.72	7.27	4.70	7.17	6.50	7.55
LiF	B1	8.78	13.10	8.94	12.94		14.20
AlAs	B3	1.35	2.16	1.40[a]		2.24	2.23
SiC	B3	1.31	2.25	1.35	2.28	2.39	2.40
BP	B3	1.19	1.86	1.31[a]		2.16	2.00
BAs	B3	1.23	1.71	1.16[a]		1.92	1.46
InP	B3	0.45	1.57		1.40[b]	1.64	1.43
AlP	B3	1.45	2.32	1.46	2.32	2.52	2.45
BN	B3	4.78	6.07	4.39	5.85	5.98	6.22
GaN	B3	1.66	2.80	1.63	2.81	3.03	3.20
CdTe	B3	0.49	1.65	0.61[a]		1.52	1.49
GaAS	B3	0.30	1.64	0.30	1.64	1.21	1.52
ZnS	B3	1.83	3.63	1.84	3.66	3.42	3.91
CdS	B3	0.87	2.63	0.86	2.66	2.14	2.42
AlSb	B3	1.14	1.79	1.29[a]		1.99	1.68
InN	B4	0.02	0.86	0.02[a]		0.71	0.69
AlN	B4	4.14	5.56	4.17	5.55		6.28
ZnO	B4	0.75	2.75	0.75	2.68		3.44

[a] Reference [3]
[b] Reference [18]

As we stated before, we have made our calculations with the new *Wien2k 2011* code. We also repeated the calculation with the *LDA* to compare with the results obtained by Blaha et al. using the same approximation. Minor differences appear. They are always less than 3%. It is worth noting, nevertheless, that for BN the difference rises to 9%. It is evident from Table 3 that in any version of the code the gap values for semiconducting systems calculated with *LDA* turn out to be

wrong as it very well known. The issue here is the improvement in the calculation of the gap for all the semiconducting systems consider so far. Comparing the results with the new *Wien2k 2011* code to the ones reported by Blaha et al.[2] previously, we find minor but non-negligible differences. Some improve the agreement with experiment some do not. For *MgO, LiF, BP, BaAs, BN, AlSb* and *ZnO Wien2k 2011* is in better agreement with experiment. For *Si, AlAs, SiC, InP, GaN* and *ZnS* the previously reported results by Baha et al, [2] agree better. When comparing the *Wien2k 2011* with *HSE* (See Table 3) again some results turn out to agree better with experiment some do not. When *Wien2k 2011* and the experimental values are compared, we find that the overall agreement of the new code values is quite better and opens the possibility to consider interfaces and superlattices of systems containing semiconductor elements. Actually we think that, in this sense, the code opens a new direction of research that was not so clearly possible before. To see better the improvement of the *Wien2k 2011* code we present the following figure.

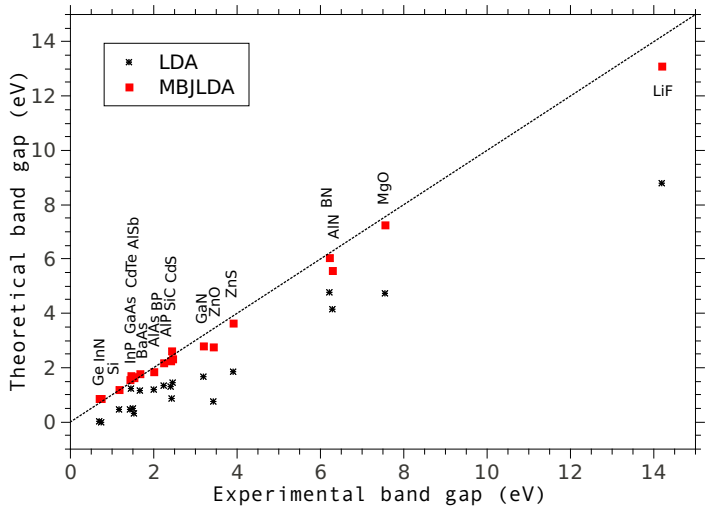

Fig. 1 Theoretical vs experimental band gaps. The are taken from Table 3

Figure 1 shows the degree of improvement from the *LDA* predictions as compare to the *MBJLDA* ones. Nevertheless the predictions of *Wien2k 2011* deviate from 0-20% which points to the fact that even

though the amount of progress is impressive, some more work is to be done in that direction. A point that still waits for a more convincing solution is the impossibility to optimize (to obtain a consistent value of the lattice constant) with the same potential with which the calculation is made.

5 Conclusions

In this paper we performed an analysis of the new progress done in the implementation of *DFT* whose most famous shortcoming was its impossibility to account for the experimental value of the band gap of semiconducting systems. We have calculated the band gap for all semiconductors reported in ref [2] and reference [3] and some other and compare the results among them and with experiment. We found that the new so-called *TB-MBJLDA* potential gives rise to gap values that represent an impressive progress as compare to the old LDA potential. This new code, the *Wien2k 2011*, allows the calculation of interfaces and superlattices with a semiconducting component with a high degree of accuracy which were impossible with the old code. For example, with the *Wien2k 2008* code, we calculated the electronic band structure of the interface *YBCO7/GaAs* and obtained [1] that two atomic planes in the GaAs side become metallic. Nevertheless since the code does not allow the correct calculation of the gap of the semiconductor, this interesting result remained uncertain [19]. In that sense, the new code opens a new field which is of interest in several disciplines as spintronics, for example. We found that the disagreement between the new code and experiment for a few semiconductors as large as 20% but on the whole, the agreement is quite good. Calculations with the *HSE* potential are also in good agreement with experiment (see Table 3). The suggestion that optimization to obtain a consistent lattice parameter should be done with the *LDA* and the result used as input in the new code, was found to give reslts in better agreement with experiment that if one would optimize with the new potential directly. Although a justification for it is given in reference [2], we find this point worst analyzing further.

References

1. A. E. Garcia, J. Camas. s. Mendoza, R Baquero-Salaguarda, L. M. Garcia-Cruz and R. Baquero, *The Icfa J. Phys.* **I**, No 4, (2008).
2. F. Tran and P. Blaha, *Phys. Rev. Lett.* **102**, 226401 (2009).
3. J. Heyd, J.E. Peralta, G.E. Scuseria, and R.L. Martin, *J. Chem. Phys.* **123**, 174101 (2005).
4. P. Hohenberg and W. Khon, *Phys. Rev. B* **136**, 13864 (1964).
5. W. Khon and L.J. Sham, *Phys. Rev.* **140**, A1133 (1965).
6. J.P. Perdew and Y. Wang, *Phys. Rev. B* **45**, 13244 (1992).
7. J.P. Perdew, S. Kurth, J. Zupan, and P. Blaha, *Phys. Rev. Lett.* **82**, 2544 (2000).
8. A.D. Becke and E.R. Johnson, *J. Chem.* **124** 221101 (2006).
9. A. D. Becke and M.R. Roussel, *Phys. Rev. A* **39**, 3761 (1989).
10. P. Blaha, K. Schwars, G.K.H. Madsen, D. Kvasnicka, and J. Luitz, *WIEN2K:Full Potential-Linearized Augmented Plane aves and Local Orbital Programs for Calculating Crystal Properties*, edited by K. Schwars, Vienna University of Technology, Austria, (2001).
11. K. Wang, R.R. Reeber, *Mat. Sci. Eng.* **R23**, 101 (1998).
12. B. Koslowski, C. Dietrich, P. Ziemenn, *Se. Sci* **557**, 225 (2004).
13. A.R. Jani, N.E. Brener an J. Calaway, *Phys. Rev. B* **38**, 9425 (1988).
14. O. Madelung, *Data in Sciene and Technology, Landolt-Borstain, Group III: Crystal and Solid StatePhysics, Vol 13 Metals; Phonon States, Electron States and Fermi Surfaces, Subvolume C.* Ed. Springer-Verlag. (1984).
15. D. Papaconstantopoulos, J. Anderson and J. McCaffrey, *Phys. Rev. B* **5**, 1214 (1972).
16. I. Petroff and C. R. Viswanathan, *Phys. Rev. B* **4**, 799 (1971).
17. S. Ada Chi, *Handbook on Physical Properties of Semiconductors, Vols. I, II, III.* Kluwer Academic Publishers (2004).
18. L. C.O. Dacal and A. Cantarero, *Solid State Comm.* **151**, 781 (2011).
19. Preliminary calculatins with Wien 2011 seem, nevertheless, to confirm the result obtained previously.

Efectos de la fijación de la polarización lineal sobre los vórtices en el condensado polaritónico

M. Toledo Solano

Abstract

Actualmente la condensación de Bose-Einstein de polaritones se ha observado en microcavidades semiconductoras a temperaturas cercanas a la temperatura ambiente. Los polaritones de la cavidad son "cuasipartículas" producidas cuando fotones de un campo de luz localizados por la cavidad, se acoplan con electrones y huecos en la forma de excitones, que a su vez se confinan dentro de la misma. De esta manera, los polaritones son parte materia y parte luz que heredan las cualidades de ambos. La observación de la condensación de Bose-Einstein de polaritones en microcavidades semiconductoras ha proporcionado una oportunidad excepcional para observar y estudiar la superfluidez polaritónica, considerada como un resultado de la transición de fase Berezinskii-Kosterlitz-Thouless (BKT). Dada a la importancia para entender esta superfluidez, se deben estudiar los vórtices en el condensado polaritónico. Los vórtices desempeñan un papel importante en diversos fenómenos físicos, tanto a nivel macroscópico como microscópico. Si bien la formación de vórtices es muy importante para la descripción de los diferentes efectos en la mecánica de fluidos, en particular, en la aerodinámica y el movimiento de flujo turbulento, la comprensión de las propiedades de los vórtices cuantizados es crucial para la descripción de varias transiciones de fase en materia condensada. Es de suma importancia entender la estructura y las propiedades de la polarización de los vórtices en los condensados de Bose-Einstein de polaritones, ya que la disociación vórtice-antivórtice define la temperatura crítica T_{BKT} de la transición de fase BKT, y además, los vórtices son objetos topológicamente estables y pueden ser usados como memorias ópticas de larga vida. Analizamos el campo efectivo originado por la anisotropía óptica de la

Facultad de Ciencias de la Universidad Autónoma del Estado de Morelos. Av. Universidad 1001. Col. Chamilpa. Cuernavaca, Mor., Mexico. e-mail: miller@uaem.mx

microcavidad que tiene como resultado la fijación de la polarización lineal del condensado. Los vórtices elementales del sistema, los semi-vórtices, en este caso adquieren cuerdas (solitones) unidas a ellos. Los semi-vórtices son detectados mediante la observación de una dislocación tipo tenedor en las franjas de interferencia de la luz emitida desde la cavidad en las dos polarizaciones circulares.

Effects of pinning of lineal polarization on the vortices in exciton-polariton condensate

Currently the Bose-Einstein condensates of exciton-polaritons have been observed in semiconductor microcavities close to room temperature. Cavity polaritons are "quasi-particles" produced when photons of a light field located in the cavity, are coupled with electrons and holes in the form of excitons, which in turn are confined within the same. Thus, polaritons are part matter and part light which inherit the qualities of both. The observation of the Bose-Einstein condensate of exciton-polariton in semiconductor microcavities has provided a unique opportunity to observe and study superfluidity of polaritons, considered as a result of the Kosterlitz-Thouless-Berezinskii (BKT) phase transition. Due to the importance in understanding this superfluidity, vortices should be studied in the Bose-Einstein condensate of exciton-polariton. Vortices play a key role in varios physical phenomena both on the macroscopic and microscopic levels. While the vortex formation is very important for the description of different effects in fluid mechanics, in particular, aerodynamics and turbulent flow motion, the understanding of the properties of quantized vortices is crucial for the description of varios phase transitions in condensed matter. It is very important to understand the sctructure and polarization properties of vortices in the Bose-Einstein condensate of exciton-polariton, since it is the vortex-antivortex unbinding that defines the critical temperature T_{BKT} for the BKT phase transition. Moreover, vortices are topologically stable objects y they can be used as long-living optical memory elements. We analyze the effective field caused by the optical anisotropy of the microcavity which results in the pinning of lineal polarization of the condensate. Half-vortices are the elemental vortices of system, in this case acquire strings (solitons) attached to them. Half-vortex are detected by observing the interference fringes of light emitted from the cavity in two circular polarizations.

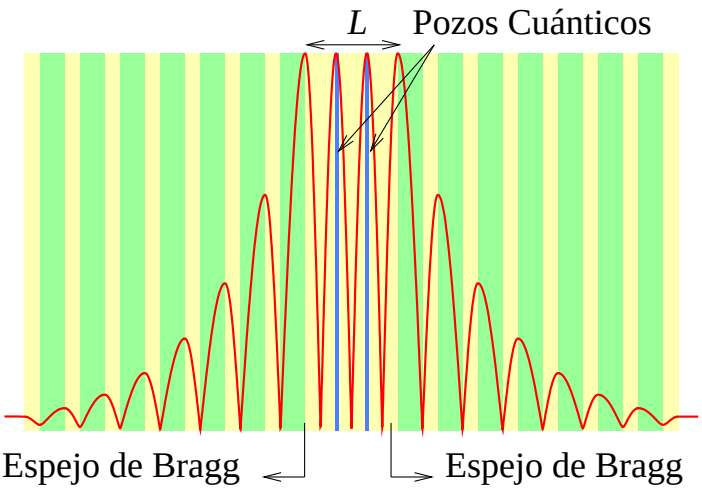

Fig. 1 Una estructura típica de microcavidad. La cavidad central tiene un espesor L igual a un número entero de media longitud de onda del modo de luz resonante. Pozos cuánticos son colocados en los antinodos del modo para proporcionar un acoplamiento más fuerte a la luz. Estos se muestran como líneas sólidas en la región activa.

1 Polaritones en microcavidades semiconductoras

El rápido avance en la tecnología del crecimiento de cristales en el siglo pasado permitió realizar microestrucutras cristalinas, con propiedades ópticas novedosas y controlables. Las microcavidades semiconductoras son materiales artificiales relativamente nuevos, crecidos mediante epitaxia de haces moleculares. Estos materiales han atraído la atención en los últimos años, ya que proporcionan un método para mejorar y controlar la interacción entre la luz y la materia. Las microcavidades semiconductoras son cavidades tipo Fabry-Perot entre dos espejos de Bragg y que pueden contener pozos cuánticos embebidos dentro de la región de activa [ver figura 1]. Un espejo de Bragg es una estructura periódica compuesta de dos semiconductores o materiales dieléctricos con índices de refracción diferentes. Cuando el espesor del pozo cuántico es comparable al radio de Bohr de un excitón, los estados excitónicos están cuantizados en la dirección de crecimiento, pero con la existencia de un continuo de vectores de onda en el plano de la cavidad. Por otro lado, la cavidad lleva a la cuantización de los estados de los fotones en la dirección de crecimiento, pero, al igual que los estados excitónicos, los estados fotónicos en el plano no son

afectados por la cavidad. La dispersión de los fotones de la cavidad se ve modificada fuertemente en relación a los fotones libres y se aproxima (en la región de pequeños vectores de onda) a una forma parabólica, caracterizada por una masa muy pequeña en el plano y que conduce a un número de propiedades, como las que se discuten abajo. Efectos muy interesantes fueron observados en el espectro de reflexión de una microcavidad, cuando existía una resonancia entre la frecuencia del excitón y la del fotón de la cavidad [1]. Cuando la magnitud del acoplamiento entre el excitón y el fotón es superior a la razón de escape de fotones y a la razón de decaimiento de los excitones, se producen dos nuevos estados propios del sistema que tienen energías diferentes a los estados de fotón y excitón solos. Éstos dos nuevos modos están asociados con partículas mezcladas de luz y materia llamados excitón-polaritones o polaritones [2].

El polaritón es visto como una cadena de procesos donde el excitón decae, emitiendo un fotón con la misma energía E y momento $\mathbf{k}$, el cual es reabsorbido por el medio, creando un nuevo excitón con los mismos valores de E y $\mathbf{k}$, y así sucesivamente hasta que la excitación se encuentra fuera de la cavidad (resultando en la aniquilación del polaritón), o el electrón o el hueco es dispersado. El hamiltoniano, en la imagen de la segunda cuantización, que describe al sistema interactuante de fotones y excitones se escribe como [2]

$$\begin{aligned}\widehat{H}_{pol} &= \widehat{H}_{cav} + \widehat{H}_{esc} + \widehat{H}_I \\ &= \sum_{\mathbf{k}} E_C(\mathbf{k})\widehat{B}^{\dagger}_{\mathbf{k}}\widehat{B}_{\mathbf{k}} + \sum_{\mathbf{k}} E_X(\mathbf{k})\widehat{X}^{\dagger}_{\mathbf{k}}\widehat{X}_{\mathbf{k}} + \sum_{\mathbf{k}} \hbar\Omega(\widehat{B}^{\dagger}_{\mathbf{k}}\widehat{X}_{\mathbf{k}} + \widehat{X}^{\dagger}_{\mathbf{k}}\widehat{B}_{\mathbf{k}}),\end{aligned} \quad (1)$$

donde $\widehat{B}$ es el operador de aniquilación de un fotón y $\widehat{X}$ su contraparte excitónica. La cavidad de ancho L proporciona la relación de dispersión $E_C(\mathbf{k})$ para el fotón [2],

$$E_C(\mathbf{k}) = (\hbar c/n)\sqrt{k_{||}^2 + (2\pi N/L)^2}, \quad (2)$$

donde $\hbar$ es la constante de Planck, c la velocidad de la luz, n el índice de refracción de la cavidad, $k_{||}$ el vector de onda en el plano de la cavidad y N es el número de modos transversales en la cavidad. Para la situación en la figura 1, $N = 3$. Para pequeños $k_{||}$, la energía puede ser escrita como

$$E_C(\mathbf{k}) \approx \hbar\omega_0 + \frac{\hbar^2 k_{||}^2}{2m_{fo}}, \qquad m_{fo} = \frac{nh}{cL}, \tag{3}$$

donde m_{fo} es la masa efectiva del fotón del orden de $10^{-4} - 10^{-5}$ veces la masa del electrón libre. La energía del excitón en el PC se escribe como

$$E_X(\mathbf{k}) = E_0 + \frac{\hbar^2 k_{||}^2}{2M_{ex}}, \tag{4}$$

donde M_{exc} es la masa efectiva reducida del electrón y el hueco en el plano del PC, $E_0 = E_g + \varepsilon_c + \varepsilon_v$ y donde $\varepsilon_{c,v}$ indican los niveles de energía dentro del PC para electrones y huecos, respectivamente. La energía de la interacción dipolar excitón-fotón $\hbar\Omega$ está dada como [3]

$$\hbar\Omega \approx \hbar \left(\frac{2\pi e^2 c N_p f_{ex}}{n_c L_{efec}} \right)^2, \tag{5}$$

donde f_{ex} es la fuerza del oscilador del excitón [4], N_p el número de pozos cuánticos en la cavidad, n_c el índice de refracción de cavidad, y L_{efec} la longitud efectiva de la cavidad debido a la penetración del modo de la cavidad sobre los espejos de Bragg.

El hamiltoniano (1) puede ser diagonalizado por la transformación

$$\widehat{a}_{\mathbf{k}}^I = x_{\mathbf{k}} \widehat{X}_{\mathbf{k}} - c_{\mathbf{k}} \widehat{B}_{\mathbf{k}}, \tag{6}$$

$$\widehat{a}_{\mathbf{k}}^S = c_{\mathbf{k}} \widehat{X}_{\mathbf{k}} + x_{\mathbf{k}} \widehat{B}_{\mathbf{k}}, \tag{7}$$

donde $c_{\mathbf{k}}$ y $x_{\mathbf{k}}$ son conocidos como los coeficientes de Hopfield [5] y satisfacen $|x_{\mathbf{k}}|^2 + |c_{\mathbf{k}}|^2 = 1$, de tal manera que la transformación es canónica y los operadores $\widehat{a}$ obedecen un álgebra bosónica. Entonces el hamiltoniano (1) se reduce a términos libres únicamente

$$H_{pol} = \sum_{\mathbf{k}} E_S(\mathbf{k}) \widehat{a}_{\mathbf{k}}^{S\dagger} \widehat{a}_{\mathbf{k}}^S + \sum_{\mathbf{k}} E_I(\mathbf{k}) \widehat{a}_{\mathbf{k}}^{I\dagger} \widehat{a}_{\mathbf{k}}^I, \tag{8}$$

para las bandas superior e inferior de polaritones con los operadores de aniquilación $\widehat{a}^S$ y $\widehat{a}^I$, respectivamente. Ya que ambos excitones y fotones son bosones, también lo son los polaritones. La relación de dispersión para las bandas es

$$E_{S,I}(\mathbf{k}) = \frac{1}{2} \left[E_X(\mathbf{k}) + E_C(\mathbf{k}) \pm \sqrt{4\hbar^2\Omega^2 + \Delta_{\mathbf{k}}^2} \right], \tag{9}$$

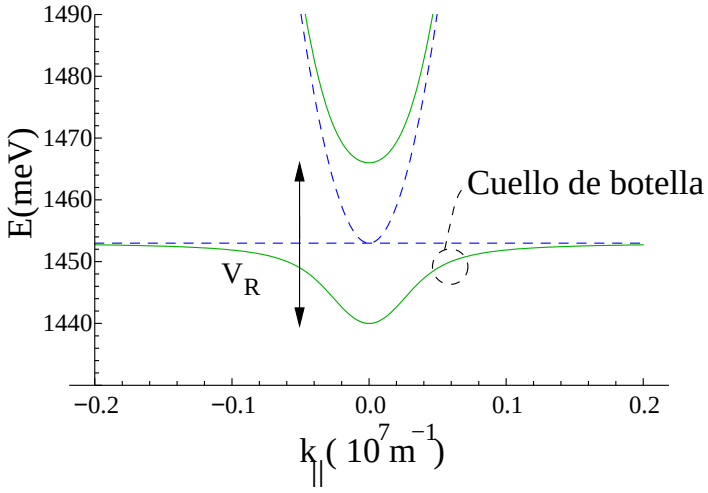

Fig. 2 Relación de dispersión de los fotones y excitones desacoplados (líneas discontinuas), y la de los polaritones de la cavidad en el régimen de fuerte acoplamiento en líneas sólidas, que corresponden a los polaritones en la banda superior y a los polaritones en la banda inferior, respectivamente. El fotón de la cavidad y el excitón del pozo cuántico están en resonancia en $k_{||} = 0$. La región de cuello de botella se explica en el texto.

donde el signo $+$ se asocia los polaritones de la banda superior (PS) y el signo $-$ se asocia a los polaritones de la banda inferior (PI). $\Delta_{\mathbf{k}}$ es la diferencia de energía entre el modo de la cavidad y el excitón, $\Delta_{\mathbf{k}} = E_C(\mathbf{k}) - E_X(\mathbf{k})$. Las fracciones de excitón y fotón para PI (y viceversa para PS) están dados por las amplitudes cuadradas de los coeficientes de Hopfield

$$|c_{\mathbf{k}}|^2 = \frac{E_S(\mathbf{k})E_X(\mathbf{k}) - E_I(\mathbf{k})E_C(\mathbf{k})}{(E_C(\mathbf{k}) + E_X(\mathbf{k}))\sqrt{\Delta_{\mathbf{k}}^2 + 4\hbar^2\Omega^2}}, \tag{10}$$

$$|x_{\mathbf{k}}|^2 = \frac{E_S(\mathbf{k})E_C(\mathbf{k}) - E_I(\mathbf{k})E_X(\mathbf{k})}{(E_C(\mathbf{k}) + E_X(\mathbf{k}))\sqrt{\Delta_{\mathbf{k}}^2 + 4\hbar^2\Omega^2}}. \tag{11}$$

En $\Delta_{\mathbf{k}} = 0$, $|x_{\mathbf{k}}|^2 = |c_{\mathbf{k}}|^2 = \frac{1}{2}$, los LP y los UP son exactamente mitad fotón y mitad excitón, y sus energías tienen una separación mínima de $2\hbar\Omega$, también conocida como separación de Rabi V_R ("*Rabi splitting*"), representando dos veces la magnitud del acoplamiento entre excitones y fotones [ver figura 2]. El anticruzamiento ("*avoided crossing*") de los modos polaritónicos, es resultado de la interacción ex-

citón-fotón. Los polaritones son los modos del sistema, mientras que los modos de excitón y fotón son estados transitorios que intercambian energía en la frecuencia de Rabi Ω.

La existencia de tales modos acoplados en las microcavidades fueron demostrados experimentalmente [1] en 1992. Trabajos adicionales [6] mostraron que la forma de las curvas de dispersión de los polaritones dependía fuertemente de la diferencia δ ("*detuning*") entre la energía del modo fotónico de la cavidad $\hbar\omega_0$ y la del modo excitónico E_0 en el vector de onda $k_{||} = 0$. El vector de onda en plano $k_{||}$ está relacionado al ángulo de incidencia φ de la luz que ilumina la estructura por la relación

$$k_{||} = \frac{\omega}{c} \operatorname{sen}\varphi. \tag{12}$$

Al medir el ángulo de la resonancia en los espectros de reflexión o de transmisión de la microcavidad, se puede obtener la verdadera relación de dispersión de los polaritones.

1.1 Condensación de Bose-Einstein y superfluidez de polaritones

La posibilidad para la condensación de Bose-Einstein (CBE) de polaritones comenzó con Imamoglu *et al.* [7] en 1996. Ellos propusieron usar el carácter bosónico de los polaritones para la construcción de un condensado polaritónico que debería emitir luz coherente de manera espontánea. Aquí y en lo que sigue, por emisión de luz por polaritones se indica el escape de luz desde la cavidad debido a la probabilidad finita de tunelamiento a través de los espejos de Bragg. La idea era crear una distribución de polaritones por bombeo óptico. La relajación de esta distribución vía su interacción con fonones acústicos se considerada capaz de porporcionar una acumulación eficiente de polaritones al estado base. Tassone *et al.* [8] desmostron teóricamente poco tiempo después a la predicción de Imamoglu que los fonones acústicos no pueden proporcionar una relajación eficiente de polaritones hacia el estado base, debido a la parte central inclinada de la relación de dispersión llamada cuello de botella [ver figura 2], donde su pendiente excede a la velocidad del sonido. La región de cuello de botella se origina por una competencia entre los fonones acústicos

que asisten a la relajación de los polaritones y la razón de incremento de escape de los polaritones de la cavidad debido a sus características fotónicas con la disminución de $k_{||}$. Sin embargo, una dependencia cuadrática de la emisión sobre la potencia de bombeo no resonante fue observada experimentalmente en microcavidades tipo II-VI [9] y III-V [10]. Esto significaba que otros mecanismos de relajación permitían a una parte de los polaritones atravesar la región de cuello de botella. La propuesta principal de estos mecanismos adicionales fue la dispersión polaritón-polaritón [11].

En años posteriores una serie de trabajos [12, 13, 14, 15, 16] reportaron la observación experimental de la dispersión estimulada de polaritones hacia el estado base. Todo esto, más el entendimiento de la dinámica de espín de estos procesos [17], hizo que se incrementara el interés sobre el efecto bosónico en microcavidades. A finales del 2002, un aumento en la coherencia de la luz emitida desde el estado base polaritónico contra la intesidad de bombeo no resonante fue reportado en una microcavidad basada en GaAs [18]. Sin embargo, en ninguno de estos trabajos se reportó alguna medición de la polarización o de la coherencia espacial, misma de la que hablamos a continuación.

Como se sabe, el ejemplo más antiguo de la CBE es la fase superfluida conocida como He II en el líquido de ^{4}He por debajo de una temperatura crítica [19]. Este efecto fue interpretado [20] como una manifestación de la CBE de una fracción macroscópica de átomos de helio, a pesar de que este líquido de interacción fuerte está lejos del gas ideal de Einstein. En este sentido, la superfluidez es una propiedad profundamente asociada a la CBE y a primera vista parece que una no puede existir sin la otra. Pero esto no es exactamente cierto. La CBE indica la apariencia de una fase homogénea en el espacio directo. Esta homogeneidad implica superfluidez. Las partículas pueden moverse a través del espacio con una fase coherente, sin disipación. La superfluidez indica que estadísticamente dos puntos en el espacio están conectados por una trayectoria de fase coherente, aun si el espacio entero no está cubierto por una función de fase coherente, por lo que un estado superfluido puede existir sin la existencia estricta de la CBE. Esto es el tipo de estado que se origina en un sistema bidimensional, donde estrictamente la CBE está prohibida. Sin embargo, debido al tamaño finito del punto de excitación en la muestra, el tamaño de la nube polaritónica es finita, y se puede alcanzar coheren-

cia completa a través de la nube a temperaturas suficientemente bajas así como la ocupación macroscópica de un estado cuántico único. Los polaritones presentan fuertes interacciones aún para densidades bajas [21, 22], además tienen un tiempo de vida finito y deben ser bombeados desde el exterior para compensar las pérdidas de polaritones que decaen, por lo que un sistema polaritónico realista está siempre fuera del equilibrio. No obstante, las principales predicciones para la CBE como la condensación en el estado base de una población en equilibrio térmico y el desarrollo de la coherencia cuántica, indicado por la coherencia espacial de largo alcance, fueron recientemente obtenidas [23, 24, 25, 26, 27], las cuales han brindado las evidencias de la CBE de polaritones en microcavidades cuánticas.

La microcavidad en [23] contenía 16 pozos cuánticos con una separación de Rabi de 26 meV. La energía de excitación estaba por arriba de la energía del estado base para asegurar que los polaritones inicialmente inyectados al sistema fueran incoherentes, condición necesaria para la demostración del CBE. En este trabajo se observó que al incrementar la intensidad de bombeo, la distribución de polaritones en el espacio recíproco se localizaba en el punto $k_{||} = 0$, por lo que la la luz emitida por la microcavidad se generaba en este estado cuántico único, tal como se muestra en la figura 2 de [23].

Del patrón de emisión de campo lejano se obtuvo la ocupación del estado base, así como su energía de emisión y su ancho de línea como función de la potencia de excitación [ver figura 3 en [23]]. Con el incremento de la potencia de excitación, la ocupación del estado base se incrementa primero linealmente y de manera exponencial inmediatamente después de la potencia umbral. La temperatura efectiva del sistema polaritónico $T_{efec} = 19\,\mathrm{K}$ fue estimada en la potencia umbral. La ocupación es cercana a la unidad en el umbral, consistente con el proceso de relajación estimulada de los polaritones por la población en el estado base, característica específica de los bosones. El notable estrechamiento espectral indica que, arriba de la potencia de estimulación umbral, el tiempo de coherencia de la población polaritónica en el estado base es más largo que el tiempo de vida polaritónico [25]. El corrimiento al azul se atribuye a la renormalización de la energía inducida por la interacción entre polaritones.

Los experimentos en las referencias [23, 24] mostraron además que la luz emitida desde el estado base es linealmente polarizada, lo cual está en excelente concordancia con las predicciones teóricas [28]. La

formación de la polarización lineal fue explicada en [29] donde se muestra que el estado energéticamente preferente del condensado polaritónico superfluido es linealmente polarizado debido a que minimiza la densidad de energía libre del sistema. Los trabajos [23, 30] muestran que la dirección de la polarización lineal sobre un eje cristalino en particular se debe a la existencia de una separación ("*splitting*") de energía en la dispersión de los polaritones. Esta energía resulta de la anisotropía óptica de la cavidad y sus efectos son mostrados más adelante en las propiedades de los vórtices.

2 Parámetro de orden y hamiltoniano del sistema polaritónico

Una propiedad importante de los polaritones es su (pseudo)espín **S** el cual está directamente conectado con el estado de polarización de la luz absorbida o emitida por la microcavidad. En óptica clásica, este pseudoespín **S** corresponde al vector de Stokes para la luz parcialmente polarizada. Los polaritones heredan esta propiedad desde el espín del excitón en el pozo cuántico y del fotón de la cavidad. Los estados excitónicos tienen proyecciones de espín ± 1 y ± 2 sobre el eje de la estructura. Los estados con ± 1 forman el doblete polaritónico ópticamente activo, y pueden ser creados por luz polarizada circularmente, mientras que con luz polarizada linealmente se excita una combinación lineal con proyección de espín total igual a cero sobre el eje de la estructura. De esta manera, los polaritones son cuasipartículas con dos proyecciones de espín [arriba (abajo) correspondiendo a polarización circular derecha (izquierda) de la luz emitida]. Por lo tanto, el parámetro de orden del condensado de polaritones ψ posee dos componentes, cada uno asociado con la funciones de onda complejas de los estados de espín arriba y abajo, respectivamente. El parámetro de orden ψ es un vector bidimensional complejo y define la dirección y fase de la componente del campo eléctrico en el plano de la microcavidad. El parámetro de orden del condensado puede escribirse como

$$\psi = \left\{ \psi_x, \psi_y \right\}, \tag{13}$$

donde ψ_x y ψ_y son funciones complejas de la posición y del tiempo, y describen las proyecciones de la polarización del condensado sobre los dos ejes correspondientes al plano de la cavidad. En microcavi-

dades bombeadas por debajo del umbral, $|\psi| = 0$, mientras que arriba del umbral, ψ se construye debido a la dispersión estimulada de los polaritones desde estados excitados al condensado [31], y sus fluctuaciones espaciales y temporales son pequeñas y pueden ser despreciadas [32].

La conservación del espín en la foto-absorción permite la orientación de los espines de los excitones por la luz polarizada, efecto que ha sido ampliamente estudiado. Como el espín de un polaritón define la polarización de los fotones emitidos, el análisis de los espectros de fotoluminiscencia polarizada de la microcavidad es una herramienta poderosa para la investigación experimental de la dinámica de espín de los polaritones [17, 33].

Por otro lado, el argumento teórico a favor de la CBE de polaritones se debe a que sus masas efectivas son muy reducidas, del orden de 10^{-4} la masa del electrón libre m_e. Gracias a esto, los polaritones exhiben varias propiedades específicas y juegan un rol importante en un número de efectos muy interesantes [2]. Sin embargo, como ya hemos mencionado antes, la característica esencial del condensado polaritónico es su naturaleza fuera del equilibrio. El tiempo de vida del polaritón es extremadamente corto, típicamente del orden de 1 ps, para alcanzar una población completamente termalizada. Los polaritones deben ser excitados en la microcavidad usando una fuente externa, ya sea por bombeo óptico o por una corriente eléctrica [34]. Además, los polaritones excitados no se quedan en la microcavidad para siempre, sino que escapan de ésta debido a la probabilidad finita de atravesar los espejos de Bragg. No obstante, se puede esperar que bajo excitación continua, con una intensidad por arriba de la condensación umbral, el sistema polaritónico alcance un equilibrio cuasi-térmico. El flujo de polaritones a través de los espejos de Bragg, se balancea por la llegada de los polaritones desde el bombeo incoherente, y este balance establece un potencial químico μ, para el sistema polaritónico.

Para el equilibrio cuasi-térmico es necesario que el tiempo de vida de los polaritones sea suficientemente grande en el condensado comparado con el tiempo de vida radiativo $\tau = \Gamma^{-1}$. La tasa de escape Γ debería ser comparada con la tasa de entrada W que define el número de polaritones entrando al condensado a partir de un reservorio excitado incoherentemente. El umbral para la condensación polaritónica está definido por la condición $W = \Gamma$ [35, 36]. Por arriba del umbral, donde $W \gg \Gamma$, el condensado se establece en equilibrio cuasi-térmico.

Otra manera para alcanzar un equilibrio cuasi-térmico es considerar una temperatura y un rango de la diferencia δ ("*detuning*") donde el tiempo de termalización espontánea de las partículas sea mucho mas corta que su tiempo de vida. Este régimen puede lograrse experimentalmente para temperaturas suficientemente altas para la red y δ positivos.

La temperatura para la CBE de polaritones en equilibrio puede ser estimada desde el modelo BKT y por la fórmula de Landau para la ocupación de los estados excitados. La temperatura crítica se incrementa con la intensidad de bombeo. Su máximo corresponde a la más alta intensidad de bombeo donde el régimen de acoplamiento fuerte en la microcavidad se mantiene. Se espera que el CBE de polaritones en equilibrio tome lugar en varias decenas de grados Kelvin en las microcavidades basadas en Ga-As, arriba de 200 K en microcavidades basadas en CdTe y a temperatura ambiente en microcavidades basadas en GAN o ZnO. Sin embargo, la temperatura efectiva del sistema polaritónico, T^*, puede diferir de la temperatura de la red a causa de las diferentes interacciones polaritón-fonón y polaritón-polaritón. El enfriamento del condensado polaritónico debido a la dispersión polaritón-polaritón y al subsecuente decaimiento no radiativo de los polaritones de más alta energía es posible, en principio. De hecho la misma tasa de entrada W define la temperatura del condensado, $T^* \propto W$. La temperatura efectiva proporcionada es todavía mucho más pequeña que la temperatura de condensación o transición superfluida, y el condensado polaritónico puede ser descrito en el marco de trabajo de la ecuación de Gros-Pitaevskii (GP) en equilibrio.

La ecuación de GP en el equilibrio generalmente se puede escribir como

$$i\hbar\frac{\partial\psi}{\partial t} = \frac{\delta H}{\delta\psi^*}, \tag{14}$$

donde H es el hamiltoniano del sistema polaritónico expresado como un funcional del parámetro de orden $\psi(\mathbf{r},t)$,

$$H = \int d^2r\left\{\mathfrak{T} - \mu n + \mathfrak{H}_{int} + \mathfrak{T}_{sep}\right\}, \tag{15}$$

donde $\mathfrak{T}$ es la energía cinética del condensado, μ el potencial químico, $\mathfrak{H}_{int}$ la energía de interacción entre polaritones y $\mathfrak{T}_{sep}$ la separación de energía en las bandas polaritónicas.

El hamiltoniano (15) describe los polaritones cerca de la parte más baja de la banda inferior y desprecia la no-parabolicidad de la dispersión. Esto implica que las energías típicas de un condensado polaritónico, en particular, el potencial químico μ pueda ser medido por el corrimiento al azul de la línea de emisión del condensado, y las energías de las excitaciones elementarías se consideren mucho más pequeñas que la separación de Rabi.

Con respecto a la configuración del campo eléctrico en el plano de la cavidad, definida por el vector bidimensional ψ y por el vector de onda $\mathbf{k}$, los modos TE y TM son transversal y longitudinal, respectivamente. De esta manera la energía cinética $\mathfrak{T}$ del condensado se puede escribir como

$$\begin{aligned}\mathfrak{T} &= \frac{\hbar^2}{2}\sum_{i,j=x,y}\left\{\frac{1}{m_t}(\nabla_i\psi_j^*)(\nabla_i\psi_j)+\left(\frac{1}{m_l}-\frac{1}{m_t}\right)(\nabla_i\psi_i^*)(\nabla_j\psi_j)\right\}\\ &= \frac{\hbar^2}{2}\sum_{i,j=x,y}\left\{\frac{1}{m_t}(\nabla_i\psi_j^*)(\nabla_i\psi_j)+\left(\frac{1}{m_l}-\frac{1}{m_t}\right)|\nabla\cdot\psi|^2)\right\}, \qquad (16)\end{aligned}$$

donde m_t y m_l son las masas efetivas transversal (TE) y longitudinal (TM). Como estamos enfocados en la banda inferior de los polaritones, uno puede considerar ya sea $m_l < m_t$ o $m_l > m_t$. Esta interrelación depende de la diferencia δ del modo de luz de la microcavidad desde el centro de la brecha para el espejo de Bragg [37]. Dado que $\nabla \to i\mathbf{k}$, en el caso de $\mathbf{k} \perp \psi$, $\nabla\cdot\psi = 0$ y los modos son puramente transversales (TE). En el caso de $\mathbf{k} \parallel \psi$ los modos son puramente longitudinales (TM).

El término $\mathfrak{T}_{sep}$ para la separación ("*splitting*") de energía en la relación de dispersión de los polaritones puede tener varios orígenes. La primera separación y objeto de estudio en este trabajo es aquella que se origina por la anisotropía óptica de la cavidad, y se debe a la debilidad en el plano de las tensiones uniaxiales, las cuales dan como resultado una birrefringencia ligera del medio. Esta separación no es cero en $k_{||} = 0$. Esto tiene como resultado la selección de la polarización lineal del condensado polaritónico en una dirección específica [30, 38, 39]. Otras separaciones de energía son la separación TE-TM entre las polarizaciones TE y TM de la luz y la separación de Zeeman debido a un campo magnético $\mathbf{B}$ aplicado perpendicularmente al plano de la cavidad ($\mathbf{B}||\hat{z}$). En microcavidades la separación TE-TM

se amplifica desde $k_{||} = 0$ debido al acoplamiento del excitón con el fotón de la cavidad [37]. Ambos efectos de estas separaciones sobre el condensado polaritónico fueron discutidos por Rubo *et al.* [29, 40].

El término de la interacción polaritón-polaritón en el integrando (15) se escribe como [29]

$$\begin{aligned}\mathfrak{H}_{int} &= \frac{1}{2}U_0(\psi^* \cdot \psi)^2 - \frac{1}{2}U_1|\psi \cdot \psi|^2 \\ &= \frac{1}{2}(U_0 - U_1)(\psi^* \cdot \psi)^2 + \frac{U_1}{2}|\psi^* \times \psi|^2, \end{aligned} \tag{17}$$

y es descrito por dos invariantes cuárticos que pueden ser construidos desde un vector bidimensional complejo. Las constantes de interacción, U_0 y U_1, están relacionadas a los elementos matriciales de la interacción de dos polaritones con la misma polarización circular $M_{\uparrow\uparrow}$ y con polarizaciones circulares opuestas $M_{\uparrow\downarrow}$. A saber, $U_0 = AM_{\uparrow\uparrow}$ y $U_1 = A(M_{\uparrow\uparrow} - M_{\uparrow\downarrow})/2$, donde A es el área de normalización (área del punto de excitación) [41]. Parece que hay un consenso de que polaritones con la misma misma polarización circular presentan una interacción repulsiva y aún cuando distintos tratamientos producen diferentes elementos $M_{\uparrow\uparrow}$, el valor de $6|x|^2 E_B a_B^2$ se utiliza con recurrencia [42], aquí E_B y a_B son la energía de enlace y el radio de Bohr del excitón, respectivamente, y x es la fracción excitónica en cada polaritón en la banda más baja. Las predicciones para la interacción de polaritones con polarizaciones circulares opuestas $M_{\uparrow\downarrow}$ son más diversas, van desde cero a la interacción atractiva de la misma magnitud que polaritones con el mismo estado de polarización [41, 43].

Cuando $M_{\uparrow\downarrow} = 0$, es decir, cuando la interacción de dos polaritones con polarizaciones circulares opuestas desaparece, $U_1 = U_0/2$. En el caso de débil atracción se tiene $U_0/2 < U_1 < U_0$. Los valores $U_0 = 2.4 \times 10^{-18}$eV m^2 y $U_1 = 0.55U_0$ se escogen preferentemente en [29].

2.1 Polarización y espectro de excitaciones en el condensado polaritónico

El mínimo de la densidad de energía libre del sistema polaritónico se busca con el parámetro de orden ψ espacialmente uniforme e independiente del tiempo. En este caso, la densidad hamiltoniana toma la

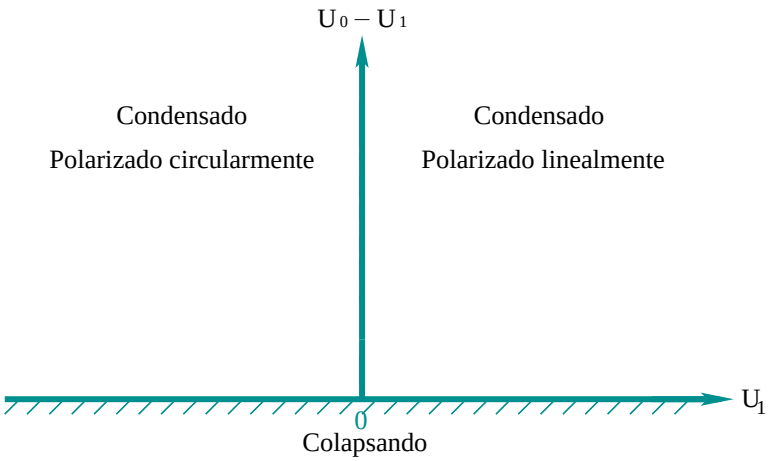

Fig. 3 Se muestran los límites donde el sistema polaritónico se encuentra en regiones estables y en donde se colapsa en el caso de una separación de energía $\mathfrak{T}_{sep} = 0$. Cuando $U_1 > 0$ el condensado se encuentra lineal polarizado, mientras que cuando $U_1 < 0$ el condensado se encuentra circularmente polarizado. Cuando $U_1 = 0$ la polarización del condensado puede ser arbitraria ya que la energía es independiente de la polarización.

forma

$$\frac{H_{uni}}{A} = -\mu(\psi^* \cdot \psi) + \frac{1}{2}(U_0 - U_1)(\psi^* \cdot \psi)^2 + \frac{U_1}{2}|\psi^* \times \psi|^2 + \mathfrak{H}_{sep} \quad (18)$$

Para obtener una densidad finita del condensado polaritónico es necesario tener términos de interacción definidos positivos. De otra manera el condensado se colapsaría. En este trabajo se consideraran los dos casos de estabilidad encontradas: $U_0 > 0$ y $U_1 < U_0$. Las regiones donde el condensado se encuentra estable y en donde se colapsa se muestran en la figura 3.

Cuando no se considera la sepación de energía $\mathfrak{H}_{sep}$, es decir, cuando $\mathfrak{H}_{sep} = 0$, la polarización del condensado polaritónico está determinada por las interacciones polaritón-polaritón. El término U_0 en (18) no depende de la polarización. De hecho el término U_1 en (18), es quién define la polarización del sistema polaritónico. Para $U_1 > 0$ la energía se minimiza para el estado de polarización lineal cuando

$$\psi^* \times \psi = 0. \quad (19)$$

Este efecto puede ser entendido debido a la asignación de $+1$ ó -1 al pseudoespín de cada polaritón, lo cual corresponde a polarización circular derecha o izquierda, respectivamente. Los polaritones con el mismo pseudoespín se repelen uno con otro, mientras que existe una atracción débil entre los polaritones con pseudoespines opuestos. Como resultado, la energía de interacción del sistema polaritónico se minimiza cuando igual número de polaritones polarizados circularmente a la derecha e izquierda están presentes. La densidad hamiltoniana (18) entonces se escribe como

$$\frac{H_{uni}}{A} = -\mu n + \frac{1}{2}(U_0 - U_1)n^2, \tag{20}$$

donde $n = (\psi \cdot \psi^*)$ es el número de ocupación del condensado. El potencial químico se obtiene por la minimización de la densidad hamiltoniana (20) sobre n, lo cual produce

$$\mu = (U_0 - U_1)n. \tag{21}$$

En el caso contrario de valores negativos de U_1, el mínimo de la energía se alcanza cuando este término se anula, esto es para la polarización circular que implica $\psi \cdot \psi = 0$. El potencial químico es entonces $\mu = U_0 n$. La formación de la polarización lineal observada en el condensado [23, 24, 30] implica que $U_1 > 0$.

Por otro lado, las excitaciones elementales del condensado en cuasiequilibrio pueden ser analizadas en términos del espectro de Bogoliubov [44]. Esto puede hacerce considerando una pequeña perturbación del estado base del sistema polaritónico cerca de su valor medio constante $\sqrt{n}$,

$$\psi = \sqrt{n}\mathbf{e} + \mathbf{A}e^{\mathrm{i}(\mathbf{k}\cdot\mathbf{r}-\omega t)} + \mathbf{B}^* e^{-\mathrm{i}(\mathbf{k}\cdot\mathbf{r}-\omega t)}, \tag{22}$$

donde $\mathbf{e}$ es el vector complejo unitario, $\mathbf{e}^* \cdot \mathbf{e} = 1$, y define la polarización del estado base. $\mathbf{A}$ y $\mathbf{B}$ son amplitudes complejas consideradas pequeñas. Al sustituir esta expresión de ψ en la ecuación (14), linealizando, y separando términos con diferentes funciones exponenciales complejas, es posible obtener un sistema de dos ecuaciones lineales, complejas y homogéneas, que definen la dispersión de las excitaciones elementales del condensado y su polarización [29, 40]. Las soluciones a dichas ecuaciones muestran que la frecuencias de las cuasipartículas

satisfacen la relación de dispersión tipo ondas de sonido del espectro de excitaciones.

Los vórtices son otro tipo de excitaciones elementales del condensado y son topológicamente diferente al estado base. A continuación se discuten sus propiedades y las características relacionadas a la transición BKT. Los vórtices en superfluidos están caracterizados por una rotación de la fase (del parámetro de orden) con multiplo entero de 2π, comúnmente conocida como carga tópologica del vórtice, y por la desaparición de la población superfluida en su núcleo. El concepto de vórtice cuantizado apareció por primera vez en conexión con el helio líquido en las ideas pioneras de Onsager y Feynman, y más tarde fueron detectados experimentalmente en el líquido ^{4}He [45]. Desde entonces, los vórtices han sido estudiados teórica [46] y experimentalmente [47, 48] en CBE en tres dimensiones de gases atómicos diluidos. En CBE cuasi-bidimensional los vórtices emergieron espontáneamente desde fluctuaciones térmicas [49, 50]. En estos sistemas, la transición entre un estado normal y un estado superfluido, fue descrita en los artículos clásicos de Berezinskii [51] y Kosterlitz-Thouless [52]. En estos trabajos se muestran una variedad de sistemas bidimendionales que experimentaron transiciones de fase inusuales cuando había una singularidad en la susceptibilidad asociada con el parámetro de orden. En todos estos sistemas la transición de fase fue impulsada por la disociación de vórtices topológicos. A baja temperatura, los vórtices están ligados en parejas pero una disociación de éstos ocurre cuando la temperatura se incrementa a través de la temperatura de transición T_{BKT}. Es por esta razón que los vórtices, característica esencial de los superfluidos son amplimente estudiados.

En un trabajo reciente [53], vórtices cuantizados han sido observados experimentalmente en CBE de polaritones formados en microcavidades basada en CdTe. Estos vórtices, fijados gracias al desorden estático presente en la microcavidad, fueron detectados por interfemometría de campo cercano. Se observa en este trabajo una clara singularidad que tiene un cambio de fase de 2π después de rodearla. Sin embargo, la polarización no fue medida, pero como ya hemos mostrado anteriormente, la polarización de la luz emitida por el condensado polaritónico está orientada a lo largo de un eje cristalino. Por todo esto, resulta esencial estudiar la estructura y las propiedades de la

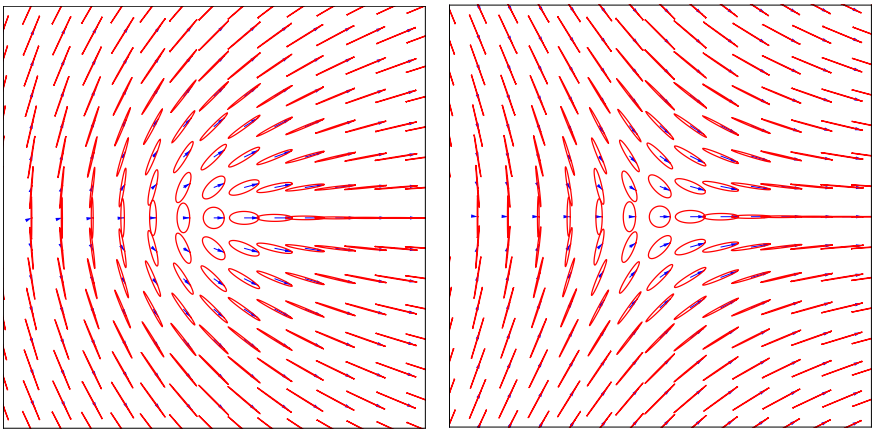

Fig. 4 Las diferentes texturas de polarización de los SVs. (a) para los SVs derecho $(1/2, 1/2)$ e izquierdo $(1/2, -1/2)$. (b) corresponde al caso de los SVs derecho $(-1/2, -1/2)$ e izquierdo $(-1/2, 1/2)$. Las fechas indican el campo eléctrico instantáneo. El campo eléctrico cambia en el tiempo siguiendo las líneas sólidas.

polarización de los vórtices para entender la superfluidez polaritónica en el marco de la teoría BKT.

Cuando se considera una microcavidad plana ideal, es decir, sin ninguna separación de energía en la banda de los polaritones de la rama inferior, un grado de libertad adicional debe aparecer ligado con la orientación de la polarización. En este caso el parámetro de orden del condensado, ya sea polarizado linealmente o elípticamente, debe ser descrito por dos variables angulares. Esto define lo que se conoce como un toro (variedad engendrada por la rotación de una circunferencia en torno a un eje que no la toca en ninguno de sus puntos). De esta manera un ángulo define la fase común y el otro ángulo define la dirección de la polarización. Cuando la polarización del condensando está fija en una dirección ó cuando el condensado está circularmente polarizado, el parámetro de orden es la circunferencia de un círculo definida por un ángulo.

Las propiedades de los vórtices en el caso cuando la variedad del parámetro de orden es un toro fueron discutidas en [54]. En ese trabajo ningún efecto, originado de la separación de energía en el condensado o algún campo magnético externo, fue considerado en la textura[1] de la polarización de los vórtices. El parámetro de orden del condensado linealmente polarizado fue escrito como

[1] La textura se refiere a la manera en la que se entreteje la polarización.

$$\psi_{lin} = \left\{ \psi_x, \psi_y \right\} = \sqrt{n} e^{\mathrm{i}\theta} \left\{ \cos\eta, \operatorname{sen}\eta \right\}, \tag{23}$$

donde $\theta(\mathbf{r})$ es la fase del fluido polaritónico coherente y $\eta(\mathbf{r})$ es el ángulo que caracteriza la orientación del campo eléctrico de los polaritones, es decir, el ángulo de polarización. El término ψ_{lin} satisface la ecuación (19). Las rotaciones del vector real bidimensional $\{\cos\eta, \operatorname{sen}\eta\}$ en el sentido a favor o en contra de la manecillas del reloj son topológicamente distintas, por lo que η proporciona la segunda carga tolopógica.

Los vórtices en esta notación son descritos por la rotación de la fase y la polarización como

$$\theta \to \theta + 2\pi m, \qquad \eta \to \eta + 2\pi k, \tag{24}$$

cuando se rodea el núcleo del vórtice. Las dos cargas topológicas k y m, pueden ser tanto enteras como semienteras simultáneamente con la suma $k+m$ entera. Así los vórtices en los condensados polaritónicos están clasificados por dos números cuánticos. Para los vórtices enteros $k, m = 0, \pm 1, \pm 2, \ldots$, y para los semi-vórtices (SVs), conocidos de esta forma dado que, $k, m = \pm 1/2$. Estos valores semi-enteros están justificados ya que si la fase θ cambia por π al rodear el núcleo del vórtice, el signo menos en el parámetro de orden es compensado por el signo menos del vector bidimendional $\{\cos\eta, \operatorname{sen}\eta\}$. Los cuatro SVs elementales, (1/2,1/2), (-1/2,-1/2), (1/2,-1/2) y (-1/2,1/2), tienen las energías más bajas. Estos SVs se separan en dos subsistemas, SVs derechos (con $km > 0$) y SVs izquierdos (con $km < 0$). Observe que cada una de las imágenes de la figura 4 representa dos SVs, uno con la rotación del vector de polarización a favor de las manecillas del reloj y el otro en contra.

Los SVs con dos cargas topológicas ya han sido estudiados en la fase superfluida ^{3}He-A [55]. En general, aparecen en condensados de varios componentes [56]. El condensado de polaritones está formado por dos componentes, a saber, polaritones con polarización circular derecha e izquierda, es en este sentido que los SVs están presentes en el condensado polaritónico.

Para revelar la fenomenología específica de los SVs con respecto a los vórtices enteros, fue conveniente escribir el parámetro de orden (23) en la base de polarización circular como

$$\psi_{lin} = \sqrt{\frac{n}{2}}\left(e^{\mathrm{i}(\theta-\eta)}|\uparrow\rangle + e^{\mathrm{i}(\theta+\eta)}|\downarrow\rangle\right), \tag{25}$$

$$|\uparrow\rangle = \frac{\{1,i\}}{\sqrt{2}}, \qquad |\downarrow\rangle = \frac{\{1,-i\}}{\sqrt{2}}. \tag{26}$$

Como se puede ver, para $\theta \to \theta + \pi$, $\eta \to \eta + \pi$, una rotación de cero ocurre en una una componente de polarización circular y una rotación completa de 2π se alcanza en la otra componente de polarización circular. Esto quiere decir que los SVs pueden verse como como un vórtice entero en una de las componentes del parámetro de orden.

La textura de polarización de los SVs también fue mostrada en [54]. Estos tienen una polarización lineal lejos de sus núcleos $r \to \infty$, misma que convierte a elíptica cuando $r \sim a$ donde a es el tamaño del núcleo del SV, y finalmente viene a ser completamente circular en su núcleo y su signo está dado por el signo del producto de dos cargas topológicas.

3 Semi-vórtices con cuerda y franjas de interferencia

Como ya hemos discutido anteriormente, la densidad de energía libre del condensado polaritónico se minimiza para la polarización lineal, es decir, cuando $\psi^* \times \psi = 0$. En el análisis de la fijación de la dirección de la polarización lineal sobre un eje cristalino, hecha en [30], un examen cuidadoso de la emisión de la luz por abajo de cierto umbral reveló una separación de energía ε del orden de 0.1 meV entre polaritones polarizados en x y en y en $k_{||} = 0$. Esta energía ε que se debe a la anisotropía óptica de la cavidad, explicó porqué la luz se orienta a lo largo de una dirección bien definida. Los experimentos en [23] también revelan esta separación de energía. Cuando solamente se considera esta separación de energía ε en el condensado polaritónico, el hamiltoniano de este sistema puede escribirse como

$$\begin{aligned} H &= H_{cin} + H_{\varepsilon} + H_{int} \\ &= \int d^2r \left[-\frac{\hbar^2}{2m^*}\left(\psi^* \cdot \Delta\psi\right) - \mu\left(\psi^* \cdot \psi\right)\right] - \varepsilon S_x \\ &+ \frac{1}{2}\int d^2r \left\{(U_0 - U_1)(\psi^* \cdot \psi)^2 + U_1|\psi^* \times \psi|^2\right\}, \end{aligned} \tag{27}$$

donde S_x es la componente del pseudoespín paralela al eje $\hat{x}$ por lo que la luz emitida se considera a lo largo de esta dirección.

Las componentes del vector pseudoespín **S** están definidas en función del parámetro de orden como

$$\begin{aligned} S_x &= (1/2)(|\psi_x|^2 - |\psi_y|^2), \\ S_y &= (1/2)(\psi_x \psi_y^* + \psi_x^* \psi_y), \\ S_z &= (i/2)(\psi_x \psi_y^* - \psi_x^* \psi_y). \end{aligned} \tag{28}$$

De esta manera, existe una relación entre sus componentes de la forma

$$S_x^2 + S_y^2 + S_z^2 = S^2 = (n/2)^2, \tag{29}$$

donde

$$n = \psi \cdot \psi^* = |\psi_x|^2 + |\psi_y|^2. \tag{30}$$

Al igual que en [54], nosotros estamos interesados en las soluciones tipo SVs de la ecuación Gross-Pitaevskii estática (14)

$$\frac{\delta H}{\delta \psi^*} = 0. \tag{31}$$

De esta manera, para poder tratar la ecuación (27), es conveniente escribir el parámetro de orden ψ como un vector con cuatro componentes reales

$$\psi = \sqrt{n}\phi_i = (\mathrm{Re}\{\psi_x\}, \mathrm{Im}\{\psi_x\}, \mathrm{Re}\{\psi_y\}, \mathrm{Im}\{\psi_y\}), \tag{32}$$

con $i = 1,2,3,4$. Con esta sustitución el hamiltoniano polaritónico ahora se escribe como

$$H = \frac{1}{2}\rho_s \int d^2 r \left[\left(\sum_i \nabla \phi_i \right)^2 - \frac{1}{a^2} \sum_i \phi_i^2 \left(1 - \frac{1}{2} \sum_i \phi_i^2 \right) + \frac{(\gamma - 1)}{a^2} S_z^2 - \frac{1}{2b^2} T \right], \tag{33}$$

donde $\rho_s = \hbar^2 n / m^*$, $T = \phi_1^2 + \phi_2^2 - \phi_3^2 - \phi_4^2$ y $S_z = \phi_1 \phi_4 - \phi_2 \phi_3$ es el pseudoespín polaritónico paralelo al eje $\hat{z}$. La primera longitud $a = \hbar / \sqrt{2m^* \mu}$ sigue siendo el tamaño del núcleo del semivórtice [54] y en donde m^* la masa efectiva de los polaritones y μ el potencial químico. La segunda longitud $b = \hbar / \sqrt{2m^* \varepsilon}$ definirá el ancho de la cuerda, tal como se muestra abajo.

La minimización $\delta H[\phi_i] / \delta \phi_i = 0$, tiene como resultado

$$\Delta\phi_i+\frac{1}{a^2}\phi_i\left(1-\sum_k\phi_k^2\right)-\frac{1}{a^2}\alpha_i\alpha_{5-i}(\gamma-1)S_z\phi_{5-i}+\frac{1}{2b^2}\mathrm{sgn}(5-2i)\phi_i=0, \tag{34}$$

para cada componente $i=1,2,3,4$, donde $\alpha_1=1$, $\alpha_2=1$, $\alpha_3=-1$ y $\alpha_4=1$ y k corriendo de 1 a 4.

Para observar los efectos de la separación ε en las propiedades de los vórtices, escribimos el parámetro de orden en la base de la polarización circular.

$$\begin{aligned}\psi&=\sqrt{n}\,(\phi_1+i\phi_2,\phi_3+i\phi_4)\\&=\frac{\sqrt{n}}{2}\left[h_1\{1,i\}+h_2\{1,-i\}\right],\end{aligned} \tag{35}$$

donde

$$h_1=\phi_1+\phi_4+i\,(\phi_2-\phi_3)\,,\ h_2=\phi_1-\phi_4+i\,(\phi_2+\phi_3)\,. \tag{36}$$

Las funciones ϕ_1, ϕ_2, ϕ_3 y ϕ_4 satisfacen al conjunto de ecuaciones dadas por (34). Usando estas relaciones y las ecuaciones (36), las funciones complejas h_1 y h_2 satisfacen el sistema de ecuaciones

$$\begin{aligned}\Delta h_1+\frac{1}{2b^2}h_2+\frac{1}{a^2}\left[1-\frac{1}{2}\left(|h_1|^2+|h_2|^2\right)\right]h_1+\frac{\gamma-1}{4a^2}\left(|h_2|^2-|h_1|^2\right)h_1=0,\\ \Delta h_2+\frac{1}{2b^2}h_1+\frac{1}{a^2}\left[1-\frac{1}{2}\left(|h_1|^2+|h_2|^2\right)\right]h_2+\frac{\gamma-1}{4a^2}\left(|h_1|^2-|h_2|^2\right)h_2=0.\end{aligned} \tag{37}$$

El sistema de ecuaciones (37) reproduce el caso conocido cuando $\gamma=3$ y cuando no hay alguna separación de energía ($\varepsilon=0, b=\infty$), ya que las soluciones al sistema de ecuaciones

$$\begin{aligned}\Delta h_1+\frac{1}{a^2}\left(1-|h_1|^2\right)h_1=0,\\ \Delta h_2+\frac{1}{a^2}\left(1-|h_2|^2\right)h_2=0.\end{aligned} \tag{38}$$

son $h_1=1$ y $h_2=u(r/a)e^{i\phi}$ donde $u(r/a)$ es la función radial del vórtice de fase usual [**?**] en un condensado sin espín.

Consideremos ahora, para cualquier valor de γ, el caso de una pequeña separación de energía xy, es decir, $\varepsilon\ll\mu$. Esto es razonable ya de otro modo el SV requeriría demasiada energía para ser ex-

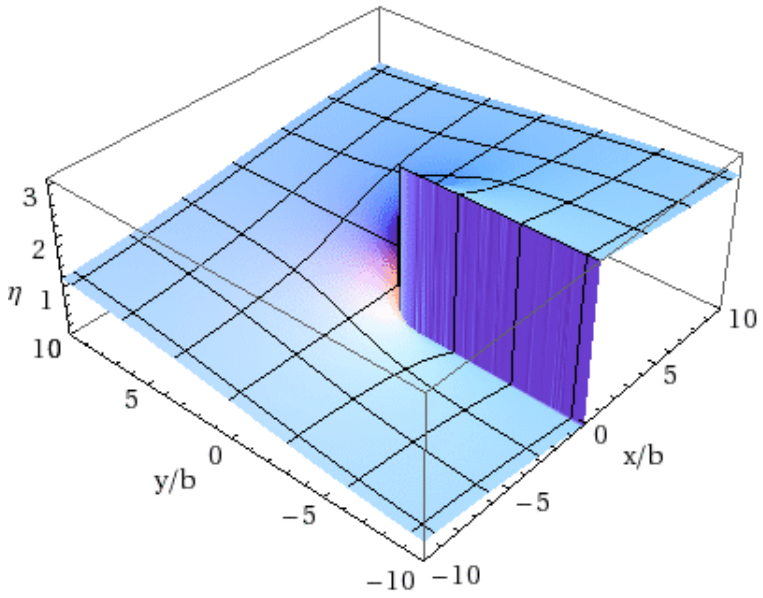

Fig. 5 Perspectiva tridimensional de la solución para ambos θ y η en el caso cuando $\varepsilon = 0$.

citado. Así que nosotros vamos a suponer que $b \gg a$. En este caso la solución del parámetro de orden ψ para distancias $r \sim a$, es decir, dentro del núcleo del SV, debería ser aproximadamente la solución sin separación de energía xy. Fuera del núcleo, cuando $r \gg a$, la concentración del condensado $n = \psi^* \cdot \psi$ viene a ser constante (región elástica) y el parámetro de orden en la base de polarización circular, como sabemos, puede escribirse como

$$\psi_{lin} = \frac{\sqrt{n}}{2}\left(e^{\mathrm{i}(\theta-\eta)}\{1,i\} + e^{\mathrm{i}(\theta+\eta)}\{1,-i\}\right), \tag{39}$$

donde $\theta(\mathbf{r})$ y $\eta(\mathbf{r})$ son los ángulos de fase y polarización y son funciones de la distancia al centro del núcleo r y del ángulo azimutal ϕ. El hamiltoniano (27) en la región elástica es

$$H_{el} = \frac{1}{2}\rho_s \int d^2r\{(\nabla\eta)^2 + (\nabla\theta)^2 - \frac{1}{2b^2}\cos(2\eta)\}, \tag{40}$$

donde hemos omitido una constante de energía.

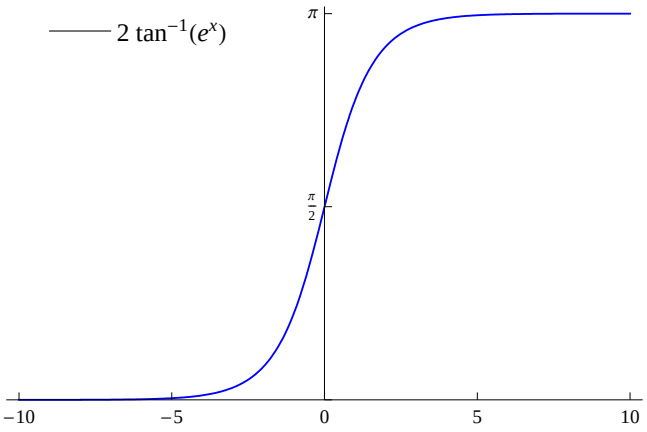

Fig. 6 Solución tipo kink de la ecuacion sen-Gordon (42b).

A partir de la ecuación (35) y de la última expresión para ψ_{lin} (39), las funciones complejas h_1 y h_2 se escriben como

$$h_1 = e^{\mathrm{i}(\theta-\eta)},\ h_2 = e^{\mathrm{i}(\theta+\eta)}, \tag{41}$$

y al sustituir estas funciones en las ecuación (37) se deduce que

$$\Delta\theta = 0, \tag{42a}$$

$$2b^2\Delta\eta = \operatorname{sen}(2\eta). \tag{42b}$$

La solución a la ecuación (42a) describe el cambio uniforme del ángulo de fase con $\theta = m\phi$ y $m = \pm 1/2$. En el caso cuando $\varepsilon = 0$, ambos θ y η son funciones suaves de ϕ, tal como se muestra en la figura 5.

La ecuación (42b) es la conocida ecuación elíptica de sine-Gordon. El nombre de esta ecuación está inspirada por la presencia de término sen al compararla con la ecuación Klein-Gordon. Esta ecuación ha sido usada en un amplio rango de fenómenos, incluyendo propagación de pertubarciones en cristales, flujo magnético en líneas de Josephson, movimiento de paredes de dominio en cristales magnéticos y movimiento bidimensionales de partículas elementales [57].

Las soluciones tipo vórtice de la ecuación de sine-Gordon, son soluciones topológicas especiales en teoría de campo y tienen aplicaciones importantes en física de materia condensada. La solución vórtice más

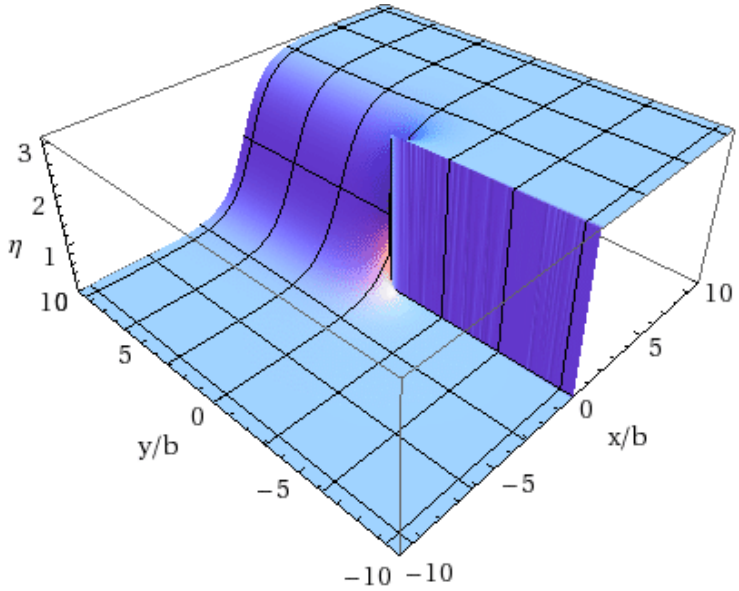

Fig. 7 Configuración tipo vórtice descrita para la ecuación sen-Gordon (42b) para η.

simple puede ser interpretada como una disminución (o incremento) de la amplitud del campo η como uno camina en la dirección positiva (con las manecillas del reloj) alrededor de la singularidad o centro del vórtice. Tal patrón está caraterizado por una carga topológica

$$k = \frac{1}{2\pi} \oint_c \nabla \eta \cdot d\mathbf{l}, \tag{43}$$

donde c es el contorno arbitrario en plano xy rodeando el centro del vórtice. Soluciones numéricas tipo vórtice fueron reportadas en [58] para las cargas topológicas $k = \pm 1$.

Nosotros buscamos soluciones tipo SVs y aplicamos las condiciones límites para resolver las ecuación de sine-Gordon (42b) para η. Consideremos el SV (1/2,1/2). En este caso $\theta = \phi/2$ en cualquier lugar. La solución para η también debería comportarse como $\eta = \phi/2$ en la región $r \ll b$. En el límite opuesto de $r \gg b$, por efectos de minimización de la energía y debido a que la polarización debe cambiar por π, una región localizada (un "*kink*") debe aparecer, por lo que una cuerda[2] se forma donde la polarización se cambia rápidamente y de

[2] Una cuerda es un solitón, ver figura 16.1 en [59]

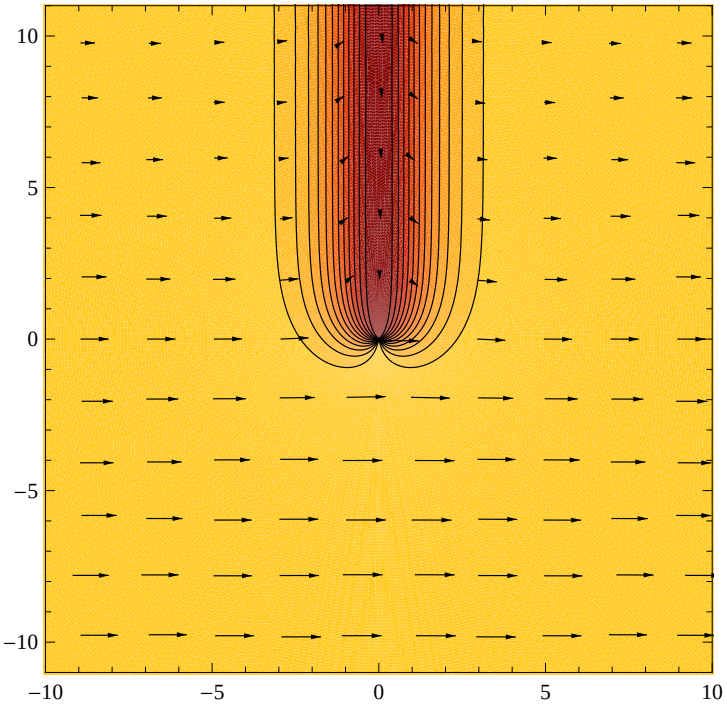

Fig. 8 Perspectiva bidimensional de la solución tipo vórtice descrita para la ecuación sen-Gordon(42b). Las flechas indican la dirección local del vector de polarización.

esta manera el ángulo de polarización η cambia únicamente en una vecindad estrecha del orden de b alrededor del eje de la cuerda. Fuera de esta cuerda, la polarización se fija lo largo de una dirección $\widehat{x}$. Entonces, para $y \gg b$ y $x \sim b$, la ecuación (42b) resulta unidimensional y puede escribirse como

$$2b^2 \frac{d^2\eta_0}{d^2x} = \text{sen}(2\eta_0), \tag{44}$$

con la solución tipo "*kink*"

$$\eta_0(x) = 2\tan^{-1}(\exp\{x/b\}). \tag{45}$$

que se muestra en la figura 6.

De esta manera, para resolver numéricamente la ecuación (42b) en todo el espacio se consideran las siguientes condiciones límites.

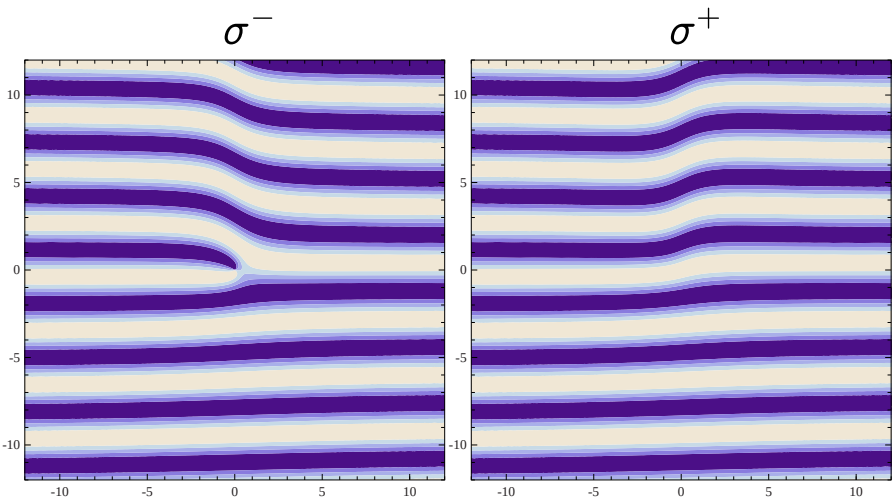

Fig. 9 Se muestran las franjas de interferencia (ver texto) en las polarizaciones izquierda σ^- y derecha σ^+, respectivamente.

$$\eta(x,y) \overrightarrow{\underset{y\to\infty}{}} \eta_0(x) = 2\tan^{-1}(\exp\{x/b\}),$$
$$\eta(x,y) \overrightarrow{\underset{y\to-\infty}{}} n\pi \begin{cases} n=0, x<0 \\ n=1, x>0 \end{cases}, \tag{46}$$

y además

$$\eta(x,y) \overrightarrow{\underset{x\to\infty}{}} 0, \qquad \eta(x,y) \overrightarrow{\underset{x\to-\infty}{}} \pi,$$
$$\eta(-\delta,y)\to 0,\ \eta(\delta,y)\to\pi,\ (\delta\to 0, y<0), \tag{47}$$

en la región $R^2 - C$, donde el corte C representa la línea $\{(0,y)| < y < \infty\}$ y asegura que $\eta(\mathbf{r})$ es univaluada.

Al usar un método numérico de relajación, junto con el conjunto de condiciones límites, se obtuvo la solución tipo vórtice para la ecuación sine-Gordon (42b) para η. Esta solución tipo vórtice se presenta en la figura 7. La región donde η cambia rápidamente define la cuerda o solitón unido al SV. La gráfica de contorno para η se muestra en la figura 8 donde la cuerda unida al SV, está definida por la línea donde la polarización es vertical. Las líneas continuas indican los valores del cambio del ángulo η de 0 a π con el paso de $\pi/12$.

En general, cualquier orientación de la cuerda es posible y los SVs orientados de manera diferente portan la misma energía en el caso que

$m_t = m_l$. Cabe mencionar que la cuerda porta una energía proporcional a su longitud. En un condensado de tamaño finito la cuerda puede terminar en los límites. En este caso el SV será atraído por el límite y puede relajarse hacia éste. La cuerda también puede terminar en otro SV pero con el signo opuesto de la carga topológica k, y esto conduce a la interacción de SVs derechos e izquierdos. La energía de dicha interacción es proporcional a la longitud de la cuerda que acopla estos SVs y crece linealmente con la distancia.

El comportamiento de las franjas de interferencia en las dos polarizaciones circulares se muestran en la figura 3 para la cuerda terminando en el SV $(1/2, 1/2)$. Estas franjas aparecen cuando se observa el patrón de interferencia de la señal emitida desde el condensado polaritónico en una componente circular y una onda plana de la misma intensidad. Experimentalmente [60], esta onda plana se origina en el condensado, pero desde un lugar diferente, donde el parámetro de orden es aproximadamente constante (y esta señal de onda plana es atenuada y reflejada). Más precisamente, la señal emitida en la polarización $\sigma^{\pm}$ es proporcional a $\exp\{\mathrm{i}(\theta \mp \eta)\}$, respectivamente, y las franjas fueron calculadas como $|e^{\mathrm{i}(\theta \mp \eta)} + e^{\mathrm{i}\kappa y}|^2$ con $\kappa = 2/b$.

Como se puede observar, el SV con cuerda está caracterizado por una dislocación tipo tenedor en una polarización circular. Por otra parte, las franjas de interferencia se desplazan media longitud de onda al atrevesar la cuerda en ambas polarizaciones circulares. La mejor opción para observar la cuerda en el patrón de interferencia es cuando el vector de onda (onda plana) es colineal con la cuerda, con las franjas perpendiculares a la cuerda.

4 Conclusiones

En este trabajo hemos presentado una visión general de las motivaciones y teorías que llevaron al logro de CBE de polaritones en microcavidades semiconductoras. Se ha discutido la importancia del estudio en los vórtices presentes en el condensado. En particular, hemos presentado la teoría de las propiedades de los SVs cuando se considera la presencia de una separación de energía debida a la anisotropía óptica de la cavidad, misma que tiene como consecuencia la fijación de polarización lineal. Hemos observado que en este caso el SV está

acompañado de la apariencia de una cuerda que define una región donde la polarización esta rotando [61]. La cuerda porta una energía proporcional a su longitud. Si la cuerda acopla un par de SVs, la energía de la interacción es proporcional a la longitud de la cuerda y crece linealmente con la distancia y no de manera logarítmica como era de esperarse si se considera que la transición superfluida sea del tipo BKT. De esta manera una nueva transición de fase debe ser considerada adicionando los efectos de la separación TE-TM [62, 63].

Agradecimientos

Agradezco al PROMEP de la Universidad Autónoma del Estado de Morelos por el apoyo otorgado para realizar mi estancia posdoctoral en esta institución.

References

1. C. Weisbuch, M. Nishioka, A. Ishikawa, Y. Arakawa, *Phys. Rev. Lett.* **69**, 3314, (1992).
2. A. Kavokin, G. Malpuech, Cavity Polaritons, Elsevier, Amsterdam, 2003.
3. V. Savona, L. C. Andreani, P. Scwendimann, A. Quattropani, *Solid State Commun* **93**, 733, (1995).
4. G. Bastard, *Mechanics Applied to Semiconductor Heterostructures*, Halstead, New York, 1988.
5. J. J. Hopfield, *Phys. Rev.* **112**, 1555, (1958).
6. R. Houdré, C. Weisbuch, R. P. Stanley, U. Oesterle, P. Pellandini, M. Ilegemd, *Phys. Rev. Lett.* **73**, 2043, (1994).
7. A. Imamoglu, J. R. Ram., *Phys. Lett. A* **214**, 193, (1996).
8. F. Tassone, C. Piermarocchi, V. Savona, A. Quattropani, P. Schwendimann, *Phys. Rev.* B **56**, 7554, (1997).
9. L. S. Dang, D. Heger, R. André, F. Boeuf, R. Romestain, *Phys. Rev. Lett.* **81**, 3920, (1998).
10. P. Senellart, J. Bloch., *Phys. Rev. Lett.* **82**, 1233, (1999).
11. F. Tassone, Y. Yamamoto, *Phys. Rev.* B **59**, 10830, (1999).
12. P. G. Savvidis, J. J. Baumberg, R. M. Stevenson, M. S. Skolnick, D. M. Whittaker, J. S. Roberts, *Phys. Rev. Lett.* **84**, 1547, (2000).
13. R. M. Stevenson, V. N. Astratov, M. S. Skolnick, D. M. Whittaker, M. Emam-Ismail, A. I. Tartakovskii, P. G. Savvidis, J. J. Baumberg, S. Roberts, *Phys. Rev. Lett.* **85**, 3680, (2000).
14. P. G. Savvidis, C. Ciuti, J. J. Baumberg, D. M. Whittaker, M. S. Skolnick, J. S. Roberts, *Phys. Rev.* B **64**, 0753111, (2001).
15. M. Saba, C. Ciuti, J. Bloch, V. Thierry-Meig, R. André, L. S. Dang, S. Kundermann, A. Mura, G. Bongiovanni, J. L. Staehli, B. Deveaud, *Nature* **730**, 74, (2001).
16. G. Messin, J.-Pah. Karr, A. Bass, G. Khitrova, R. Houdré, R. P. Stanley, U. Oesterle, E. Giacobino, *Phys. Rev. Lett.* **87**, 127403, (2001).
17. P. G. Lagoudakis, P. G. Savvidis, J. J. Baumberg, D. M. Whittaker, P. R. Eastham, M. S. Skolnick, J. S. Roberts, *Phys. Rev.* B **65**, 161310, (2002).

18. H. Deng, G. Weihs, C. Santori, J. Bloch, Y. Yamamoto, *Science* **298**, 199, (2002)
19. P. Kapitza, *Nature* **141**, 74, (1938).
20. F. London, *Nature* **141**, 643, (1938).
21. J. Keeling, P. R. Eastham, M. H. Szymanska, and P. B. Littlewood, *Phys. Rev. Lett.* **93**, 226403, (2004);
22. F. M. Marchetti, J. Keeling, M. H. Szymanska, y P. B. Littlewood, *Phys. Rev. Lett.* **96**, 066405, (2006).
23. J. Kasprzak, M Richard, S. Kundermann, A. Baas, P. Jeambrun, J. Keeling, F. M. Marchetti, M. H. Szymńske, R. André, J. L. Staehli, V. Savona, P. B. Littlewood, B. Deveaud, and Le Si Dang, *Nature* **443**, 409, (2006).
24. Balili R, Hartwell V, Snoke D, Pfeiffer L, West K., *Science* **316**, 5827, (2007).
25. M. Richard, J. Kasprzak, R. André, R. Romestain, Le Si Dang, *Phys. Rev.* B, **72**, 202301, (2005).
26. C. W. Lai, N. Y. Kim1, S. Utsunomiya, G. Roumpos, H. Deng, M. D. Fraser, T. Byrnes, P. Recher, N. Kumada, T. Fujisawa, Y. Yamamoto, *Nature* **450**, 529, (2007).
27. J. J. Baumberg, A. V. Kavokin, S. Christopoulos, A. J. D. Grundy, R. Butté, G. Christmann, D. D. Solnyshkov, G. Malpuech, G. Baldassarri Hger von Hgersthal, E. Feltin, J.-F. Carlin, N. Grandjean, *Phys. Rev. Lett.* **101**, 136409, (2008).
28. F. P. Laussy, I. A. Shelykh, G. Malpuech, A. Kavokin, *Phys. Rev.* B **73**, 035315, (2006).
29. I. A. Shelykh, Y. G. Rubo, G. Malpuech, D. D. Solnyshkov, and A. Kavokin, *Phys. Rev. Lett.* **97**, 066402, (2006).
30. J. Krasprzak, R. André, Le Si Dang, I. A. Shelykh, A. V. Kavokin, Y. G. Rubo, K. V. Kavokin, G. Malpuech, *Phys. Rev.* B **75**, 045326, (2007).
31. Y. G. Rubo, *Phys. State Solidi A* **201**, 641 (2004).
32. D. Read, P. J. Membry, T. C. H. Liew, Y. G. Rubo, A. V. Kavokin, *Phys. Rev.* B **80**, 195309, (2009).
33. M. D. Martin, G. Aichmayr, L. Viña, R. Andre, *Phys. Rev. Lett.* **89**, 077402, (2002).
34. S. I. Tsintzos, N. T. Pelekanos, G. Konstantininidis, Z. Hatzopoulos, P. G. Savvidis, *Nature* **453**, 372, (2008).
35. D. Porras, C. Tejedor, *Phys. Rev.* B **67**, 161310, (2003).
36. Y. G. Rubo, F. P. Laussy, G. Malpuech, A. Kavokin, P. Bigenwald, *Phys. Rev. Lett.* **91**, 156403, (2003).
37. G. Panzarini, L. C. Andreani, A. Armitage, D. Baxter, M. S. Skolnick,V. N. Astratov, J. S. Roberts, A. V. Kavokin, M. R. Vladimirova, M. A. Kaliteevski, *Phys. Rev.* B **59**, 5082, (1999).
38. L. Klopotowski, A. Amo, M. D. Martín, L. Viña, I. A. Shelykh, M. M. Glazov, A. V. Kavokin, D. D. Solnyshkov, G. Malpuech, R. André, *Solid State Commun.* **139**, 51 (2006).
39. G. Malpuech, M. M. Glazov, I. A. Shelykh, K. V. Kavokin, p. Bigenwald. *Appl. Phys. Lett.* **88**, 111118 (2006).
40. Y. G. Rubo, A. V. Kavokin, I. A. Shelykh, *Phys. Lett. A.* **358**, 227, (2006).
41. C. Ciuti, V. Savona, C. Piermarocchi, A. Quattropani,P. Schwendimann, *Phys. Rev.* B **58**, 7926 (1998).
42. F. Tassone, Y. Yamamoto, *Phys. Rev.* B **59**, 7554 (1999).
43. J. Inoue, T. Brnades, A. Shimizu, *Phys. Rev.* B **61**, 7926 (1999).
44. N. N. Bogoliubov, *J. Phys.*, (USSR), 11, 23, (1947).
45. W. F. Vinen, Proc. *Roy. Soc. A* **260**, 218, (1961).
46. A. L. Fetter, A. A. Svidzinsky, *J. Phys. Condens. Matter* **13**, R135R194, (2001).
47. M. R. Matthews, B. P. Anderson, P. C. Haljan, D. S. Hall, C. E. Wieman, E. A. Cornell, *Phys. Rev. Lett.* **83**, 2498 (1999).
48. K. W. Madison, F. Chevy, W. Wohlleben, J. Dalibard, *Phys. Rev. Lett.* **84**, 806 (2000).
49. T. P. Simula, P. B. Blakie, *Phys. Rev. Lett.* **96**, 020404, (2006).
50. L. Giorgetti,I. Carusotto, Y. Castin, *Phys. Rev. A* **76**, 013613, (2007).
51. V. L. Berezinskii, *Sov. Phys. JETP* **32**, 34, 610, (1970).
52. J. M. Kosterlizt, D. J. Thouless, *J. Phys. C: Solid State Phys.* **6**, 1181, (1973).

53. K. G. Lagoudakis, M. Wouters, M. Richard, A. Baas, I. Carusotto, R. André, L. S. Dang, B. Deveaud-Plédran, *Nat.Phys.* **4**, 706, (2008).
54. Y. G. Rubo, *Phys. Rev. Lett.* **99**, 106401, (2007).
55. G. E. Volovik, *The Universe in a Helium Droplet*, Oxford University Press, New York, 2003, Chap. 15.3.
56. M. M. Salomaa and G. E. Volovik, *Rev. Mod. Phys.* **59**, 533, (1987).
57. R. Rajaraman, *Solitons and instantons*. North-Holland Personal Library, (1989).
58. A. B. Bosisov, *Theoretical and Mathematical Physics*, **124**, No. 2, (2000).
59. G. E. Volovik, The Universe in a Helium Droplet, Clarendon Press, Oxford, 2003.
60. K. G. Lagoudakis, T. Ostatnický, A. V. Kavokin, Y. G. Rubo, R. André, and B. Deveaud-Plédran, *Science* **326**, 974, (2009).
61. M. Toledo-Solano, Y. G. Rubo, *J. Phys.: Conf. Ser.* **210**, 012024, (2010).
62. H. Flayac, I. A. Shelykh, D. D. Solnyshkov, and G. Malpuech, *Phys. Rev.* B **81**, 045318, (2010).
63. M. Toledo-Solano, Y. G. Rubo, *Phys. Rev.* B **82**, 127301, (2010).

Index